TECHNICAL REPORTS SERIES NO. 477

Development and Applications of Residual Stress Measurements Using Neutron Beams

IAEA
International Atomic Energy Agency

IAEA SAFETY STANDARDS AND RELATED PUBLICATIONS

IAEA SAFETY STANDARDS

Under the terms of Article III of its Statute, the IAEA is authorized to establish or adopt standards of safety for protection of health and minimization of danger to life and property, and to provide for the application of these standards.

The publications by means of which the IAEA establishes standards are issued in the **IAEA Safety Standards Series**. This series covers nuclear safety, radiation safety, transport safety and waste safety. The publication categories in the series are **Safety Fundamentals**, **Safety Requirements** and **Safety Guides**.

Information on the IAEA's safety standards programme is available on the IAEA Internet site

http://www-ns.iaea.org/standards/

The site provides the texts in English of published and draft safety standards. The texts of safety standards issued in Arabic, Chinese, French, Russian and Spanish, the IAEA Safety Glossary and a status report for safety standards under development are also available. For further information, please contact the IAEA at: Vienna International Centre, PO Box 100, 1400 Vienna, Austria.

All users of IAEA safety standards are invited to inform the IAEA of experience in their use (e.g. as a basis for national regulations, for safety reviews and for training courses) for the purpose of ensuring that they continue to meet users' needs. Information may be provided via the IAEA Internet site or by post, as above, or by email to Official.Mail@iaea.org.

RELATED PUBLICATIONS

The IAEA provides for the application of the standards and, under the terms of Articles III and VIII.C of its Statute, makes available and fosters the exchange of information relating to peaceful nuclear activities and serves as an intermediary among its Member States for this purpose.

Reports on safety in nuclear activities are issued as **Safety Reports**, which provide practical examples and detailed methods that can be used in support of the safety standards.

Other safety related IAEA publications are issued as **Emergency Preparedness and Response** publications, **Radiological Assessment Reports**, the International Nuclear Safety Group's **INSAG Reports**, **Technical Reports** and **TECDOCs**. The IAEA also issues reports on radiological accidents, training manuals and practical manuals, and other special safety related publications.

Security related publications are issued in the **IAEA Nuclear Security Series**.

The **IAEA Nuclear Energy Series** comprises informational publications to encourage and assist research on, and the development and practical application of, nuclear energy for peaceful purposes. It includes reports and guides on the status of and advances in technology, and on experience, good practices and practical examples in the areas of nuclear power, the nuclear fuel cycle, radioactive waste management and decommissioning.

DEVELOPMENT AND APPLICATIONS OF RESIDUAL STRESS MEASUREMENTS USING NEUTRON BEAMS

The following States are Members of the International Atomic Energy Agency:

AFGHANISTAN
ALBANIA
ALGERIA
ANGOLA
ARGENTINA
ARMENIA
AUSTRALIA
AUSTRIA
AZERBAIJAN
BAHAMAS
BAHRAIN
BANGLADESH
BELARUS
BELGIUM
BELIZE
BENIN
BOLIVIA
BOSNIA AND HERZEGOVINA
BOTSWANA
BRAZIL
BRUNEI DARUSSALAM
BULGARIA
BURKINA FASO
BURUNDI
CAMBODIA
CAMEROON
CANADA
CENTRAL AFRICAN REPUBLIC
CHAD
CHILE
CHINA
COLOMBIA
CONGO
COSTA RICA
CÔTE D'IVOIRE
CROATIA
CUBA
CYPRUS
CZECH REPUBLIC
DEMOCRATIC REPUBLIC OF THE CONGO
DENMARK
DOMINICA
DOMINICAN REPUBLIC
ECUADOR
EGYPT
EL SALVADOR
ERITREA
ESTONIA
ETHIOPIA
FIJI
FINLAND
FRANCE
GABON
GEORGIA
GERMANY
GHANA
GREECE
GUATEMALA
HAITI
HOLY SEE
HONDURAS
HUNGARY
ICELAND
INDIA
INDONESIA
IRAN, ISLAMIC REPUBLIC OF
IRAQ
IRELAND
ISRAEL
ITALY
JAMAICA
JAPAN
JORDAN
KAZAKHSTAN
KENYA
KOREA, REPUBLIC OF
KUWAIT
KYRGYZSTAN
LAO PEOPLE'S DEMOCRATIC REPUBLIC
LATVIA
LEBANON
LESOTHO
LIBERIA
LIBYA
LIECHTENSTEIN
LITHUANIA
LUXEMBOURG
MADAGASCAR
MALAWI
MALAYSIA
MALI
MALTA
MARSHALL ISLANDS
MAURITANIA
MAURITIUS
MEXICO
MONACO
MONGOLIA
MONTENEGRO
MOROCCO
MOZAMBIQUE
MYANMAR
NAMIBIA
NEPAL
NETHERLANDS
NEW ZEALAND
NICARAGUA
NIGER
NIGERIA
NORWAY
OMAN
PAKISTAN
PALAU
PANAMA
PAPUA NEW GUINEA
PARAGUAY
PERU
PHILIPPINES
POLAND
PORTUGAL
QATAR
REPUBLIC OF MOLDOVA
ROMANIA
RUSSIAN FEDERATION
RWANDA
SAN MARINO
SAUDI ARABIA
SENEGAL
SERBIA
SEYCHELLES
SIERRA LEONE
SINGAPORE
SLOVAKIA
SLOVENIA
SOUTH AFRICA
SPAIN
SRI LANKA
SUDAN
SWAZILAND
SWEDEN
SWITZERLAND
SYRIAN ARAB REPUBLIC
TAJIKISTAN
THAILAND
THE FORMER YUGOSLAV REPUBLIC OF MACEDONIA
TOGO
TRINIDAD AND TOBAGO
TUNISIA
TURKEY
UGANDA
UKRAINE
UNITED ARAB EMIRATES
UNITED KINGDOM OF GREAT BRITAIN AND NORTHERN IRELAND
UNITED REPUBLIC OF TANZANIA
UNITED STATES OF AMERICA
URUGUAY
UZBEKISTAN
VENEZUELA
VIET NAM
YEMEN
ZAMBIA
ZIMBABWE

The Agency's Statute was approved on 23 October 1956 by the Conference on the Statute of the IAEA held at United Nations Headquarters, New York; it entered into force on 29 July 1957. The Headquarters of the Agency are situated in Vienna. Its principal objective is "to accelerate and enlarge the contribution of atomic energy to peace, health and prosperity throughout the world''.

TECHNICAL REPORTS SERIES No. 477

DEVELOPMENT AND APPLICATIONS OF RESIDUAL STRESS MEASUREMENTS USING NEUTRON BEAMS

INTERNATIONAL ATOMIC ENERGY AGENCY
VIENNA, 2014

COPYRIGHT NOTICE

Marketing and Sales Unit, Publishing Section
International Atomic Energy Agency
Vienna International Centre
PO Box 100
1400 Vienna, Austria
fax: +43 1 2600 29302
tel.: +43 1 2600 22417
email: sales.publications@iaea.org
http://www.iaea.org/books

Printed by the IAEA in Austria
April 2014
STI/DOC/010/477

IAEA Library Cataloguing in Publication Data

Development and applications of residual stress measurements using neutron beams. — Vienna : International Atomic Energy Agency, 2014.
p. ; 24 cm. — (Technical reports series, ISSN 0074–1914 ; no. 477)
STI/DOC/010/477
ISBN 978–92–0–113313–7
Includes bibliographical references.

1. Neutron beams — Experiments. 2. Nondestructive testing. 3. Residual stresses — Measurement. I. International Atomic Energy Agency. II. Series.

IAEAL 14–00892

FOREWORD

The deep penetration and selective absorption of neutrons make them a powerful tool for the non-destructive testing of large samples of material or large objects. Residual stress that is formed in a material during manufacturing, welding, utilization or repair can be measured by means of neutron diffraction. In fact, neutron diffraction is the only non-destructive testing method which can facilitate three dimensional mapping of residual stress in a bulk component. Stress measurement using neutron beams is a technique that enables this kind of high quality non-destructive investigation, and provides insight into the material strain and stress state deep within engineering components and structures under various conditions representative of those which might be experienced in service. Such studies are of importance to improve the quality of industrial components in production and to optimize design criteria in applications. Anisotropies in macroscopic properties such as thermal and electrical conductivities, for instance of fuel elements, and mechanical properties of materials depend on the textures developed during their preparation or thermal treatment. Such textures also can be studied using neutron diffraction techniques.

There is currently substantial scientific and industrial demand for high quality non-destructive residual stress measurements, and the continuing competitive drive to optimize performance and minimize weight in many applications indicates that this demand will continue to grow. As such, the neutron diffraction technique is an increasingly important tool for mechanical and materials engineering in the search for improved manufacturing processes to reduce stress and distortion. Considering this trend, and in accordance with its purpose of promoting the peaceful use of nuclear applications, in 2006–2009 the IAEA organized a Coordinated Research Project on the Development and Application of the Techniques of Residual Stress Measurements in Materials. This project relied on the participation of practitioners from highly specialized user facilities from various Member States, including the Czech Republic, Germany, Hungary, India, the Netherlands, Pakistan, Romania, the Russian Federation and South Africa.

This report is the culmination of the project, and provides guidance on the basic principles, requirements, preparation, design, execution and standardization of residual stress measurements using neutron beams. It includes details of experimental techniques; associated equipment and instrumentation; their commissioning, calibration and control; and, finally, data acquisition. A separate section is dedicated to data analysis and interpretation. The publication also provides a number of selected examples of applications of residual stress measurements as well as future trends for the development and use of this powerful technique. Finally, complete information on a number of round robin

exercises with standard samples, as well as detailed information on a dozen residual stress instruments worldwide, has been included. Ultimately, the report is intended to promote the use of neutron beams in residual stress measurements; facilitate the preparation, design and standardization process at less well equipped smaller research centres around the world; and to serve as a guidance text for young researchers and graduate students new to the field.

The IAEA officer responsible for this publication was D. Ridikas of the Division of Physical and Chemical Sciences.

CONTENTS

1. INTRODUCTION

1.1. BACKGROUND

Nuclear technologies such as fission and fusion reactors, including associated waste storage and disposal, rely on the availability not only of nuclear fuels but also of advanced structural materials. Various techniques have been developed to measure material properties at the microscopic and macroscopic level. Neutron scattering has played an important role in studying the structure and dynamics of condensed matter. The special nature of neutron interaction with matter provides important data which is complementary and supplementary to data gathered through other techniques. The location of hydrogen atoms in the presence of heavy elements, for example, can only be determined by means of neutron diffraction studies. Crystal structures of biological systems, such as amino acids and polypeptides, have been elucidated using single crystal neutron diffraction. The properties of magnetic materials can be studied at the microscopic scale using neutrons and such studies have been useful in both scientific and industrial applications.

The substantial penetration depth and selective absorption of neutrons make them a powerful tool in the non-destructive testing of materials with large and bulky samples. Residual stress formed in a material during manufacturing, welding, utilization or repairs can be investigated by means of neutron diffraction. In fact neutron diffraction is the only non-destructive testing method which can facilitate three dimensional mapping of residual stress in a bulk component. Such studies are important in order to improve the quality of engineering components in production and to optimize design criteria in applications. The technique has applications in nuclear technology such as testing pipes and tubes, weld joints or structures under various conditions representative of those which might be experienced in service. Anisotropies in macroscopic properties such as thermal and electrical conductivities, for instance, of fuel elements, and mechanical properties of materials depend on the textures developed during their preparation or thermal treatment. Such textures can also be studied using neutron diffraction techniques.

The IAEA conducted a Coordinated Research Project (CRP) on the Development and Application of the Techniques of Residual Stress Measurements in Materials (2006–2009). This project relied on the participation of practitioners from highly specialized user facilities from various Member States, including the Czech Republic, Germany, Hungary, India, the Netherlands, Pakistan, Romania, the Russian Federation and South Africa. Various activities were implemented to increase Member State capabilities in the development and applications of

residual stress measurements. The project participants initiated and contributed significantly to the preparation of this report, which will certainly be useful for other Member States interested in residual stress measurements using neutron beams.

1.2. PURPOSE AND SCOPE

The CRP objectives, among others, were:

— To optimize neutron beams for residual stress measurement using modern simulation techniques;
— To enhance beam intensity using modern neutron optics;
— To develop and test standardized procedures for the comparison of data from various instruments.

This publication is the main output of the project, and its purpose is to relate guidance on the basic principles, requirements, preparation, design, execution and standardization of residual stress measurements using neutron beams in a single publication. The publication will promote the use of neutron beams in residual stress measurements both at the microscopic and the macroscopic scale; facilitate preparation, design and standardization processes at less well equipped smaller research centres around the world; and offer guidance for young researchers and graduate students new to the field.

1.3. STRUCTURE

This report consists of nine sections including references. Section 2 defines the terms and techniques discussed in the report. Section 3 includes details of experimental techniques, while Section 4 describes associated equipment and instrumentation and their commissioning, calibration and control as well as data acquisition. Section 5 is dedicated to data analysis and interpretation. Section 6 of the report provides a number of selected examples for applications of residual stress measurements and Section 7 discusses future trends for development and use of this powerful technique. In addition, Annex I contains complete information on a number of round robin tests with standard samples and some results reported by the IAEA project participants. Finally, information on a dozen residual stress instruments worldwide and their characteristics is provided in Annex II.

2. RESIDUAL STRESS

2.1. DEFINITION

Residual stresses are self-equilibrating stresses within a stationary solid body in the absence of externally applied forces. Residual stresses arise due to shape misfits or incompatibilities, occasionally termed eigenstrains, between the unstressed shapes of different parts, regions or phases of the material and can occur over a wide range of length scales.

Residual stresses may develop at any stage of a manufacturing process or in-service history that introduces permanent inhomogeneous deformation into a component or structure. Welding, machining, forming, hardening, casting and forging can all cause residual stresses to remain in the finished product. Additional processes are also often used for the specific purpose of inducing beneficial compressive residual stresses at critical locations.

It is useful to divide residual stresses into three classes defined by length scales. Type I residual stresses, also known as macrostresses, are homogeneous over many crystal domains in a material, i.e. at the macroscopic scale of the structure. The internal forces and moments associated with macrostresses are equilibrated and balanced on all planes and axes of the volume. Type II and Type III residual stresses, collectively defined as microstresses, act at microscopic and submicroscopic levels. Type II residual stresses are homogeneous within a small crystal or intergranular scale of the material (a distinct grain or phase), typically 3–10 times the grain size. The internal forces associated with Type II stresses are balanced between dissimilar grains or phases. Type III residual stresses are homogeneous on the smallest crystal domain, over a few interatomic lengths, and consequently the internal forces coupled to Type III stresses are equilibrated at subatomic domains (smaller than a grain size). Type III residual stresses are typically related to defects in crystals, e.g. coherency at interfaces, dislocations, interstitials and vacancies [1].

It is the Type I residual stresses that have a significant effect on the mechanical performance of materials and, thus, quantitative knowledge of these stresses is useful for manufacturers, operators and regulators of mechanical and structural components and structures, especially in safety critical applications. However, the assessment of residual stress is far from easy and there is a substantial and growing technical and industrial demand for high quality non-destructive residual stress measurements.

Neutron stress measurement is such a technique and provides insight into strain and stress fields deep within engineering components and structures [2]. Elastic strain and stress distributions measured with neutrons can be directly

compared to predictions produced with finite element models of material deformation. As such, it has become an increasingly important tool for mechanical and materials engineering in the search for improved manufacturing processes to reduce stress and distortion, as precise knowledge of stresses within structures allows the definition of more precise structural integrity and resistance procedures. The continuing drive to optimize performance and minimise weight in many applications in order to maximise competitiveness will ensure that this field continues to grow.

The technique was first developed in the late 1970s and, after initial slow expansion, has developed significantly since then, with an increase in the number of available instruments and an expansion in the user community. This expansion resulted from the fact that for many problems, neutron strain scanning is still the only non-destructive means of measuring stresses deep within engineering components and structures, under conditions representative of those experienced in service (temperature, stress, atmosphere, etc.). The popularity and maturity of neutron strain scanning is reflected in a series of international standards and review books covering this topic. An ISO standard dealing with residual stress measurement by neutron diffraction was proposed by the Versailles Project on Advanced Materials and Standards Technical Working Area 20 in 2001 and ratified in 2005 [3]. A comprehensive introduction to the technique is found in Ref. [4]; and a description of the state of the art of stress measurements using neutron and synchrotron radiation is given in Ref. [5].

The present report covers various topics essential to the establishment of neutron strain scanning instruments at neutron sources. It is the culmination of IAEA CRP on the Development and Application of the Techniques of Residual Stress Measurements in Materials, and its purpose is to relate guidance on the basic principles, requirements, preparation, design, execution and standardization of residual stress measurements using neutron beams in a single publication. The goal of this report is to promote the use of neutron beams in residual stress measurements; facilitate preparation, design and standardization process for newcomers; and to serve as a guidance text for young researchers and graduate students in the field.

2.2. RESIDUAL STRESS MEASUREMENT BY NEUTRON DIFFRACTION

As noted above, residual stress measurement by neutron diffraction has gained momentum from its widespread applications in industry and technology and is now a well-established technique. The crystallites, which form the polycrystalline solid aggregate, act as built-in strain gauges for the analysis of internal stresses using diffraction methods. Indeed, the analogy of the technique

as an atomic or crystal strain gauge is useful as just as in the case of mechanical strain gauges fixed to the surface of a component or structure, strain is actually measured and stress is then calculated.

Comprehensive descriptions of neutron diffraction based stress analysis can be found in textbooks [1, 4, 6–8]. The technique is conceptually simple but its practical application can be time consuming. Its main advantages are:

— Penetration power of the order of centimetres in most engineering materials.
— High spatial resolution that is adjustable to resolve strain gradients in engineering components.
— Its non-destructive nature, meaning that it can be used to mimic the evolution of residual stress in simulated environments and loading conditions in situ.
— Its suitability for characterizing bulk macroscopic engineering stresses, average phase-specific stresses and inter-granular stresses.

2.2.1. The basic principles

The crystal lattice, which is the natural building block of crystalline solids, presents as a natural and ever present atomic plane strain gauge embedded in each crystallite or grain. Although the neutron diffraction technique does not probe the deformation with atomic spatial resolution, it does probe the average deformation of the lattice planes in a certain sample volume. Detailed descriptions of the scattering of waves by regular arrangements of atoms are the essential basis for diffraction based techniques for strain and hence stress characterization based on Eq. (1), which is the general description of Bragg's law as illustrated in Fig. 1.

$$2d_{hkl} \cdot \sin \theta_{hkl} = \lambda \tag{1}$$

Through the nature of the diffraction process, which focuses on the lattice plane spacings of specific subsets of crystallites, or grains, with favourable orientations relative to the scattering geometry, the technique provides unique insights for both fundamental and applied materials science. This grain selective character facilitates the separation of the strain response of different phases in a multiphase material, provided that the phases are distinguishable in a crystallographic sense.

The average elastic lattice strain in the sampled volume of the component under investigation is given in terms of the difference in its lattice plane spacing d_{hkl} relative to that of a strain or stress free reference $d_{0,hkl}$. In many circumstances, the determination of the stress free lattice parameter is the most challenging aspect of measuring stress by neutron diffraction and this subject will be returned to later in this report.

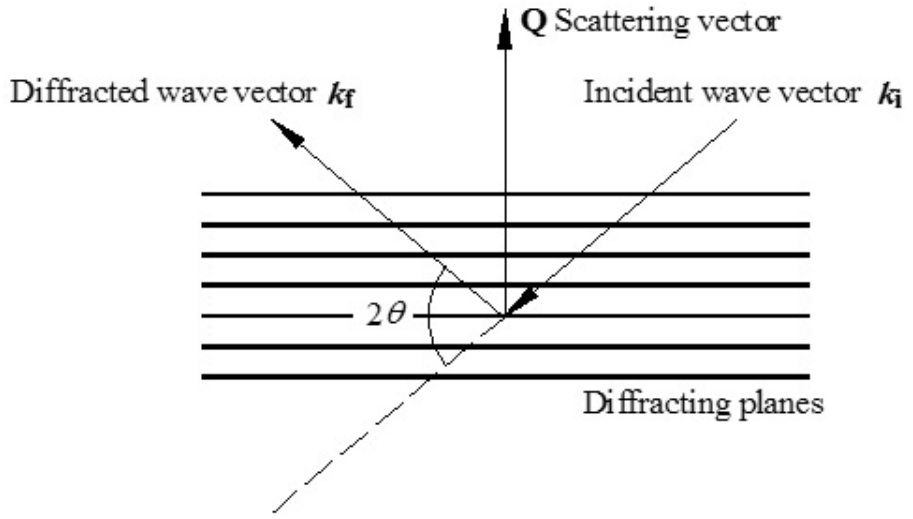

FIG. 1. Schematic illustration of Bragg scattering geometry.

The strain is measured in the direction of the scattering vector, $\boldsymbol{Q} = k_f - k_i$, which bisects the angle between incident and diffracted beams and is perpendicular to the diffracting planes as shown in Fig. 1. Lattice spacings are determined from the measured angular position of the diffraction peak (Bragg reflection) by probing the specimen with a monochromatic collimated beam of neutrons. If the specimen contains no strain, the lattice spacings are the strain free (stress free) values for the material and are denoted by $d_{0,hkl}$. In a stressed specimen, lattice spacings are altered, a shift in each Bragg peak position occurs and the elastic strains are then given by:

$$\varepsilon_{hkl} = \frac{d_{hkl} - d_{0,hkl}}{d_{0,hkl}} = \frac{\Delta d_{hkl}}{d_{0,hkl}} = \frac{\sin\theta_{0,hkl}}{\sin\theta_{hkl}} - 1 \tag{2}$$

Strain is a second rank tensor and the strain calculated in Eq. (2) represents one component of this tensor. Measurements of other strain components from the same volume will enable the complete strain tensor to be obtained. The related second rank stress tensor can then be calculated by combining this data, provided the elastic constants of the materials are known as they are the critical data in the fourth rank compliance tensor which links stress/strain as shown in Eq. (3).

$$\sigma_{ij} = C_{ijkl}\,\varepsilon_{kl} \tag{3}$$

In practice, simplifying assumptions about both the elastic constants and the strain or stress tensors can often be made, and methodologies for calculating stress from strain in such situations are described later in this report.

2.3. OTHER FACTORS

Although they are not going to be treated in detail within this report, it is worth briefly describing the ancillary factors that are necessary for the successful operation of a neutron based residual stress measurement programme.

The first factor is recognizing the requirement to improve communication and collaboration between neutron diffraction experts and their potential customers. Whilst the benefits of using large scale facility methods are often understood by scientists, they are less known by engineers in industry who may think of research reactors as being test facilities for nuclear power plants or only of use for research in fundamental science. Indeed, considering the manifold benefits of neutrons as a research tool, it makes sense to work closely together with industrial engineers representing the non-destructive testing and structure-mechanical simulation field, despite possible limited knowledge among them regarding the methods available at neutron facilities.

The second related issue is the requirement to develop human capital in both the research reactor and user environments. A successful experiment requires both a trained person who understands the technique and is motivated to find a proper solution and an engaged user who understands the strengths and weaknesses of the technique. Often this ideal can only be achieved through dedicated education and training programmes which may be delivered either through intensive, highly interactive ‘neutron schools’ which offer in person lectures, tutorials and problem classes over the course of one or two weeks, or increasingly by well designed distance or virtual learning environments.

3. EXPERIMENTAL TECHNIQUES

3.1. NEUTRON SOURCES

3.1.1. Introduction

At present, two types of neutron source — steady state (or continuous) and pulsed — are used for neutron scattering studies of condensed matter. Nuclear

research reactors are a common example of the first type of source, while the second type mostly comprises a few remaining sources based on high energy proton accelerators. With pulsed sources, proton interactions with the target cause spallation of the nuclei of the heavy metal atoms, releasing a considerable number of neutrons per nucleus.

For neutron production in nuclear reactors, fission reactions with radioactive elements are used. The first nuclear reactors appeared in the middle of the 1940s, and it was demonstrated soon after that slow neutrons can be used for diffraction [9] and inelastic scattering [10] studies of the structure and dynamics of crystals and liquids. The design of nuclear reactors improved quickly; their power and neutron flux increased and already in the 1960s a number of research reactors with 10–20 MW power, and several with 50–100 MW power, were designed and built in various countries. One of the most well known is the high flux reactor at the Institut Laue-Langevin (ILL) in Grenoble, France, with 58 MW power and 1.5×10^{15} $cm^{-2} \cdot s^{-1}$ thermal neutron flux, which was put into operation in 1971 [11].

At this level, steady state research reactors are close to the limit of achievable neutron flux, and their further development as neutron sources for condensed matter studies focuses on the upgrading of beamlines with various average neutron energies (cold, thermal and epithermal).

Starting in the 1960s, neutron sources based on particle accelerators have appeared as an alternative to nuclear reactors. At first, in 1959, electron linear accelerators, known as Harwell linacs, with heavy metal (Pb, W) or fission element (^{235}U, ^{238}U) targets, were constructed. However, the neutron flux provided by this type of source was not enough for condensed matter studies and soon they were substituted by sources based on proton accelerators. The first successful example of this series was the ZING-P′ source at Argonne National Laboratory in 1973, which combined a proton linac, a synchrotron and a metal target made from W or ^{238}U [12]. Using this positive experience as a basis, in the 1980s several pulsed neutron sources of this spallation source type were put into operation. In the twenty-first century a third new generation of pulsed spallation neutron sources (SNS) was introduced. Their main feature is their higher average power level, which exceeds 1 MW, while the power of the previous spallation sources was not higher than 200 kW.

3.1.2. Steady state nuclear reactors

In nuclear reactors, neutrons are produced from the result of a nuclear chain reaction with heavy radioactive elements such as ^{235}U or occasionally ^{239}Pu. These isotopes undergo fission with thermal neutrons producing 2–3 fast neutrons and the release of 100–200 MeV of energy per fission. The central part of a reactor

consists of [13] an active core with fuel, neutron guides, a main moderator and in some reactors, additional moderators. The active core is formed with a number of fuel elements and the chain reaction is controlled by neutron absorbing control rods. The total amount of fuel packed in fuel elements is around 10 kg. The active core is surrounded by the main moderator (for reducing the energy of fast neutrons), which can be H_2O or D_2O depending on the enrichment of the fuel. The moderator is simultaneously used as a reflector of slow neutrons back into the core to support the chain reaction and as the reactor coolant. The moderator tank is quite large: 2–3 m in diameter and 3–4 m in height. At modern reactors, the neutron density in the moderator is very high; consequently, a high neutron flux can be provided. For instance, at the FRM II (Technical University of Munich, Germany) reactor, which was put into operation in 2004, the nominal thermal power is equal to 20 MW and the neutron flux is as high as 8×10^{14} $cm^{-2} \cdot s^{-1}$ [13].

Neutron beam tubes pass through the shield of the reactor into the moderator. Some of them are radial, whilst others are tangential to the core. The former have a more intense neutron flux than the latter, and their background gamma and fast neutron flux is also higher. A number of beam tubes are used for the transportation of thermal neutrons to spectrometers, which measure scattered neutrons from various samples or objects under investigation. In addition, there are beam tubes, which view special hot or cold moderators (sources), so that the neutron spectral distribution is shifted to the side of lower or higher energies. The temperature of the hot moderator can be as high as 1000°C. Cold moderators are used, as a rule, in the range of 20–100 K. An important feature of powerful reactor operation is the burnup of fuel, which must be regularly exchanged with a normal cycle length of 2–3 months.

Placed around the reactor are spectrometers for neutron scattering studies of condensed matter. Some of them are located in an experimental hall close to the reactor; others are placed in neutron guide halls at a greater distance from the source [14]. Usually the spectrometers for thermal and epithermal neutrons are placed in the reactor hall, while the neutron guide hall is provided with cold neutrons.

The active construction of steady state research reactors was carried out in the 1960s and 1970s. Since 1990, their number worldwide has been decreasing, as their lifetime is 30–50 years, and the construction of new steady state research reactors has practically stopped. A current overview of extant research reactors can be found in the IAEA Research Reactor Database [15].

3.1.3. Pulsed neutron sources

At present, pulsed neutron sources are classified according to the time width of the neutron pulse, Δt_0. Those with $\Delta t_0 \leq 50$ μs are considered short

pulse sources, and those with $\Delta t_0 \geq 300$ μs are considered long pulse sources (Fig. 2). This is because of the strong influence of the neutron pulse width on the resolution function of neutron spectrometers and the consequent possibility of realizing certain kinds of experiments. All but one of the existing spallation sources are short pulse sources. At the moment, the only operational source with a long pulse is the IBR-2 pulsed reactor in Dubna in the Russian Federation. At both types of pulsed neutron sources, the time of flight (TOF) technique is used for data acquisition.

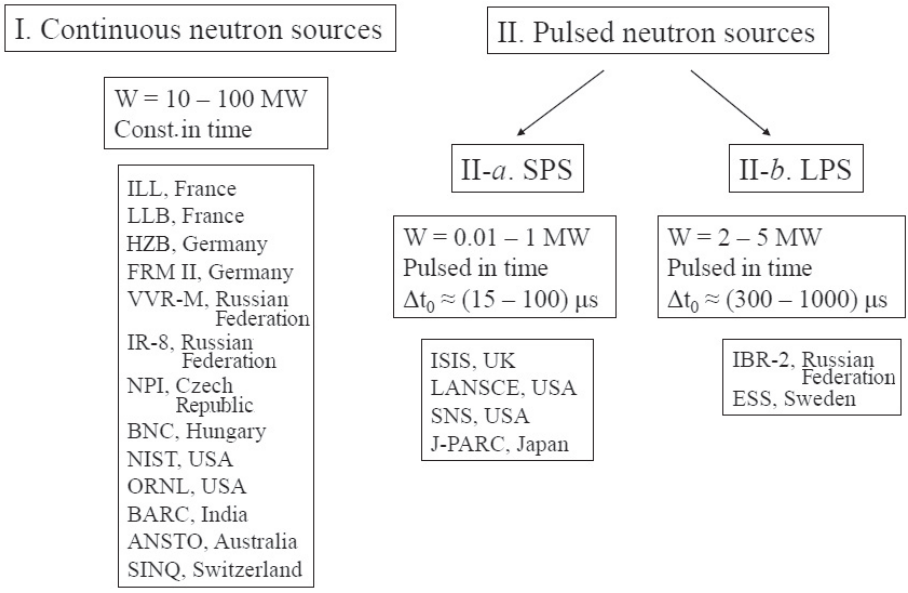

FIG. 2. Research neutron sources for condensed matter studies (name of the source or laboratory are indicated). For continuous neutron sources, only a few representative reactors are mentioned. One should note separately that the SNS (United States of America) and J-PARC (Japan) pulsed sources had started operation a short time before the publication of this report but had not reached their nominal power by the time of writing, while the ESS (Sweden/Europe) is at the detailed design stage.

To produce neutrons, spallation sources use the spallation process, which is a nuclear reaction that occurs when high energy charged particles bombard a heavy atom (e.g. tungsten, tantalum or mercury) target. For example, protons with an energy of around 1 GeV can produce close to 30 neutrons per incident particle.

The principle of operation of the ISIS spallation neutron source, which is a combination of a linear accelerator and a synchrotron, can be found in Ref. [16]. At this source, a 200 μA, 800 MeV proton current impinges on a tantalum target

producing approximately 2×10^{18} fast neutrons per second at a frequency of 50 Hz with pulses of <1 μs in width. The target is surrounded by four moderators, two of which are water moderators at room temperature, while the third is liquid methane at ≈100 K and the fourth is liquid hydrogen at ≈20 K. In the course of moderation, the initial short pulse of fast neutrons is transformed into a longer pulse of low energy neutrons. Its width depends on its energy, which is roughly proportional to the neutron wavelength, and could be from 20 to 100 μs.

Neutrons are provided to spectrometers through the biological shielding via beam tubes or neutron guides. The spectrometers are arranged differently to steady state reactors. Near to the source, at a flight path around L = 8–15 m, spectrometers that do not need high TOF resolution are placed. At longer flight paths of 50–100 m, high resolution spectrometers are constructed, sometimes in a dedicated pavilion.

At present, four pulsed spallation sources are operational: ISIS (Rutherford Appleton Laboratory (RAL), United Kingdom), LANSCE (Los Alamos National Laboratory (LANL), USA), SNS (Oak Ridge National Laboratory (ORNL), USA) and J-PARC (Tokai, Japan). The last two are new sources of the next generation with an average power of 1–1.5 MW. In 2009, it was decided to construct a new pulsed neutron source in Europe, which was named the European Spallation Source (ESS) and will be located in Lund, Sweden. It will have 5 MW power and is planned to be of the long pulse source type [17]. The commissioning of ESS is expected before 2020.

3.1.4. Specific neutron sources

In addition to powerful steady state reactors and spallation sources, two rather unique neutron sources are successfully used for condensed matter studies: SINQ (Paul Scherrer Institute (PSI), Switzerland) [18] and IBR-2 (Joint Institute of Nuclear Research, Russian Federation) [19]. SINQ, operational since 1997, is a spallation type source with a proton accelerator of 590 MeV in energy at a current of up to 2.3 mA and a heavy metal (lead or mercury) target station. The target is surrounded by a D_2O moderator and H_2O reflector with one D_2 cold source (T = 25 K) inside the moderator tank. The frequency of proton pulses is approximately 50 MHz, meaning that the neutron flux is practically constant in time similar to the steady state reactors. Consequently, neutron spectrometers are placed either near the source or in the neutron guide hall. The average neutron flux at SINQ is comparable to the flux at a medium power nuclear reactor.

The IBR-2 reactor, operational since 1984, has a PuO_2 active core as a normal nuclear reactor does; however, neutrons are periodically produced in pulsed mode. Thus, the IBR-2 combines a high average power, as at a steady state reactor, and a pulsed mode of operation, like a pulsed spallation type source.

Its nominal parameters are 2 MW average power and 5 Hz pulse frequency with fast neutrons having a pulse duration of 215 μs. The active core is surrounded by water moderators, after passing through which the width of the thermal and cold neutron pulse is approximately 350 μs. The total average neutron flux from the moderator surface is about 10^{13} $cm^{-2} \cdot s^{-1}$. The pulse power and pulse flux are very high, amounting to 1.4 GW and 10^{16} $cm^{-2} \cdot s^{-1}$, respectively.

3.1.5. Two types of stress diffractometers

All neutron scattering techniques, including diffraction for stress analysis, can be realized successfully at both steady state and pulsed neutron sources. At the latter, all spectrometers operate with a continuous (white) neutron spectrum and the TOF technique is used for energy or wavelength scanning. The majority of the spectrometers at steady state sources operate with a monochromatic incident beam, though sometimes mechanical choppers are used for creating a pulsed regime with TOF analysis.

In accordance with the source type, two main modes for neutron diffraction experiments are considered (Fig. 3):

— Monochromatic incident beam; the diffraction pattern is a function of the scattering angle.
— Continuous incident spectrum; the diffraction pattern is a function of the TOF.

Examples of strain diffractometers with a monochromatic incident beam are STRESS-SPEC (FRM II), SALSA (ILL) and E3 (HZB). The TOF mode is used at ENGIN-X (ISIS), SMARTS (LANSCE) and VULCAN (SNS). The strain diffractmeters pulse overlap diffractometer (POLDI) at SINQ, Fourier stress diffractometer (FSD) and high resolution Fourier diffractometer (HFRD) at IBR-2 are special cases. They are TOF instruments but with a correlation method of data acquisition, which provides a better relation between intensity and resolution.

An advantage of TOF instruments is that texture information on several peaks can be measured simultaneously. As a rule, strain diffractometers with monochromatic incident beams are optimized for the collection of diffraction patterns over a short range of scattering angles, ideally close to $2\theta = 90°$, which only includes 1–2 diffraction lines; however, measurements can also be made very quickly (for instance by using the pyrolytic graphite monochromator of the STRESS-SPEC diffractometer of the FRM II, which has a flux of 1×10^{-8} $cm^{-2} \cdot s^{-1}$). Also, a new continuous texture measurement method has been developed by Christian Randau at the Helmholtz Zentrum Berlin (HZB) and FRM II [20], which allows the inclusion of all the grain reflections from

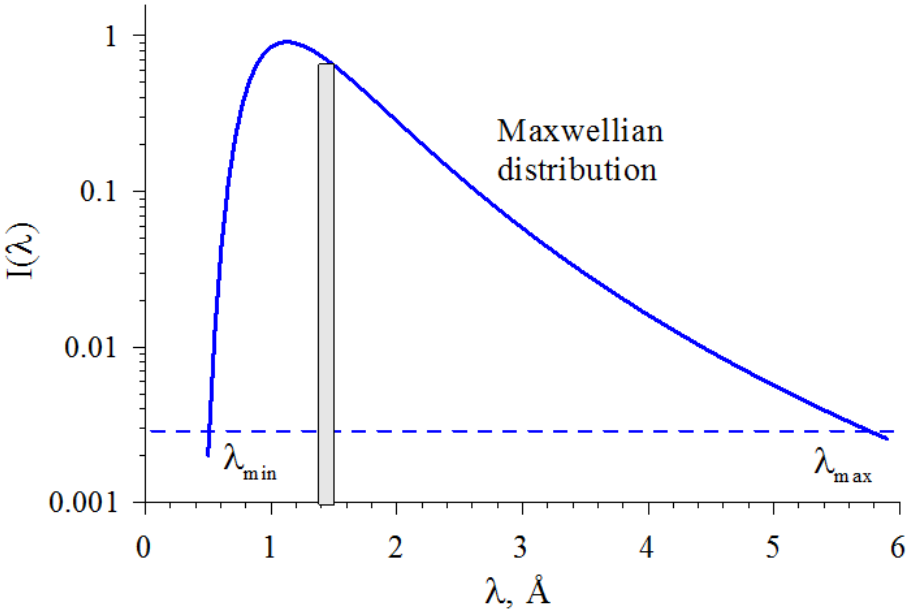

FIG. 3. At all neutron sources a 'white' wavelength distribution is produced. At a steady state reactor, as a rule, the monochromatic neutron beam is formed (shown as a narrow strip). At a pulsed neutron source, the continuous incident spectrum is used. The limits λ_{min} and λ_{max} are selected in accordance with the intensity arguments.

a polycrystalline sample into a number of scan steps which are captured on the detector without discretization. A specially developed software called STRESS-TEX [21] processes the measured data.

The total neutron flux at a TOF diffractometer is comparable with the monochromatic flux at a conventional diffractometer, but the intensities of the individual peaks are much lower owing to spectrum distribution over the wide wavelength range. The positive consequences of a continuous spectrum are nevertheless important: in parallel with the measurement of strains, an estimation of texture and anisotropy effects is possible and the analysis of multiphase materials is straightforward. Because a complete diffraction pattern is recorded with a TOF diffractometer, it is natural to fit the entire diffraction spectrum using a Rietveld refinement.

On the whole, both types of strain diffractometers should not be considered as alternative, but rather as complementary instruments. Correspondingly, depending on a particular problem, an experiment at a diffractometer must be planned either with a monochromatic diffractor or with a continuous spectrum. Moreover, some complicated tasks can be properly solved if the experiment is realized at both types of strain diffractometers.

3.2. TYPES OF INSTRUMENTS

A typical set-up of a monochromatic instrument for strain measurement at a steady state source is shown in Fig. 4. The 'white' neutron beam is monochromated to the desired wavelength (close to Maxwellian) using a suitable monochromator. Today, double-focusing bent silicon crystals represent the state of the art because of their superior combination of resolution and intensity. The monochromatic beam is subsequently shaped by beam defining optics such as slits or collimators to produce a beam of controlled dimensions. This beam is then diffracted from the specimen as a Debye-Scherrer cone and partially captured by a neutron detector. An example of a diffraction peak from a monochromatic instrument is shown in Fig. 5.

TOF diffractometers are typically used at pulsed sources, where each pulse provides a diffraction profile across a large range of lattice spacings. A typical TOF diffractometer used at a pulsed source for strain measurement in two directions simultaneously is shown in Fig. 6. As a fixed scattering angle is used, most instruments at spallation sources use radial (focusing) collimation. This allows neutrons to be detected over a wider solid angle than would be possible using a slit, yet ensures that most of the detected neutrons come from a defined gauge volume. The signals from the individual elements of the detector array are combined, taking into account their different angular positions. Two or more detectors with radial collimators can be used to enable more than one $\boldsymbol{Q}$ (strain) direction to be measured simultaneously. A typical diffraction pattern from such an instrument is shown in Fig. 6, right, which also shows the result of a Rietveld profile refinement where a crystallographic model of the structure is fitted to the diffraction data using least squares analysis.

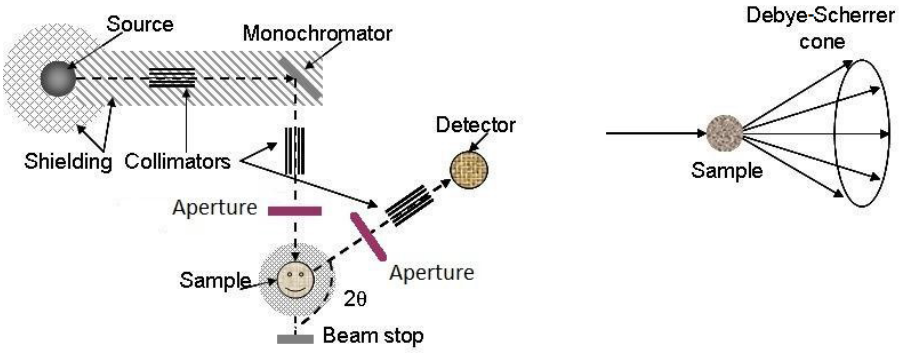

FIG. 4. Schematic illustration of a steady state source based diffractometer for strain measurement.

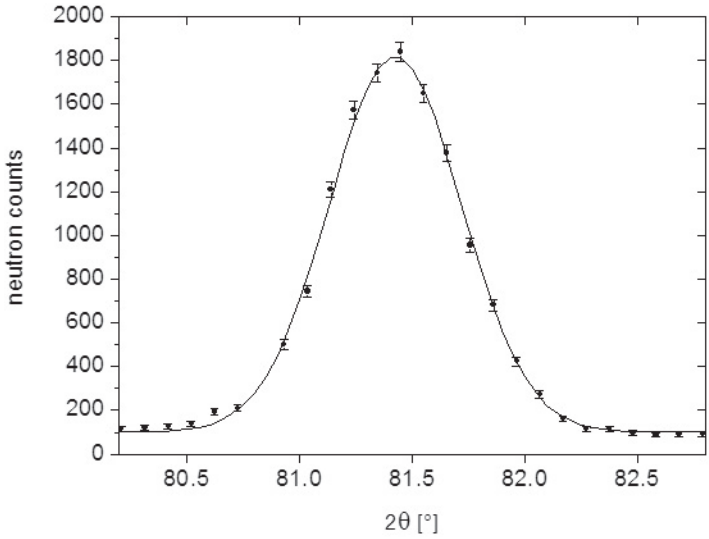

FIG. 5. Diffraction peak recorded at the High Flux Reactor in the Netherlands, presented in combination with a Gaussian fit of the neutron data.

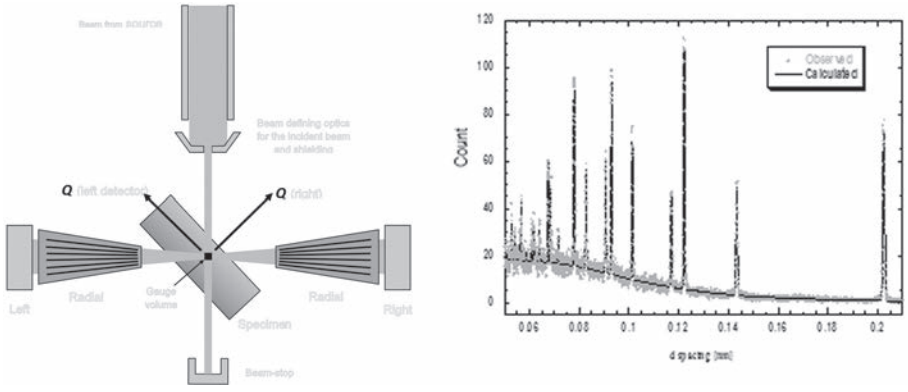

FIG. 6. Left: Schematic of a TOF diffractometer [3]. Right: TOF diffraction pattern as measured in each of the two detectors.

An overview of the neutron diffraction facilities for residual stress measurement currently in operation is provided in Annex II. In addition, the authors of the present report have provided detailed information on the instruments at their home institutions. These details can also be found in Annex II.

3.3. STANDARD EQUIPMENT

3.3.1. Introduction

In this section, an overview is provided of the standard equipment that is now used when measurements of stress/strain are made by neutron diffraction. This only comprises the necessary elements for simple measurements: the neutron source and moderators, beam tubes and neutron guides for the transport of neutrons from the source to the instrument, beam conditioning equipment for collimation and wavelength selection, beam defining optics, sample positioning stages, neutron detectors and data acquisition systems. Ancillary equipment, for example, to facilitate measurements at elevated temperatures or under applied loads, is covered in Section 3.8. Furthermore, the postprocessing of measured data is not addressed here, as it is at least partially described in other sections.

The neutron diffraction technique for residual stress measurement is still relatively young. An overview of its early history can be found in Ref. [22]. The possibility of applying neutron diffraction for strain measurement was first considered in the middle of the 1970s in the USA. The first journal article on neutron strain measurements was only published in the early 1980s by a UK based group [23]. X ray diffraction had been used for stress analysis and neutron powder diffraction decades earlier. The first neutron diffractometers used for strain analysis were derived from those used in powder diffraction facilities. In principle, there are only two points in which diffractometers for the measurement of residual stresses distinguish themselves from powder diffractometers: (a) the sampling volume, i.e. the volume in space from which scattered neutrons reach the detector needs to be carefully selected for residual stress analysis by means of beam defining optics in the incident and diffracted beams, and (b) a sample positioning stage facilitating the change both of the location of the sampling volume and of the orientation of the scattering vector with respect to the sample. The equipment necessary to address these requirements could simply be added to typical powder diffractometer set-ups and in the earliest days of neutron strain scanning this was often done.

Since the early 1980s, the design of residual stress diffractometers has improved. The arrival of position sensitive detectors and multidetectors allowed the simultaneous measurement of complete diffraction peaks, while dedicated instrument design facilitated the optimization of incident beam optics for stress measurement (e.g. second order filtering is now not always required, dedicated monochromators were developed, beam focusing was made possible) and manipulation tables for heavy samples with extended ranges of translation facilitated investigations of large engineering components. The introduction of TOF methods in the early 1990s, e.g. at pulsed spallation sources, gave access to

simultaneous observation and analysis of complete diffraction spectra, allowing new insights into the response of materials to mechanical loads.

The elements described in the following sections are common to the majority, or even to all of the neutron diffractometers for residual stress analysis operating in the world today. Where possible, some attention is also given to special equipment existing at individual facilities fulfilling similar functions.

3.3.2. The neutron source and neutron moderation

The topic of neutron sources has already been covered in Section 3.1. Only a few points will therefore be reiterated here. Nowadays two types of neutron sources are suitable for this application: nuclear reactors and spallation sources, as described above. Only these types of sources can currently provide the neutron fluxes required for neutron scattering applications such as strain analysis. It must also be kept in mind that (quasi) parallel beams of neutrons are needed at a distance from the source (mostly in the range 5–50 m) for experiments involving neutron scattering.

After fission or spallation, neutrons are characterized by their high kinetic energy, which is normally in the MeV range. These neutrons are called fast neutrons. For the measurement of strains and stresses by diffraction, neutrons with wavelengths similar to the lattice spacings under investigation are needed. For most crystalline materials of engineering relevance, this range of lattice spacings is 0.1–0.4 nm. In accordance with the de Broglie principle [24], suitable neutron energies for strain measurements are in the meV range. Neutrons in the energy range of up to about 100 meV are called thermal neutrons. The process of transferring the neutrons from fast to thermal energy levels is called moderation. This requires the interaction of the neutrons with matter at a particular temperature, so that the average temperature of the neutrons shifts towards the temperature of the medium they are interacting with. The excess energy of the neutrons is thereby transferred to the surrounding material. Materials containing hydrogen, deuterium or both are the most efficient moderator materials for this purpose. The principle is described in Section 3.1.3. The most commonly used moderator materials are water and heavy water at reactor sources and liquid methane at spallation sources. Liquid hydrogen and liquid deuterium moderators are rarely used for strain measurement installations as they generate neutrons with overly long wavelengths.

3.3.3. Transfer of neutrons from the source to the facility

As stated in the previous subsection, a diffractometer for stress analysis is typically located at a considerable distance from the source. There are two main

reasons for this. The first reason is to provide radiation protection, both for the experimenter and for the experiment itself, e.g. sample activation and reduction of measurement background. The second reason is that it would be difficult to provide a relatively parallel beam of neutrons at facilities in close proximity to the source.

Beam ports, beam tubes and neutron guides facilitate the travel of neutrons from the source to the diffraction facility. Beam ports in the context of this description are simply holes in the biological shielding of the source in order to facilitate neutrons reaching experimental installations outside of the biological shield in sufficient amounts.

A neutron beam tube is basically a rather straight tube. Its main function is to facilitate relatively undisturbed travel of neutrons from the source to the instrument. For this purpose, the beam tube must begin close to the neutron source and will ideally end close to the facility. Within the tube, the amount of neutron–matter interaction has to be limited so that a good fraction of the neutrons entering the tube at the source can reach the facility. For this purpose, the tube should be filled with a gas; air is a possibility, as is helium, the latter having significantly less interaction with the neutrons.

In common with any other radiation emanating from a point source, the flux of a neutron beam decreases at a $1/r^2$ relationship to the distance from the source. In order to facilitate the installation of instruments at large distances from the source in spite of this rule, neutron beams have to be transported through neutron guides. Neutron guides are narrow beam tubes with interior wall coatings that reflect neutrons under certain conditions [25], i.e. the travel of such neutrons can be contained within these guides and much lower losses of flux than in accordance with the $1/r^2$ relationship can be achieved for these neutrons. In fact, low energy (cold) neutrons can be transported over tens of metres with virtually no loss in flux (provided that the guide is either under vacuum or filled with helium).

Neutron reflection on such coated surfaces is subject to certain conditions. The impinging angle of the neutron has to be small; how small depends on the neutron energy and the type of coating. Relatively low neutron energy is also required, but coatings for guides for thermal neutrons are available, albeit with a somewhat lower reflectivity and therefore a higher rate of loss in flux.

These conditions, which on the one hand make the application of neutron guides complicated and expensive, on the other hand provide a significant additional advantage for neutron guides. They can be used to suppress the background of high energy neutrons and gammas at the instruments. For this purpose, curved guides are constructed with high radii of curvature. While low energy neutrons — subject to reflection at the inner surfaces — are contained within the curved guide tube, fast neutrons and gammas are not reflected at the

guide walls; therefore, they leave the guide following a straight line and can be absorbed in the biological shielding surrounding the guide without reaching the experimental facilities.

3.3.4. Beam conditioning: Collimation–monochromatization

3.3.4.1. Collimating elements

Collimation of the neutron beam is necessary to ensure that the beam reaching the specimen or the monochromator is sufficiently parallel or that the sampling volume seen by a particular element of the neutron detector is sufficiently small, or both.

This can be achieved by linear collimators in the incident or diffracted beams, but also by radial collimators focusing on the location of measurement.

Such collimators are normally arrangements of foils coated with a neutron absorbing material so that the travel of neutrons is only possible through the gaps between the foils. This limits the angular divergence of the neutron beam passing through the collimator. The arrangement of the foils can be parallel to each other or in a radial configuration. The beam divergence admissible depends on the spacing between the foils and their length in the direction of the beam. The more the beam divergence is limited by a collimator, the lower the neutron flux that can be transmitted through it.

In many cases, the collimation given by the geometry of the instrument suffices, and no dedicated collimation equipment is necessary for the successful execution of stress measurements. This can be true for the incident and the diffracted beams. For example, an effective monochromator width of 50 mm and a beam opening of 2 mm close to the specimen, at 2.5 m from the monochromator, will already render an angular range of admissible neutron flight paths of only ±0.6°, which is sufficient for the execution of stress measurements without using extra equipment for beam collimation. For other configurations, the use of collimating elements can be necessary, for example, when the distance between the monochromator and the measurement location is relatively short. Also, in a case where a single wire neutron detector of several cm width is used, it might be necessary to install a monochromator in the diffracted beam in order to achieve the angular and spatial resolution required for the measurement.

At many beamlines, in-pile collimators are installed in the beam tubes relatively close to the source in order to reduce the beam divergence further away from the instrument itself. These contribute more to a reduction of the measurement background rather than to the angular or spatial resolution of the measurement.

3.3.4.2. Monochromatization — wavelength determination

Figure 6 in Section 3.1.5 illustrates the beam intensity distribution in a typical neutron beam emanating from a thermal moderator at a steady state source. With a neutron beam containing this spectrum of neutron energies impinging onto the specimen, it would not be possible to obtain distinguishable diffraction peaks. For this reason, the following techniques are applied:

— At most steady state source based instruments the neutron beam is monochromatized by means of single crystal or highly orientated polycrystal monochromators. This leads to a neutron beam with a narrow band of neutron wavelengths being directed to the specimen (see Fig. 3 in Section 3.1.5) and the response of one chosen set of lattice planes (*hkl*) is studied in the experiment.
— At pulsed sources, the flight time of neutrons between the source and the neutron detector is measured in addition to the location where the neutron is registered on the detector. This measurement of neutron travel time (TOF) can either be facilitated through the use of narrow neutron pulses (narrow both in terms of their length in time and their velocity spread) or through the installation of rotating choppers in the incident beam in order to establish a starting point in time and space for the travel of the neutrons.

Through this TOF technique, which is also described in other sections, measurements with a white neutron beam are possible and multipeak diffraction spectra are obtained, as opposed to the monochromatic instruments where measurements are mostly based on a single diffraction peak.

3.3.5. Equipment for the definition of the sampled gauge volume

In neutron diffraction stress measurements, it is important that the signal is obtained from a defined volume in space that contains part of the specimen material. This is achieved by placing beam defining apertures for the incident and diffracted beams, either in the form of slits, or in the form of radial collimators. The simplified sketch in Fig. 7 illustrates how a sampling volume is defined through apertures (in this case, slits) placed in the incident and diffracted beams. The intersection of the thus defined incident and diffracted beams is called the sampling volume or the gauge volume. The signal recorded on the detector in neutron strain and stress measurements originates from this volume.

Beam defining equipment, i.e. slits or radial collimators, is manufactured from materials with a very high absorption cross-section for thermal neutrons. There are four elements with isotopes with such a high cross-section: gadolinium,

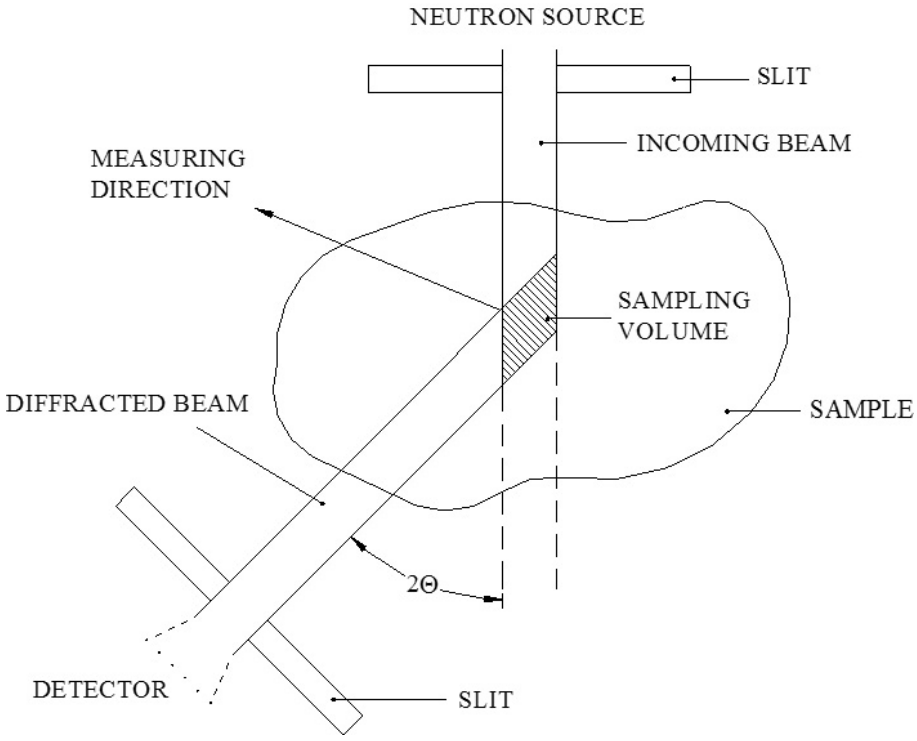

FIG. 7. Simplified representation of the definition of the sampling volume within a specimen through the intersection of the incident and diffracted neutron beams. The beam defining apertures are indicated as slits, but radial collimators can also be used for bean definition.

cadmium, boron and lithium [26]. For collimators, in most cases, materials containing gadolinium are applied because the high absorption of gadolinium allows the use of thin layers, thus reducing 'dead' area. For slits, cadmium is often used, with which a thickness of 1–2 mm is usually sufficient. Also, cadmium can be cut, bent and formed easily. An obvious disadvantage is the high toxicity of cadmium, and, where this constitutes a problem, alternative materials such as boron nitride or boron carbide can be used to manufacture slits.

The ISO technical specification [3] for the method for stress determination by neutron diffraction introduces three definitions for the sampling volume. These refer to the nominal gauge volume, the instrumental gauge volume and the sampled gauge volume.

The sampling volume depicted in Fig. 7 corresponds to the nominal gauge volume. This definition is based on the simplifying assumption of non-diverging parallel beams with sharp edges defined by the beam apertures, and the size of the nominal gauge volume is given by the openings provided through the

apertures installed and the diffraction angle. In most cases, experimenters refer to this nominal gauge volume when specifying the sampling volume size for a given experiment.

In reality, a neutron beam will be characterized by a flux distribution across the beam and an angular divergence of the beam. This results in the sampling volume being different from the nominal gauge volume. Normally, there is a gradually decreasing neutron intensity around the edges, and because of the beam divergence, the volumetric extent of the sampling volume is usually larger than the nominal gauge volume would indicate. This 'real' sampling volume is defined as the instrumental gauge volume. The term sampled gauge volume refers to a situation where the instrumental gauge volume is not completely filled by the material under investigation. This special case is not discussed here.

The discussion of the different sampling volume definitions should help the reader to understand two important differences between the use of slits and radial collimators as beam defining equipment.

Figure 8 illustrates the definition of a sampling volume through slits. Figure 8(a) shows the idealized situation where non-diverging beams define the nominal gauge volume, whereas Fig. 8(b) shows exactly the same situation, but with diverging neutron beams. It can be seen that the spatial extent of the instrumental gauge volume in Fig. 8(b) is larger than that of the nominal gauge volume. The consequence of this is that the beam defining apertures, i.e. the front opening of the slits, have to be placed as close as possible to the location of the sampling volume. Otherwise, with a larger distance the instrumental gauge volume becomes larger because of the beam divergence and the spatial resolution of the measurement is compromised.

The use of radial collimators is shown in Fig. 9. Radial collimators for both the incident and the diffracted neutron beam are positioned such that the gauge volume is located at the focal distance that corresponds to their geometries. The effect of beam divergence is limited because the sampling volume is located at the narrowest point of the diverging beams. At the same time, radial collimators can be positioned at a much greater distance from the sampling volume than slits, so more space is available for specimen translation or rotation. This can be important when measurements are performed on large specimens or on specimens with an irregular shape. Additional effects associated with the use of radial collimators in neutron strain measurements have been analysed by Pirling [27].

At most monochromatic instruments, slits are used nowadays for the sampling volume definition. Nevertheless, radial collimators are becoming more popular and are used on a regular basis at the stress measurement facilities at ILL (SALSA), HZB (E3) and FRM II (STRESS-SPEC). For TOF instruments, it is normal practice that radial collimators are used in front of the detector systems.

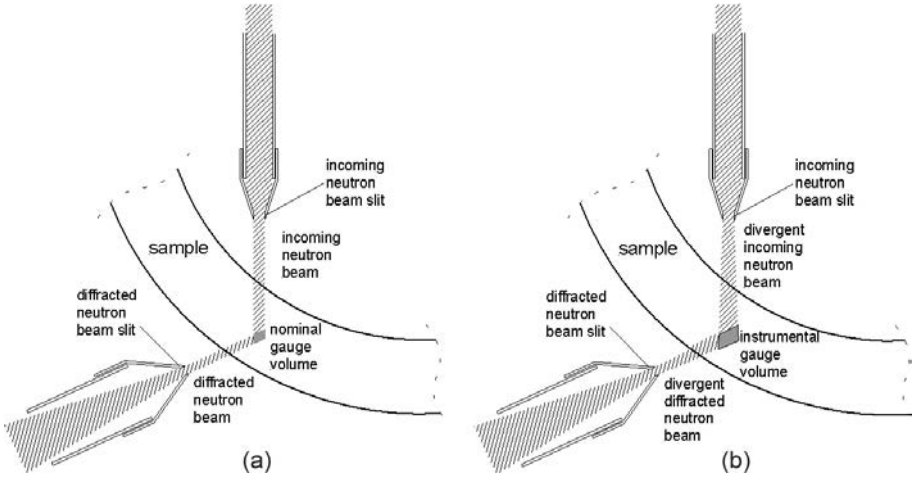

FIG. 8. Illustration of 'nominal' and 'instrumental' gauge volumes as generated by slits in the incoming and diffracted neutron beams: (a) nominal gauge volume, based on the assumption of non-diverging incoming and diffracted neutron beams; (b) instrumental gauge volume, reflecting the more realistic situation of diverging neutron beams.

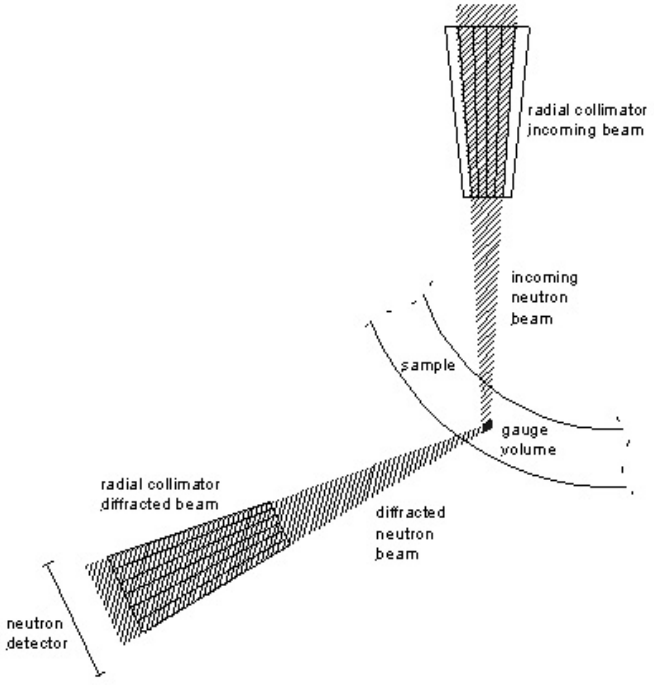

FIG. 9. Illustration of sampling volume as generated by radial collimators in the incident and diffracted neutron beams.

3.3.6. Specimen positioning table

Positioning table assemblies are an important element of neutron diffraction stress measurement facilities. Figure 10 illustrates, in a simple way, why sample positioning assemblies are necessary. In most stress investigations, the objective is to measure the distribution of stresses within the specimen. Consequently, measurements have to be obtained from different locations within the specimen. Hence, a specimen positioning table is needed to change the location of the sampling volume within the specimen (Fig. 10(b)). Furthermore, in accordance with Eq. (4) in Section 5.2.2 and Eq. (5) in Section 5.2.3, measurements of strain have to be obtained in different directions at each location of measurement in order to facilitate the calculation of stresses. Hence, a specimen rotation table is needed to change the orientation of the specimen with respect to the incident and diffracted neutron beams (Fig. 10(c)).

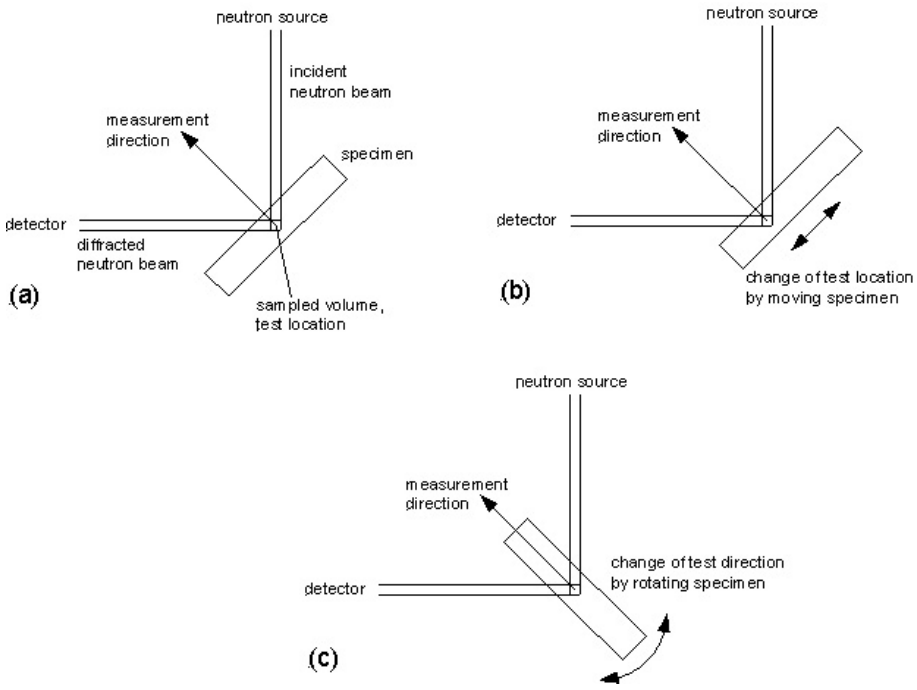

FIG. 10. Schematic illustration of the function of sample positioning equipment in neutron diffraction stress measurements: (a) Basic set-up of a measurement; average lattice spacing is measured over the sampling volume that is positioned at the location of interest, the test location within the specimen, in a direction normal to the long side of the specimen; (b) in order to change the test location, the specimen is moved with respect to the neutron beams; (c) in order to change the measurement direction, the specimen is rotated.

A corresponding assembly of positioning and rotation stages facilitates linear specimen translation along three mutually orthogonal axes (called x, y and z by most experimenters), and specimen rotation about at least one axis through the centre of the sampling volume. At most instruments, a horizontal stage, i.e. with a vertical axis of rotation, is installed. Figure 11 depicts a typical existing sample positioning stage. The linear stages for positioning in the x and y directions can be clearly seen, as can the sample rotation stage underneath.

Different facilities have different capabilities in terms of weight capacity and movement ranges. The assembly design has a significant impact on what a diffractometer for neutron stress measurements can accomplish.

Linear movement ranges are typically in the range 50–500 mm, with a resolution of 0.01 mm easily available with modern positioning equipment. The equipment shown in Fig. 11 has a linear movement range of 250 mm in the x, y and z directions. The range of rotation is often larger than 270° with a stepping resolution of 0.01° or better.

FIG. 11. Specimen positioning and rotation assembly as installed at the HFR in Petten, the Netherlands.

Every component must be able to carry and position the weight of the specimen and the ancillary equipment that might be installed together with the specimen. There are currently instruments available that can position specimen assemblies of one or several thousand kg (for example at PSI, ILL, RAL, LANL, ORNL and the Joint Research Centre). A small weight capacity, but in particular a small range of linear movement (100 mm or less), constitutes a substantial limitation to the application for stress measurements in engineering components. One has to concede that it is complicated to design an instrument with large movement ranges because of the size of the equipment necessary.

In addition to the positioning equipment described above, which is available in one form or another at all instruments, some facilities have Eulerian cradles that can be mounted on the specimen positioning stage. Figure 12 shows an Eulerian cradle that is available at instrument E3 at the BER-II reactor in Berlin. This device enables the experimenter to select more specimen orientations than would be available with the standard equipment described above, where only one rotation axis is possible. An Eulerian cradle provides two additional rotation axes. This is very useful for full stress tensor determination based on Eq. (5) in Section 5.2.3, where strain measurements in at least six independent orientations are necessary.

3.3.7. Neutron detectors

Neutron detectors sample the neutrons diffracted from the specimen under investigation. They are located at a given distance from the sampling volume at the diffraction angle chosen for the particular measurement. The preferred diffraction angles for residual stress analysis by neutron diffraction are as close as possible to 90° and preferably not outside the range 60°–120°. This requirement is related to the geometries shown in Figs 7–9. When the measurement angle is too far from 90°, the sampling volume becomes skewed and its diagonals very different from each other. The sampling volumes for different testing directions then occupy to a large degree different parts of the specimen material, hence compromising the reliability of three dimensional stress measurement. In addition, the neutron path through the specimen material becomes very long in at least one of the test directions with such measurement angles.

Various detector types can be applied, but the most common for this application are gas proportional detectors and scintillator arrangements. Gas proportional detectors for neutrons function in a similar way to Geiger counters for other types of ionizing radiation. However, the neutrons themselves do not ionize the medium they travel through. Therefore, gases containing isotopes that react with neutrons are needed. Helium-3 and BF_3 are the gases most commonly used for this.

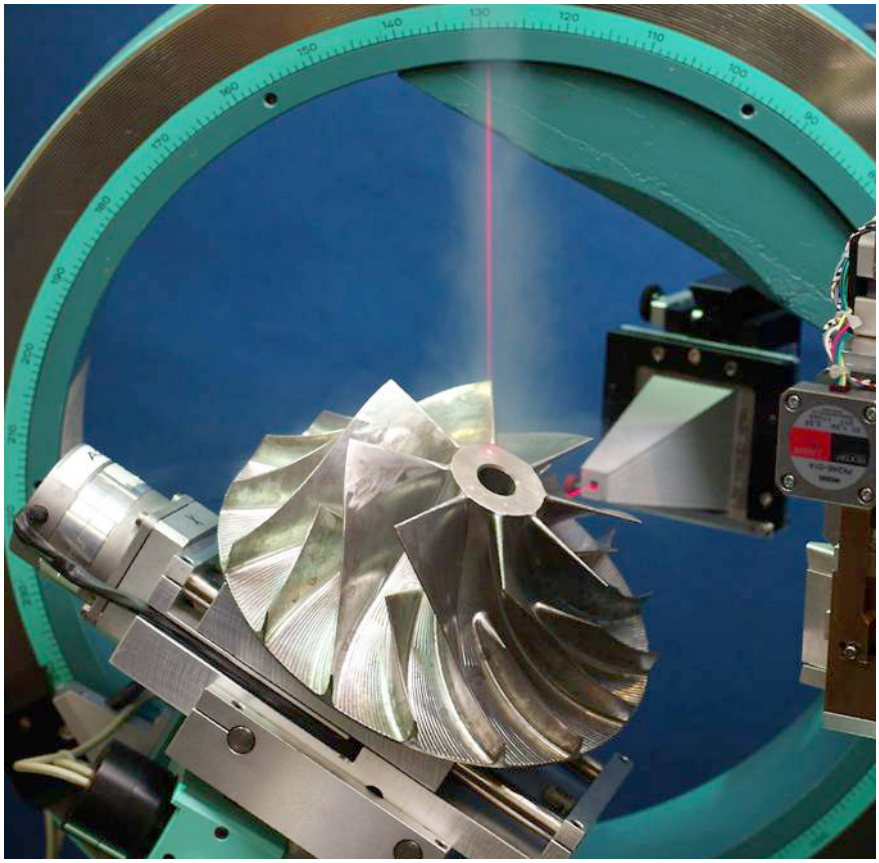

FIG. 12. Eulerian cradle carrying an impeller wheel at the E3 diffractometer at HZB Berlin.

The following nuclear reaction takes place in ^{3}He:

$$^{1}n + {}^{3}He \rightarrow {}^{1}H + {}^{3}H + 0.764\ MeV$$

and in ^{10}B:

$$^{1}n + {}^{10}B \rightarrow [{}^{11}B] \rightarrow \alpha + {}^{7}Li + 2.31\ MeV$$

Accordingly, the interaction results in the emission of highly energetic charged particles that can be readily detected in a high voltage chamber.

It should be mentioned here that there is currently a world shortage of ^{3}He [28] and alternatives are starting to be used, for instance, BF_3. However ^{10}B has a smaller thermal neutron cross-section of 3840 b, making it less

sensitive to detection than ^{3}He, which has an absorption cross-section of 5330 b for thermal neutrons.

Other alternatives to ^{3}He are scintillation detectors based on materials (e.g. ^{6}Li) producing flashes of light upon reaction with neutrons. Various types of material are available for this. Event detection is facilitated by the use of photomultipliers or photodiodes. Scintillation detectors have long been used in particular at TOF facilities because of the spatial resolution they offer, which is not achievable with gas detectors.

It is currently common practice for ^{3}He detectors to also be position sensitive covering one or several complete diffraction peaks in a single measurement. Position sensitive detectors can simultaneously record neutrons impinging at different angular positions. In the past, measurements were performed by scanning a single wire detector across the diffraction peaks in sequential steps.

Spatial resolutions that can be obtained in a position sensitive gas detector are normally in the range of one to several mm. Figure 5 shows a diffraction peak recorded at a monochromatic instrument with a position sensitive detector. The spatial resolution of this particular detector was 2 mm, and the detector was set up in such a way that the angular spacing between neighbouring bins was 0.1°.

At some instruments (e.g. SALSA at ILL or E3 at HZB), the detectors used are position sensitive in two dimensions; this permits visualization of grain size effects and the umbrella effect [29] for scattering angles deviating strongly from 90°. With this information available, such effects can be taken into account in data analysis or setting up the measurement procedure. Two dimensional detectors with sensitive areas as big as 30 cm × 30 cm are installed at some steady state facilities. The detector arrays installed at TOF instruments based at spallation sources are often even larger than this. With such large detectors, more neutrons can be collected to contribute to measurement sensitivity and better counting statistics. On the other hand, a large detector collects neutrons from a wide range of scattering angles, which is only acceptable in stress measurement within certain limits. A range of ±10° to ±15° for the opening angle of the neutron detector is considered acceptable.

The major difference between monochromatic and TOF instruments is normally that the flight time of the neutrons is recorded in addition to the angle of scattering. Consequently, at a TOF instrument the entire detector surface contributes to the diffraction signal, while at a steady state instrument only the detector area covered by the diffraction peak contributes. TOF instruments record the entire diffraction pattern from the specimen while monochromatic instruments measure only one or two peaks simultaneously.

When the instrument is located at a limited distance from the neutron source, e.g. less than 10 m, it is normally necessary to place the neutron detector inside a shielding cavity in order to reduce the background of neutrons not

associated with the experiment that would otherwise be recorded by the detector. Such a shielding can comprise a thick layer of plastic, e.g. polyethylene, for thermalizing the fast neutrons, and a thinner layer of a neutron absorbing material, i.e. a material containing neutron absorbers such as lithium, boron, cadmium or gadolinium. In this case, plastics containing added boron compounds are often used. The shielding provides a small opening for neutrons to reach the detector only from the direction of the sampling volume.

3.3.8. Data acquisition

The registration of a neutron event by a neutron detector delivers an electronic pulse to the data acquisition system that should be connected at this point of the measurement chain. The data acquisition system provides for pulse discrimination to separate recorded events not associated with neutrons from those caused by the neutrons passing through the detector. The neutron events are counted and the counts are registered together with the position on the detector where the neutrons were detected. This process renders a record of a distribution of neutron counts over the detector, see for example Fig. 5.

Various systems fulfilling the described function have been put in place at different facilities. In most cases, data acquisition is embedded in a fully automated measurement system providing for programmable measurement sequences of sample positioning and recording of neutron counts. In some cases, novel systems even foresee intermittent data analysis leading to the automatic adaptation of measurement programs without the need for operator interference.

3.4. INSTRUMENT COMMISSIONING AND BENCHMARKING

Although the methodology involved in continuous beam and pulsed beam instruments differ, many of the instrumental components are the same. The first step in performing diffraction at a reactor based source is to narrow the beam to a selected band of wavelengths. This is typically accomplished with single crystal monochromators. The monochromatic beam scatters from the sample with sharp peaks as dictated by Bragg's law. Either a linear or scanning point detector is used to collect the diffracted neutrons. A pulsed source allows the use of the TOF technique employing white radiation for diffraction because of the dependence of the neutron velocity on wavelength. A short pulse (in the μsec range) with a broad energy spectrum leaves the moderator at time $t = 0$. As the pulse travels towards the sample, it spreads out as higher energy (shorter wavelength) neutrons travel faster, reaching the sample and the detector sooner. Because a wide spectrum of neutrons is incident on the sample, a multipeak diffraction pattern is collected

simultaneously, which is an advantage over the monochromatic instruments. Further information on instrument commissioning and benchmarking can be found in Ref. [3].

The aim of using a neutron strain scanner is to maximize useful intensity whilst maintaining the required instrumental resolution. In the instrumental set-up, the monochromatic wavelength will ideally be selectable to render a detector angle close to 90° at which the gauge volume shape is most symmetrical (i.e. cuboidal). This is easily achieved with a TOF instrument as the detector angles can be permanently set at +90° and −90° irrespective of the material being investigated. With a constant wavelength instrument, this can only be achieved with a variable monochromator take-off angle. With the tuning of the monochromator take-off angle it becomes possible to investigate different materials close to the 90° gauge volume geometry. Alternatively, a compromise set-up may be used, for example using a Si(331) monochromator at 83.5° take-off giving a wavelength of 1.67×10^{-1} nm. This puts the 211 α-Fe, 311 γ-Fe and 311 Al reflections within ±10° of the 90° optimum geometry. Adherence to this condition is not essential but should be striven for within the capabilities of the facility configuration.

3.4.1. Minimization of radiation background levels

It is normally the background radiation levels that limit the maximum depth to which materials can be probed. Shielding is best achieved as close to the neutron source as possible. In general, every set of measurements should be preceded by checks that the background from the monochromator chamber and the beam paths are minimized by absorbing the unwanted beams as close as possible to the monochromator, and that only the desired beam cross-section impinges on the sample. An important check is to verify that when this beam is blocked, such as by inserting a high thermal neutron absorbing material (Cd or B) at the beam aperture position, no counts above background are recorded by the detector. Another useful check is to ensure that with no sample in the beam only the expected background level is measured.

3.4.2. Instrument axes and reference point

An accurate knowledge of the effective position in the sample at which the strain is measured is equally as important as the accurate measurement of strain itself. As well as the normal rotation of the sample table about a vertical axis, it is necessary to be able to translate the sample in three mutually perpendicular directions relative to the incident beam. Such an x–y–z translator should be able to position the sample in a repeatable way to better than 10% of the minimum

gauge volume dimension. This means to 0.1 mm for many cases, but even 0.01 mm if very fine gauge volumes are used. A positional error of 0.05 mm would give a strain error of 100 με if the strain gradient were 2000 με/mm.

The calibration of an instrument is described in Section 3.5. Calibration is essential for checking the consistency of measurements, for comparison between instruments and for the first set-up and commissioning of new machines. It also helps to reduce the measurement uncertainty.

As strain measurements are always made relative to a stress free sample, the wavelength and zero angle needn't be precisely known as long as they remain constant. However, it is recommended that the 2θ offset of the instrument should be known to much better than ±1°, ideally to ±0.1°, especially if measuring at 2θ angles much lower than 90°. It is essential that the instrument reference axis and beam reference height be aligned at the centre of the instrumental gauge volume, to which the position of the sample may also be referred. The usual convention is to use the axis about which the sample table and the detector arm rotates. The reference point on this axis is the centre of the incident beam height in the vertical direction. The gauge volume is then arranged to have this reference point as its centre by carefully positioning the apertures in the horizontal and vertical planes. One method is to first centre an accurately machined vertical pin on the sample rotation table so that its tip defines the reference point. This centring can be done by viewing the pin through a theodolite, or using a micrometre contact gauge and adjusting the position of the x–y translator until there is no movement of the tip while rotating the sample table omega axis through at least 180°.

3.4.3. Gauge volume

The size and shape of the gauge volume is defined by slits or radial collimators placed in the incident and diffracted beams (see Section 3.3.5). The angular divergence of the incident and diffracted beam and the wavelength spread of the incident beam give rise to a penumbra. In a sample filling the gauge volume, the effective gauge volume over which the average strain is measured is larger than the nominal gauge volume.

The gauge volume should ideally be aligned with the reference point of the instrument, i.e. with the vertical rotation axis of the specimen table. The best alignment source is to use the neutron beam itself to verify that the centre of the gauge volume coincides with the reference point by observing the diffraction from a cylindrical sample of diameter close to the aperture dimension, with its axis on the reference axis. With the detector at the correct scattering angle and the aperture wide open, the sample is tracked in position in a direction perpendicular to the diffracted beam, and the corresponding horizontal aperture position adjusted to ensure that the centre of the intensity profile versus the translator

position is at the encoder values corresponding to the reference axis position. If the aperture position is capable of being scanned, an alternative method is to centre the sample at the reference axis position and then scan each aperture position. The positioning in the vertical direction can be carried out in a similar fashion. Hereafter, the diffracted beam aperture is aligned by scanning the diffracted beam aperture set at the appropriate gauge volume size and positioning at the maximum intensity position.

The size of the instrumental gauge volume can be measured experimentally. The horizontal section may be measured by tracking through it a scattering medium of much smaller dimension using the x–y translation stage. Ideally, the scattering medium will be of the same material as the sample under measurement, for example, a thin wire, but the grain size must be relatively very small in order to diffract uniformly. The vertical dimension may be measured by using similar horizontal wires.

In TOF instruments, the gauge volume is defined by radial collimators rather than apertures. The alignment of radial collimators with the reference point can be made using a nylon thread, which scatters neutrons incoherently, first positioned on the reference axis, and then scanned in position along the incident beam. The collimators are adjusted to give maximum summed detector intensity when the thread is at the reference point. The positioning of the radial collimators and thus of the gauge volume is particularly important on a time pulsed source instrument, since any change in flight path may be interpreted as a strain.

3.4.4. Detectors

Linear and area position sensitive detectors are the most suitable choice for neutron strain scanners. Using any type of detector, it is important to ensure that the dead time after each detected neutron is short enough to not affect the accuracy of the measured count. The extreme condition is saturation when using intense beams such as during initial instrument alignments. The detector needs to be protected by using appropriate beam absorbers.

3.4.5. Instrumental resolution

The uncertainty in the determination of the angle of the Bragg reflection, or the uncertainty in timing of a detected neutron, determines the error in the measured strain. This needs to be determined to an accuracy of $\Delta d/d \sim 10^{-4}$. The measurement of Type I residual stresses is concerned with accurate measurement of the shift or difference in angle or time of the Bragg peak centre from that of the reference sample, rather than the absolute peak centre. A change Δd in the lattice spacing due to internal strains will result in a shift of a Bragg peak

position $\Delta\theta$ when a single wavelength is used. The shift of the peak positions is typically in the range of 0.005°−0.2°; thus, diffraction strain measurements are precision measurements and all components of the diffractometer are required to be sufficiently precise and stable. Since residual stress distributions are always inhomogeneous, precise and reproducible positioning of a sample in the beam is required. For this, the precision of the positioning devices has to be sufficient and appropriate sample positioning procedures have to be used.

Good instrumental resolution is important in the region of the diffraction angle because the uncertainty of the peak position determination is proportional to the full width at half maximum (FWHM) of the peak. The measurement of Type II and III residual stresses through the measurement of Bragg peak widths requires even better instrumental resolution.

3.4.6. Verification of instrument performance

Instrument performance should be verified using a real practical stress investigation such as benchmarking against well characterized samples. A good benchmarking sample is the ring and plug specimen [26] used in the VAMAS initiative that has been well characterized and which rendered very good correlation in positional accuracy and strain resolution between approximately 20 different laboratories. More challenging samples exist within the NeT programme [30]. A good way of judging the accuracy (as opposed to the precision) of a stress measurement is to assume an unknown tri-axial stress state on a sample with an independently known applied stress (e.g. through a load frame with calibrated load cell). The application of Eq. (4) allows the evaluation of the stresses from the measured strains.

3.4.7. Other relevant comments

Partially filled gauge volumes can give rise to serious errors in the measured scattering angle. It is therefore most effective to use fully submerged gauge volumes as far as possible. There are practical techniques to correct for partially submerged gauge volumes as described elsewhere in this report. One way of reducing the background and improving the definition of the gauge volume is to use a radial collimator.

A similar effect can be obtained by a large grain size of the material under investigation (see Section 3.6.7). In this case, the effect might be reduced by increasing the sampling volume or by specimen rocking during the measurement.

At scattering angles other than 90°, the curvature of the Debye-Scherrer cone sections is visible on area detectors and has to be taken into account when

integrating the intensity vertically. Detector channels have to be converted to angles.

The neutron wavelength has to be known with a high precision only when absolute lattice parameters are to be determined, which is normally not required for strain measurements. For the latter, only the difference between a sample peak position and the stress free reference peak position has to be determined with high precision. However, it is recommended that the 2θ offset of the instrument should be known to much better than ±1°, ideally to ±0.1°, especially if measuring at 2θ angles much lower than 90°.

3.5. INSTRUMENT ALIGNMENT AND CALIBRATION

3.5.1. Introduction

For residual stress measurement, the calibration and alignment of the instrument is important and the principles are similar for both angular dispersive and TOF techniques [3, 31]. It can be quite a time consuming procedure, and methods facilitating much faster alignment and calibration have been developed over the years. It is an area where automatization can also be implemented. In the future, it is envisioned that automatization, coupled with simultaneous simulation of the instrument, will allow a quick alignment and calibration suitable for the particular measurement about to take place.

The following sections provide an overview of the steps to be taken for the alignment and calibration of a residual stress diffractometer, irrespective of whether these processes are automated or not.

3.5.2. Calibration

Calibration of the instrument in relation to neutron diffraction strain measurement usually means determining the wavelength of the incident neutron beam and the angular response of the neutron detector accurately.

At a monochromatic source, the detector angular response and the wavelength are normally calibrated using a powder sample with a known and well defined lattice parameter, typically silicon, ceria, alumina or calcium fluoride. These materials are strong neutron scatterers with little intrinsic peak broadening. Repeated measurement on a reference sample is a method of quantifying the stability of the instrument settings and can be compared to the estimated fitting uncertainties. At TOF instruments, the same process is applied, but here the flight time recording of the detector banks needs to be calibrated, instead of the angular response.

At a TOF source it is additionally necessary to calibrate the detector efficiency as a function of wavelength. This is done using isotropic neutron scatterers with very weak or no diffraction peaks of their own, such as vanadium.

Another component of an instrument that should be calibrated from time to time is the movement of the sample positioning stage. In view of the importance of location in strain measurements, it is clearly necessary that the positioning equipment accurately executes the movements requested by the operator. Positioning tables tend to be mechanically quite stable so that frequent recalibration is not necessary. Care should be taken with older installations where spindles and bearings could be worn out.

Residual strain determination by neutron diffraction in most cases is based on relative measurements in accordance with

$$\varepsilon_{hkl} = \frac{\sin\theta_{0,hkl}}{\sin\theta_{hkl}} - 1 \tag{4}$$

for monochromatic instruments, and

$$\varepsilon_{hkl} = \frac{\Delta a_{hkl}}{a_{0,hkl}} \tag{5}$$

for TOF installations. Hereby θ is the observed Bragg angle and a is the lattice parameter obtained after profile refinement of the TOF spectrum.

As a consequence, it is also possible to obtain strain measurements of acceptable quality from instruments where the detector angular response and wavelength have not been calibrated. Doing this introduces an additional uncertainty in the measurement that needs to be considered correctly in the uncertainty analysis. A small error can have significant impact on the uncertainty of the strain measurement [32]. Therefore the detector position should be known to within ±1°, ideally to ±0.1°, especially if measuring at 2θ angles much lower than 90°. The measurement of lattice spacings in accordance with Bragg's law (Eq. (1) in Section 2.2.1) is absolute and must therefore be done on a fully calibrated instrument. Lattice spacings obtained from non-calibrated instruments should never be cited.

3.5.3. Alignment

Most components of an instrument need to be calibrated and aligned, some more often than others. This is especially important when an instrument is set up

for the first time and at the start of neutron beamtime cycles. Alignment should also be checked after accidental collisions of components during measurement (especially the neutron optics).

3.5.3.1. Sampling volume

In accordance with Ref. [3], it is good practice to position the centroid of the sampling volume at the reference point, i.e. the centre of rotation of the specimen table. This allows for easier changing of the measurement direction by simply rotating the specimen without any need for specimen realignment.

The alignment of the sampling volume with the centre of rotation is facilitated through readjustment of the beam defining apertures, either slits or radial collimators as described above. This type of alignment occurs on a regular basis as the sampling volume is often changed when a measurement series on a new specimen starts.

It is normally possible to position the centroid of the sampling volume to within 0.1 from the centre of rotation of the specimen table. Although this is a good accuracy to aim for, it can often be improved upon if needed. The level of accuracy required depends on the type of measurement being performed. The highest positioning accuracy is needed in the case of large strain gradients and where measurements are made close to surfaces. Several methods can be used to align the sample table and the neutron optics, such as using neutron intensity scans, optical instruments and neutron cameras.

3.5.3.2. Neutron monochromator, beam defining optics

Occasionally, in particular when monochromator settings are changed, it is necessary to realign the monochromator and collimators that may be placed in the incident beam, in order to obtain the highest possible neutron flux or the desired level of beam focusing at the measurement position.

3.5.3.3. Specimen positioning table

For specimen positioning, it is important that the movements of the specimen table are as intended. The horizontal movements should indeed be horizontal and the vertical should be vertical. The movement axes should be orientated orthogonally with respect to one other and their angle with the direction of the incident beam should be known. As the specimen table set-ups are mostly mechanically quite rigid, a realignment of the specimen table is not normally frequently performed.

3.6. MEASUREMENT PROCEDURES

3.6.1. Introduction

The execution of a series of stress and strain measurements by neutron diffraction involves a number of steps. These include mainly planning and preparation in view of the requirements for the measurements and the technical capabilities of the instrument, the setting up of the instrument, the mounting and aligning of the specimen(s), the execution of the actual measurement and the subsequent data analysis. In the following sections, detailed accounts are provided of the actions to be taken. Alignment and calibration of the instrument and data analysis are already covered in Section 3.5 and Section 5.

The final subsection contains information about dealing with grain size and surface effects. While these are not everyday occurrences in neutron diffraction strain measurements, they occur frequently enough to justify the inclusion of a brief section on these phenomena.

3.6.2. Measurement planning

Before a stress measurement is executed it is often helpful to carefully prepare the experiment. Whereas not every aspect of a measurement can always be fixed prior to its execution, careful consideration of the circumstances during preparation can result in an efficient measurement. Things to take into consideration are the size and shape of the specimen, the material of the specimen, the neutron wavelength at the instrument to be used, the total beam time available, the availability of reference material and, of course, the measurements that have been requested.

An area of interest within a specimen would be a region containing residual stresses of considerable magnitude and usually also considerable stress gradients (except for composition related stresses in composite materials). The measurement objective in most such cases is to determine the strains and stresses along one or several lines through that region of interest, or even across one or several planes in that region.

When the lines or areas of measurements have been identified, it should first be established whether the specimen can be positioned and orientated on the specimen table so that all the desired measurement positions can be reached for the necessary specimen orientations. For some positions and orientations, the specimen geometry can be prohibitive, for example in thick walled tubes or even in I-beams or T-junctions. It is also possible that the specimen is too thick for the neutron beam to penetrate it.

In a case where (part of the) measurements have been found to be impossible it may be necessary to cut into the specimen. Cutting alters the residual stress distribution within the specimen; hence, the cutting has to be planned so that the measurements become feasible, while the impact on the stresses to be measured is minimized.

In some cases, it can be useful to prepare dedicated specimen holders for mounting the specimen on the specimen table during the measurements. Such holders should be designed and built well in advance of the actual measurements.

As a next step, the instrument settings in terms of neutron wavelength (if changeable), sampling volume and diffraction angle are selected. The sampling volume is selected in accordance with the required measurement resolution, but also taking into account the time constraints that apply. A small sampling volume provides for a high spatial resolution, which is useful when measuring near interfaces or on high stress gradients; a larger sampling volume reduces measurement time and makes measurements in thick walled components feasible. The final choice is usually a compromise between these requirements. The scattering angle should be chosen in the vicinity of 90°. The choice depends on the neutron wavelength and the crystallographic lattice plane used for the measurement in accordance with Bragg's law.

The alignment and calibration of the instrument (see Section 3.5) should be performed in correspondence with the settings thus chosen for the measurements to be made.

In case dedicated reference specimens are needed, for example in the case of measurements in welds, these should also be designed and cut prior to the actual measurements. Even in a case where measurements have been well prepared, it can happen that adjustments to the scheduled measurement programme are necessary while measurements are ongoing. Such adjustments, while occurring at short notice, should still be undertaken with as careful planning as possible in order to minimize the losses of time involved.

3.6.3. Specimen handling

3.6.3.1. Main specimen

Although neutron diffraction is nominally a non-destructive method for the determination of residual stresses, it sometimes occurs that a specimen requires extra preparation prior to the measurements. Reasons for this could be a specimen size too big for the diffractometer, a wall thickness prohibitive for the penetration of neutrons, the need for auxiliary equipment for specimen mounting or handling, the optimization of the measurement process or the need for cutting a reference specimen from the stressed specimen itself.

As every neutron diffraction strain measurement is different from the next it is not possible to provide a universal instruction concerning the preparation of specimens. Hence, a few general remarks on items to be considered can be made.

All steps that might be necessary prior to measuring should be considered with care in the measurement planning phase. This is particularly the case when the specimen itself needs to be altered before the measurements. When the specimen needs to be cut for any of the reasons given above, the experimenter must always consider the possibility for changes in the stress field under investigation through the alterations applied.

The specimen, as stated above, needs to be prepared in such a way that measurements in all foreseen directions are subsequently feasible without the need for additional modifications.

Measures should be implemented in order to assess the magnitude of the stress changes (in the region of interest), e.g. through the monitoring of the (surface) strain evolution during cutting. It is advisable to apply the modifications as far as possible from the area where measurements are to be taken. Electrical discharge machining methods are often the most appropriate techniques for the machining process. Section 6.3 discusses an example of thick walled tubes where a window needed to be cut in order to facilitate neutron measurements in the circumferential direction [33]. In a similar case, the cutting was accompanied by strain gauge measurements on the specimen surface in order to demonstrate that the influence of the cutting on the stresses at the measurement location was negligible.

3.6.4. Reference specimen

The determination of strain and ultimately stress by neutron diffraction is critically dependent on the evaluation of the stress free lattice spacing $d_{0,hkl}$. Indeed, it often represents the largest uncertainty in residual stress measurements since there are many factors that may cause the strain free lattice spacing to vary in a specimen. Some of these, for example, local changes in alloy chemistry, can give rise to changes in lattice parameter greater than those that arise from the residual stress in the body. If unaccounted for, these can substantially reduce the accuracy of the stress measurement.

Interestingly, there is no requirement to measure a stress free lattice spacing. For example, if it is known that a component of stress is strictly zero, this may be used to circumvent the need for an accurate $d_{0,hkl}$ value. This boundary condition is used extensively in laboratory based X ray measurements of surface stresses, and forms the basis of the so-called $\sin^2 \psi$ technique (e.g. Ref. [34]).

Furthermore, if only the deviatoric stress is required, any referenced spacing can be used. The average of the three diagonal strain components (11, 22, 33) measured relative to this arbitrary reference can then be subtracted from the diagonal elements of the measured strain tensor to yield the traceless deviatoric strain tensor. Unfortunately, this is rarely of any practical value since most materials failure processes are driven by the non-deviatory parts of the stress tensor.

Presently, the most common ways of determining a stress free reference are:

— Stress free powder: Notwithstanding the need to ensure that a powder is really stress free, it also needs to be ensured that the powder is representative of the bulk as the powder may not have undergone the same thermomechanical treatment as the stressed material.
— Performing measurements in a stress free region of a component: Identification of a suitable area in the sample where d_0 has been verified to be independent of position and direction at that region in the material.
— Sectioning of the material: Fabrication of 'combs' or small coupons (cubes) cut from an identical companion component into small stress free regions by taking care that the cutting operation relaxes the residual macrostresses without introducing new residual stresses. Metals can often be electro-discharge machined. The coupon sizes need to be small enough so that the macrostresses are substantially relieved and that d_0 variations are captured sufficiently. This way the macroscopic stresses are relaxed and the d_0 value is accessible at the end of the comb teeth or from the cubes by ensuring full gauge volume submerging [3].
— Residual stress equilibrium: The component of stress perpendicular to any plane through the body must integrate to zero.

An excellent review of the most common methods of determining d_0 was produced by Withers et al. [35].

3.6.5. Specimen alignment

As stated in Section 3.6.2, the experimenter should plan where measurements of strain and stress are to be taken in a specimen. Reference [3] recommends the definition of one or several coordinate systems within the specimen. These facilitate the mathematical description and graphical representation of the measurement locations. The specimen coordinate axes should be aligned with at least one of the lines, along which locations of measurements are placed. In most practical cases, measurement locations are chosen in a way that a straight

line connects several or all of the foreseen locations. In this way, a meaningful representation of the stresses and strains along that straight line can be obtained.

When mounting the specimen on the sample table, the defined specimen coordinate axes should ideally be aligned with the directions of motion of the sample positioning stages. This should be done as accurately as possible, especially along the axes where the longest distances between measurement locations exist. An alignment to at least within ±1°, or preferably much better, is recommended, depending on the individual situation. Optical mechanical means or multiple neutron surface scanning techniques can be used to achieve the alignment requirements.

After the specimen has been mounted on the sample table with the desired orientation, it is necessary to determine the position of the specimen coordinate system with respect to the centroid of the sampling volume. This positioning of the specimen should be achieved with a relatively high accuracy; 0.1–0.2 mm is normally desired, as this determines how accurately the real locations of measurement are known. The determination of the measurement position can be achieved by high precision optical equipment (theodolites), within limits by mechanical means, or by neutron surface intensity scanning.

If the centroid of the sampling volume has been aligned with the centre of rotation of the sample table, it is possible to rotate the specimen about the axis of the sample table for measurements in different directions without the need for a realignment of the specimen position. Otherwise, the specimen position must be redetermined for every new measurement orientation.

With the specimen orientated and aligned this way it should be possible to position the centroid of the sampling volume at the desired locations of measurement within the specimen for all measurement orientations within the scattering plane.

At most of the existing instruments the specimen mounting, orientation and alignment process needs to be repeated for those measurement directions that are not in the original scattering plane. For the most common measurement setting, i.e. three mutually orthogonal measurement directions, this means the process has to be repeated once for one out-of-plane direction. When special equipment for specimen positioning and orientation is available, e.g. an Eulerian cradle, a robot or a hexapod, it might be possible to measure in all desired directions without realignment of the specimen.

In recent years, new ways to facilitate faster specimen set-up have been developed. Particularly at high performance facilities, integrated systems combine high precision mechanics and computerized tools that facilitate off-line specimen mounting, so that the neutron diffraction instrument itself is not blocked during the set-up of a specimen. An example for such a set of tools is the SScanSS set-up at ENGIN-X at ISIS [36].

3.6.6. Measurement execution — data recording

When all the preparation steps described in Sections 3.6.2–3.6.5 have been completed, it is straightforward to execute the measurements themselves. The specimen is orientated such that the desired measurement direction bisects the incident and diffracted neutron beams, i.e. it is aligned with the scattering vector. The specimen is then positioned such that the centroid of the sampling volume coincides with a chosen measurement location. Subsequently, the distribution of neutron counts over the angle of scattering or the TOF, or both, is recorded for this position and orientation. The duration of neutron counting depends on the required measurement accuracy and the total time available for the measurement campaign. Longer counting leads to better data statistics and results in a lower fitting uncertainty of the data.

When the counting for a measurement position has finished, the specimen is moved to the next position, and may also be rotated for a new measurement direction, and the counting process is repeated, possibly with a different duration of counting as deemed appropriate.

This process is repeated for all foreseen measurement locations and orientations. Where necessary, the specimen has to be realigned in between different measurements. This occurs mainly when the orientation of the specimen in the beam is changed. A data file is usually generated that associates the recorded neutron counts over angle/time with the related position and orientation of the measurement. It is advisable to pre-analyse the measurement data while the measurements are ongoing. This way, the measurement programme can still be adapted if unexpected features are discovered in the observed strain distributions.

Measurement in the reference specimen(s) are performed in the same way as the measurements in the specimen(s) with residual stresses. It is important not to change the settings of the instrument between the measurements in the specimen and the corresponding reference measurements. Note that data analysis is addressed in Section 5.

3.6.7. Grain size and surface effects

Through Bragg's law, the peak positions measured in a neutron diffraction experiment are associated with the average lattice spacing at the location of measurement. One has to keep in mind that the position of the neutron peaks can also be influenced by an inhomogeneous distribution of the diffracting material within the sampling volume. This can occur when the material under investigation is coarsely grained or when surfaces or material interfaces cut through the sampling volume. This situation is described and analysed in Refs [26, 37].

These phenomena can have a significant impact on the measurement results. In fact, grain size and surface effects can exceed the peak position shifts that are caused by the strains under investigation in magnitude.

Therefore, these effects must be controlled and in many cases it is necessary to apply experimental techniques for mitigation. Surface–interface effects on strain measurements can be reduced by the use of radial collimators instead of slits for the definition of the incident and diffracted beams [26]. It is also possible to replicate the measurement geometry with surface–interface cutting through the sampling volume when performing the reference measurements, so that both strain and reference measurement are affected in the same way. Additional care is required with the alignment of the samples in this case.

Grain size effects can be mitigated through the use of a larger sampling volume, which is, however, not always feasible. Another technique for reducing grain size effects is specimen rocking during measurement. Rocking means continuous back and forth rotation by several degrees about the rotation axis of the specimen table (see Fig. 13). This can significantly reduce grain size effect, as the example in Fig. 14 shows (from Ref. [38]).

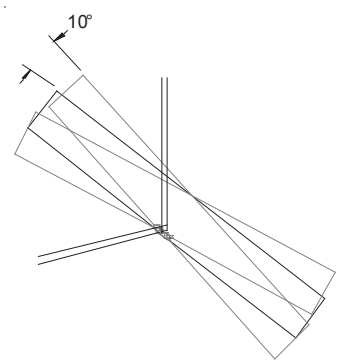

FIG. 13. Rocking of a rectangular cross-section specimen by ±10° about the measurement position.

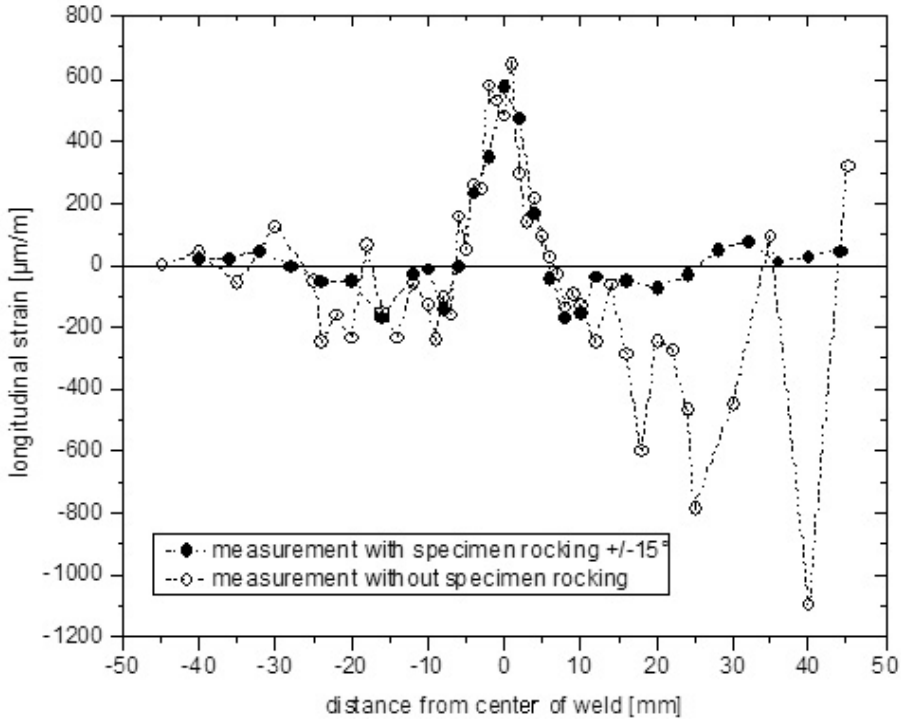

FIG. 14. Measurement of strain in a welded stainless steel specimen with and without rocking; the right hand side of the graph exhibits significant grain size effect in measurement without rocking.

3.7. SPECIALIZED SAMPLE ENVIRONMENT

3.7.1. Introduction

The expansion of research using neutron diffraction for materials behaviour at non-ambient conditions, such as under applied pressure, temperature and electric or magnetic fields, requires specialized equipment which will be discussed in the following subsections.

3.7.2. Bending device

Bending devices (see Fig. 15) can be used for the investigation of e.g. elastic–plastic behaviour of polycrystalline components under an applied external load, and of structure changes in substrate or coating structures where the coatings have thicknesses ≥0.5 mm and are measurable with the strain scanner etc.

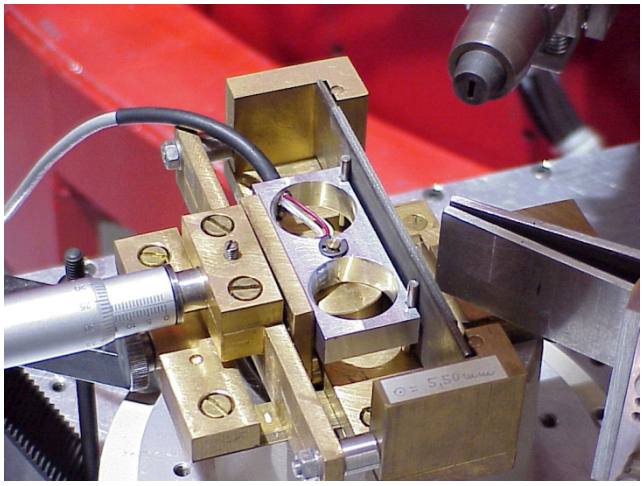

FIG. 15. Four point bending device used for bending a sample with a plasma sprayed coating.

3.7.3. Heating and cooling devices

Cryostats and furnaces are commercial products allowing neutron diffraction measurements for different sample sizes and temperature ranges. They can be used in special experiments investigating structure changes, structure phase transformations, phase specific stresses in components made from multiphase materials, etc. It should be pointed out that cryostats and furnaces create an extra background in scattering and sometimes unwanted diffraction maxima. Therefore, special care should be taken in the choice of construction material and beam windows.

3.7.4. Uniaxial stress or combined measurements

At present, many dedicated strain and stress diffractometers are equipped with devices for applying uniaxial stress, sometimes in combination with applied heating. In the case of a metallic sample a 'brute force' method for heating, i.e. a high electric current flowing through the sample, can be used (see Fig. 16). Owing to such equipment, the instrument can be used for the thermomechanical testing of materials, i.e. to study the deformation and transformation mechanisms of types of newly developed materials. Neutron diffraction performed in situ upon external loads (tension and compression or heating, or both), reveals a wide range of valuable information about structural and sub-structural parameters (e.g. grain size, dislocation density and macrostrain development) of the studied material, which is easy to correlate with parameters of external loads.

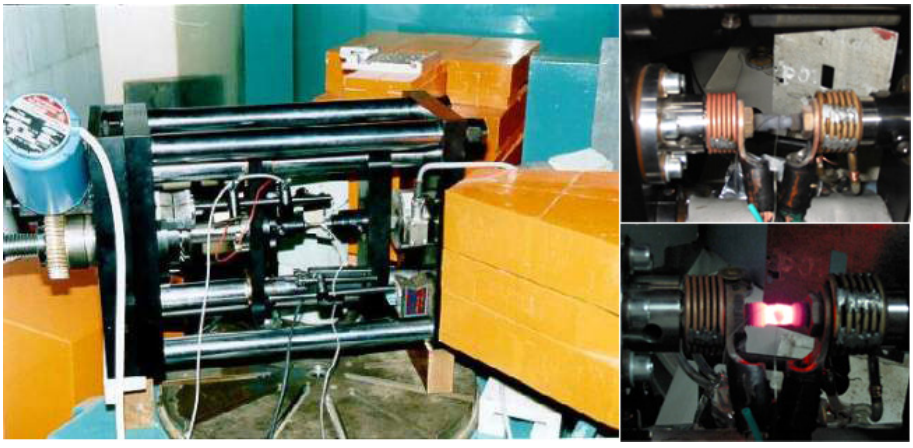

FIG. 16. Tension/compression rig at NPI Řež, Czech Republic, equipped with a sample heating system.

If the sample requires isolation from air, a combination of vacuum furnace and stress device should be constructed. A possible construction of a furnace with a tensile loading device is shown in Fig. 17.

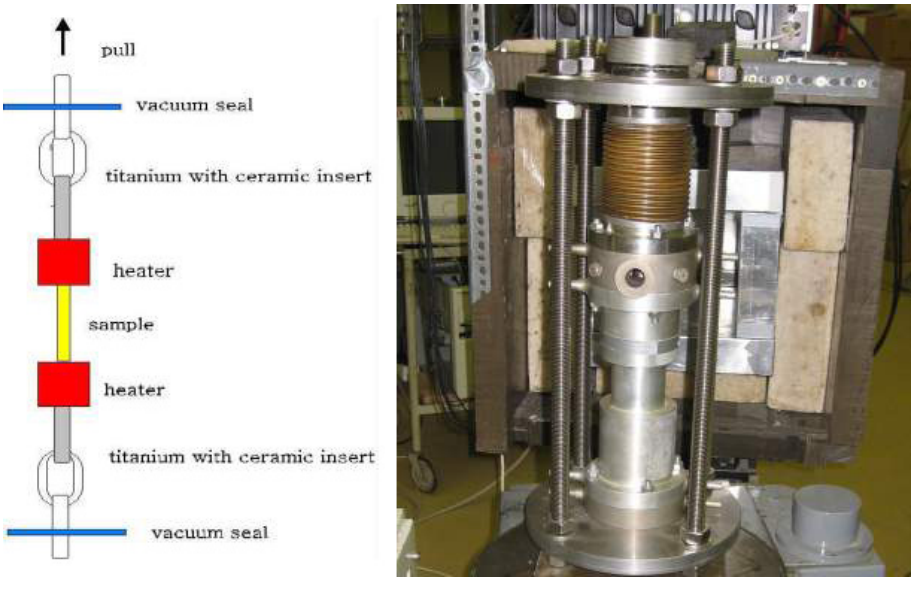

FIG. 17. Furnace with applying tension rig at the Budapest Neutron Centre in Hungary.

3.7.5. Activated samples

Irradiation can strongly change the mechanical properties of materials. Therefore, it is desirable to investigate the resulting structure changes and stress fields in components after irradiation. However, irradiated samples, in particular steels, are usually highly activated and for diffraction measurements a special sample environment has to be used. For highly activated samples it is necessary to manufacture a special shielding block with extra equipment for handling of activated samples. Safety measures should be followed for storage, transportation and final positioning of an activated sample on the neutron beam. Construction of a special shielding block is required not only for safety reasons but also to avoid a high level of gamma radiation resulting in a high background level. Figure 18 shows a set-up for stress measurements on irradiated specimens constructed at the Joint Research Centre (JRC), Petten.

FIG. 18. Shielding installation for strain measurements in highly activated specimens.

3.8. ADVANCED INSTRUMENTATION FOR RESIDUAL STRESS/STRAIN SCANNING

Advanced neutron diffraction techniques and instrumentation for residual stress/strain measurements are always connected with the optimal deployment

of neutron optics elements such as neutron guides, mirrors and supermirrors and focusing monochromators in combination with position sensitive detectors. In this section, two very advanced strain scanners installed at ISIS RAL and at the ILL are introduced. Furthermore, the principles of new high resolution neutron diffraction techniques which use Bragg diffraction optics based on cylindrically bent perfect crystals are discussed. These crystals are used as monochromators and analysers in the context of stress/strain measurements. Their unique resolution and good luminosity is achieved by focusing in real space and momentum space, und this makes them not only suitable for macrostrain scanning but also for microstress/strain studies through analysis of the diffraction profiles. The combination of good luminosity and sufficient resolution permits investigations of both macrostrains and microstrains in gauge volumes in the range of cubic millimetres with strain resolutions $\Delta d/d$ of approximately $5 \times 10^{-5} - 1 \times 10^{-4}$, even at medium power neutron sources.

Residual or applied stresses displace atoms from their original positions in a crystalline material. The resulting change of lattice parameters can be measured non-destructively and with sufficiently high precision using neutron or X ray diffraction. If the neutron source is sufficiently strong, TOF neutron diffraction technique appears the most efficient method. One of the most powerful stress/strain instruments based on the TOF technique is ENGIN-X, which is installed at the pulsed neutron source ISIS [39]. As shown in Fig. 6, the instrument determines the stress in a polycrystalline material by means of a change of the positions and shapes of many diffraction lines, and thus provides more complex information about the material properties. Moreover, as the resolution is the same on both sides of the incident beam (right–left symmetry), in many cases two strain components can be measured simultaneously. On the other hand, in cases where the stress effect can be measured by means of one reflection line, as it is usually the case at instruments installed at steady state sources, the average neutron flux on the sample plays a decisive role and the use of a strain scanner at a steady state source appears to be more effective. For sample manipulation, ENGIN-X is equipped with an xyzω positioner with 1500 kg capacity, which is capable of positioning xyz accurately to 5 μm, at 500 mm maximum travel, and ω accurately to 0.002° with the possibility of a full 360° rotation. It has standard VAMAS base plates with pre-drilled holes for accurate sample mounting. The available sample environment consists of a 100 kN servo-hydraulic stress rig for in situ loading, cycling and fatigue experiments, a radiant furnace which allows heating and thermal cycling of samples mounted on the stress rig, a cryo-cooler for experiments at liquid nitrogen temperatures or lower, and a coordinate measuring machine (CMM) for off-line determination of the sample geometry for easier experimental set-up (including a laser scanning arm). A dedicated software system takes care of experiment design, measurement point definition

and sample alignment. Because ISIS is a pulsed source, pulses can be timed and summed cumulatively for high frequency experiments.

Another example of a very advanced instrument is the strain scanner SALSA (see Fig. 19) installed at the most powerful steady state neutron source at the ILL in Grenoble [40]. Thanks to the improved flux after installing a new supermirror guide and to improved optics, SALSA has increased the range of potential engineering applications by improving resolution and shortening measurement times. It is designed to allow measurements in components of up to 2 m in length and more than 500 kg in weight at a depth of up to several centimetres, yet with a spatial resolution better than $0.5 \times 0.5 \times 0.5$ mm^3. On the other hand, precise surface measurements are standard, owing to the presence of collimators and to a positioning precision better than 50 μm. Special features include:

— A special sample stage using a Stewart platform (hexapod) allowing six axis sample movement in sample centric coordinates. This platform, on which specimens are mounted, is supported on six hydraulic jacks, which facilitate highly accurate positioning, but also tilting of the specimen through coordinated movement. Figure 19 illustrates the functioning of this equipment.
— A double focusing bent Si monochromator, offering high resolution, and high intensity.
— A flexible optical system for the incident and diffracted beams. It allows the use of combinations of different collimators and variably sized slits for automated definition of the gauge volume.

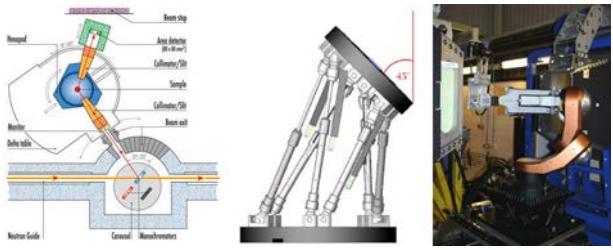

FIG. 19. Layout of the SALSA strain scanner equipped with a positioning of the sample using a hexapod (permitting tilting, translation, a load of up to 500 kg and xyz accuracy to <10 μm) and robotic positioning.

SALSA has a double focusing bent Si crystal monochromator with adjustable curvature. Its dimensions are $209 \times 170 \times 12$ mm^3. The monochromator provides neutrons in the wavelength range of 1.23–3×10^{-1} nm through a take-off angle

which is variable in the 55–125° range. Beam definition is provided by computer controlled primary and secondary slits (0.3–5 mm horizontal, 0.3–25 mm vertical). The distance of the slits to the gauge volume is motorized. The highest spatial resolution is given by primary and secondary radial collimators with the following parameters: focus (full width at half maximum) — 0.6 mm; distance to gauge volume — 150 mm; and oscillation — ±1°. A sample stage hexapod with a maximum load of 500 kg and a x,y translation of ±300 mm, z translation of 150 mm, rigid translation of 700 mm; a tilt (x, Φ) of ±30°, a rigid rotation of (Ω) 360° and a rotation (ω) of ±45°. The detector is a two dimensional position sensitive detector, with a distance to the gauge volume of between 0.5–1.5 m and an angular resolution of 0.02°.

Another recent entry to the family of positioning and orientation apparatus for neutron diffraction stress measurements is the robot arm that has been installed at the instrument STRESS-SPEC at the FRM II in Garching, Germany [41]. This device facilitates specimen positioning with movement ranges of 500 mm in the x, y and z directions. This particular device can carry a load of up to 30 kg. Next to the ranges for linear positioning, the robot arm provides for 3 axes of rotation for orientation of the specimen in the beam. This facilitates measurements in several independent orientations for the application, for example, of the $\sin^2 \psi$ method. Furthermore, this device will also be used for texture investigations at STRESS-SPEC. Figure 20 shows this robot.

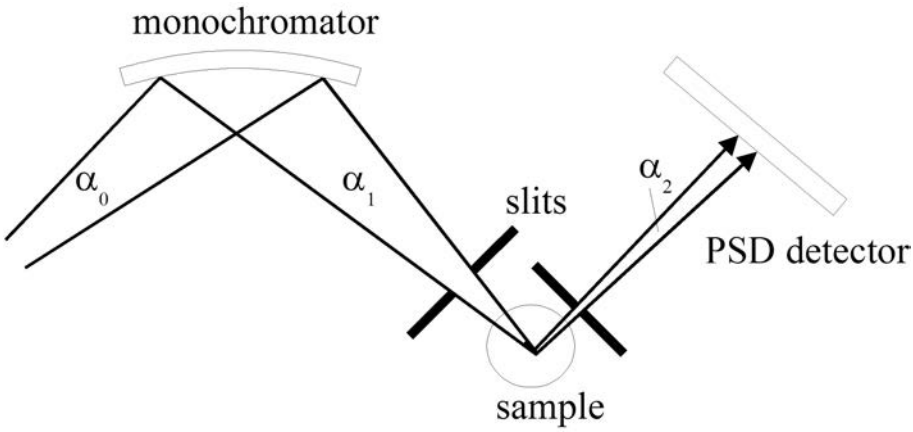

FIG. 20. Robot arm for specimen positioning and orientation at the spectrometer STRESS-SPEC at FRM II.

3.8.1. Bragg diffraction focusing

This option is often used at strain scanners installed at steady state neutron sources. It is based on the Bragg diffraction angle analysis used for high precision measurements of the change of the Bragg angle $\Delta\theta_{hkl}$ related to a chosen *hkl* reflection arising from a change of the lattice spacing $d(hkl)$ brought about by stress in the material. This change is described by a simple formula: $\Delta d/d_0(hkl) \cong \cot\theta\Delta\theta_{hkl}$. As mentioned before, stress and strain measurements require high resolution and sufficiently high neutron flux at the gauge volume. The application of Bragg diffraction optics, namely by using focusing monochromators with elastically bent perfect crystals (BPCs), fulfils both requirements simultaneously [42–48]. An example is shown in Fig. 21.

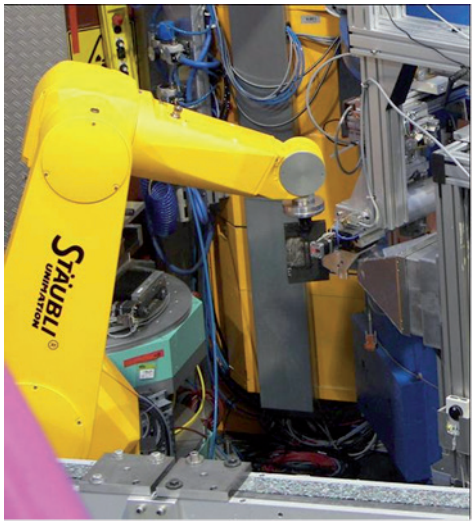

FIG. 21. Schematic sketch of the two axis Bragg diffraction focusing performance of the strain scanner.

Thus, the dedicated diffractometers using Bragg diffraction optics provide substantially higher luminosity as well as better $\Delta d/d(hkl)$ resolution which results in a figure of merit more than one order of magnitude better in comparison with the instruments equipped with conventional mosaic monochromators. The optimization of the monochromator curvature uses both resolution and intensity as shown in Fig. 22.

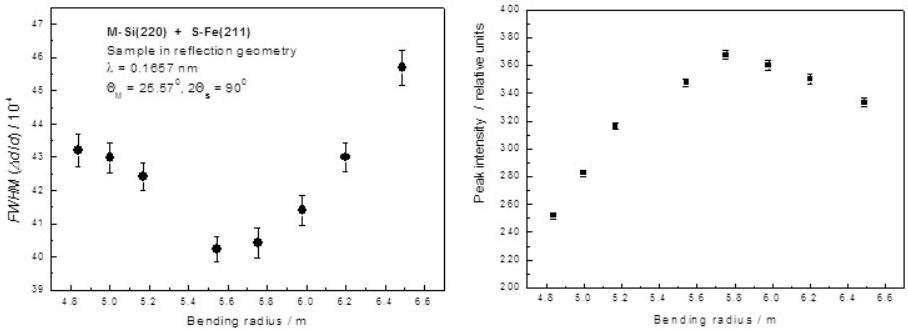

FIG. 22. Example of the optimization curves of the BPC Si(220) monochromator at $2\theta_s = 90^o$.

The focusing procedure consists basically of the following steps and properties:

- Monochromatic neutrons selected by a bent monochromator from the white spectrum are focused on a sample (real space focusing) leading to high luminosity of the device.
- The monochromatic beam is diffracted by a chosen volume element (determined by a pair of input and output slits) into the scattering angle $2\theta_s = 2\theta_{hkl}$.
- The quasi-parallel diffracted beam is directly analysed using a position sensitive detector (PSD). There are small resolution uncertainties influencing the instrumental resolution, $\Delta\alpha_{2t}$ and $\Delta\alpha_{2w}$, which arise from a non-negligible thickness t_M of the monochromator and from the finite width w of the irradiated volume of the sample determined by the input and output slits.

In the last case and for a point-like sample, the monochromator of a thickness t_M and the sample width w [45] the following is valid:

$$\Delta\alpha_{2t} = 2t_M\, a_{SM} \cot\theta_M/R_M, \quad \Delta\alpha_{2w} = w(2a_{SM} - 1)/L_{MS} \tag{6}$$

In addition, there is a strong correlation between the divergences α_0, α_1, α_2 and λ as:

$$\alpha_1 = 2\varepsilon(R_M) - \alpha_0,\ \alpha_2 = \alpha_1\,[2\, a_{SM}(1 - L_{MS}/2f_M) - 1] \tag{7}$$

$$\Delta\lambda/\lambda = \alpha_2 \cot\theta_M\,(1 - L_{MS}/2f_M)/[2\, a_{SM}(1 - L_{MS}/2f_M) - 1] \tag{8}$$

which all can be easily manipulated by changing the monochromator radius R_M. $\varepsilon(R_M)$ is the total change of the angle of incidence (exit) over the illuminated crystal length and $a_{SM} = -\tan\theta_S/\tan\theta_M$ is the dispersion parameter. By setting a proper value of the radius R_M,

$$R_M = (2L_{MS}/\sin\theta_M)/(2 - 1/a_{SM}) \quad (9)$$

at $\alpha_2 = 0$, a quasi-parallel and highly luminous detector signal can be obtained for a chosen scattering angle $2\theta_S$. Unlike with the conventional powder diffractometers equipped with mosaic monochromators, the minimum resolution, e.g. at $2\theta_S = 90°$, can be achieved even for monochromator take-off angles far below 90°.

Both $\Delta\alpha_{2t}$ and $\Delta\alpha_{2w}$ bring about a slightly divergent diffracted beam (quasi-parallel) and directly determine the instrumental resolution. The resolution can be easily estimated and adjusted according to experimental requirements [49–51]. Also, no soller collimators are required.

Of course, the total resolution of the instrument is strongly dependent on the spatial resolution of the PSD. The employment of Bragg diffraction optics results in a considerable improvement of the luminosity or an improved resolution of the dedicated strain scanners compared with the performance achieved at conventional counterparts, or both. Moreover, strain scanners can be equipped with a two crystal slab sandwich monochromator (e.g. combinations of Si(111)+Si(220) or Si(111)+Ge(311) reflections) which permits working with two neutron wavelengths simultaneously [45, 52]. This feature enables the investigation of an increased number of sample reflections under the same experimental conditions within an angular range of scattering angles covered by one setting of the PSD. Owing to to a remote control of the bending device and a remote manipulation of the crystal curvature, the optimum focusing conditions can be achieved for practically any scattering angle $2\theta_{hkl}$.

3.8.2. Correlation technique for stress/strain experiments

As mentioned before, the TOF technique is very effective for the solution of various problems connected with strain measurements in bulk samples, especially questions about microstrain anisotropy and stresses in individual phases of multiphase samples. A drawback of TOF diffractometers is the lowered intensity of individual diffraction peaks owing to the spread of the total intensity over the whole diffraction pattern. Moreover, to obtain a good resolution ($\Delta d/d \approx 0.002$), the flight path of a conventional TOF diffractometer must be quite long, at least 30–50 m. However, such a long flight path results in a considerable drop of intensity and the problem of pulse overlapping.

The main idea of advanced neutron TOF correlation techniques is the gain in intensity associated with keeping resolution at a high level. At present, two neutron diffractometers using a correlation method of data acquisition are successfully used for strain measurements: POLDI [53] at SINQ (PSI), which employs a pseudorandom chopper and FSD [54] at IBR-2 (JINR), which uses a Fourier chopper.

SINQ at PSI is a proton accelerator based continuous spallation neutron source with a neutron flux comparable to a medium flux reactor. The pulse overlap diffractometer (POLDI) is a multiple pulse overlap diffractometer mainly designed for strain measurement in bulk materials.

The use of the multislit chopper at POLDI leads to a substantial gain in intensity, but since the arrival time of a single neutron does not unambiguously determine its TOF, additional information is needed to evaluate the data. For evaluation, the dependence of the TOF on the scattering angle is recorded.

The layout of POLDI is shown in Fig. 23. Its key parts are the fast disk chopper (highest speed of 15 000 rpm) with 32 slits, which are arranged in four identical sequences with a pseudo-random distribution within each sequence, a flight path of approximately 12 m to the sample position and a one dimensional position sensitive ^{3}He detector with good spatial resolution. The chopper slits have a width of 4 mm, which yields a pulse width of 8 μs at 15 000 rpm and a TOF contribution to the resolution function of $\sim 8.6 \times 10^{-4}$ for the total flight path (chopper–detector) of about 14 m.

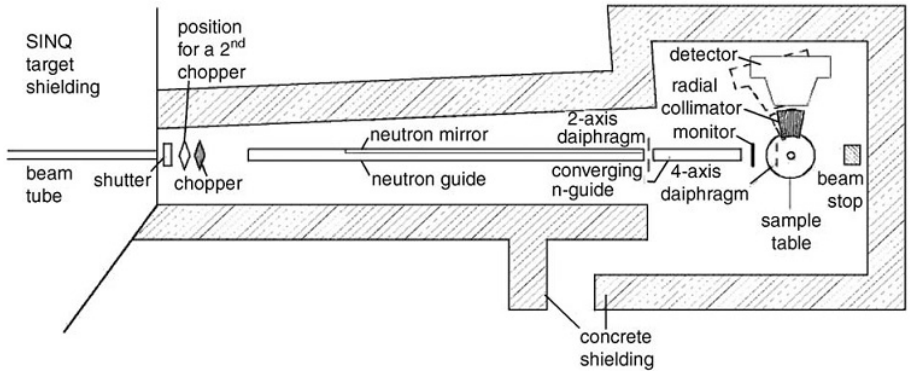

FIG. 23. Layout of the POLDI instrument (from Ref. [53]). The distance between chopper and sample table corresponds to 11.8 m.

The test experiments (Fig. 24) showed that POLDI can provide high quality data for a steel sample within 20 min, with a gauge volume of $1.5 \times 1.5 \times 10$ mm^3.

A resolution of approximately 2×10^{-3} over the whole d range was achieved at an average scattering angle of 90°.

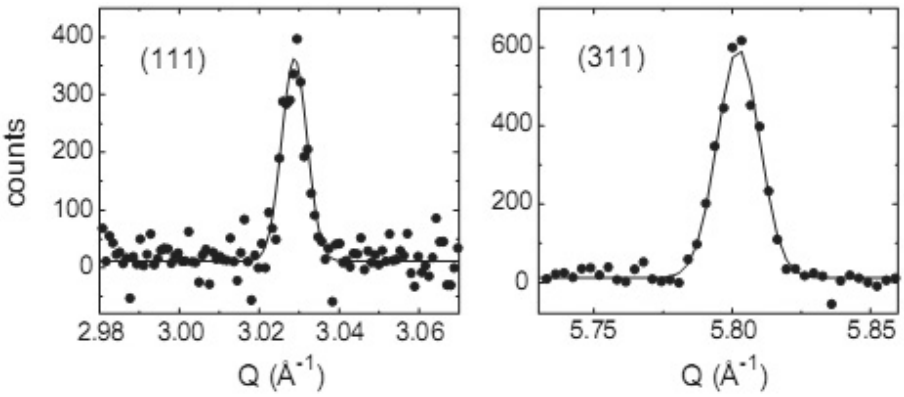

FIG. 24. A diffraction pattern measured from the centre of a 12 mm thick steel plate in transmission geometry (from Ref. [52]). The data have been collected over 20 min with a gauge volume of 23 mm^3. Experimental points and the corresponding fit result (solid line) are shown.

The IBR-2 reactor is a long pulse neutron source with a thermal neutron pulse of about 350 μs in duration, which can provide a TOF component of the resolution function of not better than 0.01 for a flight pass of 25 m. To improve the resolution at the FSD, the so-called reverse time of flight (RTOF) method is used. This technique assumes the application of a fast Fourier chopper for neutron beam intensity modulation and measuring of many TOF spectra, which are almost fully overlapping. Data acquisition is conducted while continuously changing the Fourier chopper rotation frequency from zero to a maximum frequency ω_m. The correlation analysis of the spectra measured at different frequencies make it possible to obtain a conventional TOF diffraction pattern. Because of the correlation nature of this pattern, it contains an additional background component, which is proportional to the intensity of the diffraction lines.

In the Fourier method, the time component of the resolution function depends on the maximum modulation frequency of the beam intensity $\Omega = N\omega_m$, where N is the number of transparent slits of the Fourier chopper. The effective neutron pulse width Δt_0 is equal to Ω^{-1} and for $N = 1024$, $\omega_m = 100$ Hz (FSD parameters) $\Delta t_0 \approx 10$ μs. This means that for a flight path from Fourier chopper to detector of 6.5 m, the time component of the resolution function equals $\Delta t_0/t \approx 2 \times 10^{-3}$ at $d = 2 \times 10^{-1}$ nm. The geometrical part of the resolution function

depends on the scattering angle in the same way as for any TOF diffractometer (~cot θ $\Delta\theta$) and finally $\Delta d/d \approx 2.3 \times 10^{-3}$ at $2\theta = 140°$ and $\Delta d/d \approx 4.0 \times 10^{-3}$ at $2\theta = 90°$ (for $d = 2 \times 10^{-1}$ nm) are obtained at the FSD. An example of a diffraction pattern measured with FSD by the 90º detector is shown in Fig. 25 (also see Fig. 30).

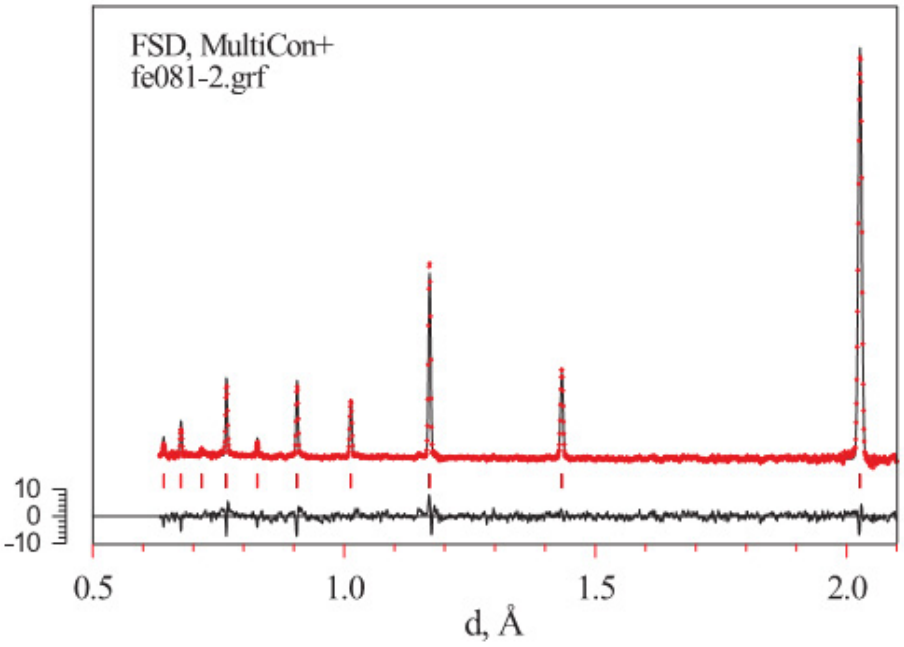

FIG. 25. Part of a neutron diffraction pattern from an α-Fe standard sample measured on FSD in high resolution mode. The experimental data, the profile calculated by the Rietveld method and the difference curve are shown (from Ref. [54]).

3.9. INSTRUMENT SIMULATION AND OPTIMIZATION

3.9.1. Numerical simulations for instrument design

The modelling of neutron optics components as well as complete neutron scattering instruments, mainly by the Monte Carlo (MC) ray tracing method, has been developed intensively over the past decade. It has become indispensable for any project building a new instrument. Rapidly growing demand for MC modelling comes particularly from large neutron scattering centres with their ambitious instrument development programmes. The Millennium Programme of the ILL in Grenoble, new instrumentation for the FRM II reactor in Munich, the

second target station of ISIS and the ESS project are the best known examples. This effort, which results in up to an order of magnitude more efficient use of otherwise limited neutron sources, opens many new experimental possibilities in various fields of science, particularly in condensed matter physics, materials research, macromolecular chemistry and microbiology. Such progress in neutron instrumentation is possible thanks to the introduction of new concepts in the application of neutron optics, such as focusing reflective and refractive optics, adaptive multicrystal Bragg mirrors, fast position sensitive neutron detectors, etc. In this respect, MC simulations proved to be very useful for the quantitative estimation of future instrument properties and in the optimization of the design of neutron optical systems in order to achieve a maximum possible gain in intensity, resolution or both. The higher neutron fluxes achieved by focusing neutron optics often lead to a more complicated non-Gaussian instrumental response compared with older instruments employing tightly collimated beams. As a result, data analysis methods developed earlier for non-focusing instruments with Gaussian response become inadequate. Here, MC simulations are also useful, as they yield a more realistic description of instrumental response function, which can be taken into account when analysing experimental data.

Tools for realistic MC simulations of neutron experiments have been developed. At present, development of the method of virtual experiments is in progress, which will be useful for instrument building, experiment planning and advanced data analysis. Simulations should become an everyday tool for instrument builders, instrument scientists and even for user groups. Reliability in simulation results will be ensured by extensive tests and comparisons with experiments.

While the development of neutron ray tracing software began in the 1970s, it has been significantly accelerated by the advent of powerful desktop computers in the 1990s and led to the creation of several software packages capable of the realistic modelling of modern neutron optics devices. They include the programs NISP [55], IDEAS [56], McStas [57], VITESS [58] and RESTRAX [59]. Of course, MC simulations always involve a trade-off between the level of physical reality implemented in the description of neutron transport and computing speed. Consequently, these programs differ in both the physical models underlying the simulation of particular components and the structure of their code, depending on the different purposes they have been written for. While some put emphasis on modularity (McStas, VITESS, NISP), which permits easy the incorporation of new components and testing of new ideas of experimental techniques, others, like RESTRAX, trade part of their flexibility for a highly efficient sampling strategy. Thanks to this approach, RESTRAX is significantly faster in many situations and hence more suitable for applications requiring a large amount of simulated data, such as optimization of one instrument configuration and analysis of experimental

data. As such, RESTRAX has proved to be useful in a growing number of instrument development projects, including those carried out by leading edge neutron facilities such as the ILL in Grenoble, HZB, FRM II [60–66]. Unlike the other programs, RESTRAX provides integrated tools for analysing experimental data from two- and three axis neutron scattering instruments, with more realistic (simulated) description of instrumental response than can be achieved with analogous analytical methods. It is thus useful not only for instrument scientists, but also for neutron users, who need to plan their experiments, treat experimental data more accurately or to resolve problems related to instrumental artefacts.

Recently, SIMRES has been upgraded to allow for simulations of a much larger variety of instrument configurations. During the past decade, SIMRES has been checked several times against other ray tracing packages (McStas, VITESS, NISP) and has proved to be reliable, providing identical results when simulating identical configurations. The main advantages of using SIMRES in simulating crystal diffractometers are (a) the ability to describe diffraction on bent and mosaic crystals realistically and (b) high speed, which permits the scanning of wide ranges of multiple variable instrument parameters. Nevertheless, as with all other simulation packages, the depth of physical reality implemented in the software is limited.

In relation to the CRP project, very successful MC simulations have been performed for optimization of parameters of stress diffractometers in HZB [66], South African Nuclear Energy Corporation (Necsa) in South Africa, Korea Atomic Energy Research Institute (KAERI) in the Republic of Korea [67] and China Institute of Atomic Energy (CIAE) in China [68]. The following paragraphs summarize the approximations adopted in description of individual diffractometer components used in this work:

— Information on a neutron source can be given in various ways. The most accurate one is a lookup table, which may include nearly arbitrary energy, spatial and angular flux distribution. The source is usually assumed to be homogeneous and isotropic with Maxwellian flux distribution.
— All collimators and slits are assumed to perfectly absorb, i.e. no trajectories through the walls or missing the collimator opening are processed.
— For the crystal monochromator, elastically bent perfect crystals are assumed. For neutron trajectories, the bent crystals are deterministic and approximated by straight lines with the turn points, which are determined from Bragg's law, calculated for a uniformly (cylindrically) bent perfect crystal. The events are weighted by diffraction probability derived from dynamical diffraction theory. This model is in very good agreement with experiments and with theory for the curvatures used on monochromators ($1/R_H >\sim 0.001$ m^{-1}). Reflectivity is calculated from table values of

scattering amplitudes and includes the Debye-Waller factor. Absorption is calculated on the basis of the semi-empirical model developed by Freund [69]. This model describes beam attenuation due to neutron capture, incoherent scattering, single and multiphonon scattering. It provides energy and temperature dependent absorption coefficients in good agreement with experimental data on single crystals, within the energy range of thermal neutrons.

— For simulations, a simplified model of a polycrystalline α-Fe sample is usually assumed, neglecting texture, microstrains, grain size effects and the Debye-Waller factor.
— A position sensitive detector with 100% efficiency is assumed. The spatial resolution is described by Gaussian response with a required variance e.g. 1 mm (in both directions).
— In the simulation program, all parameters related to the instrument configuration are included (e.g. the cross-section of the beam, the dimensions of the horizontally and vertically focusing monochromator, monochromator take-off angle, the scattering angle on the sample, the monochromator–sample distance, the sample–detector distance, etc.). The vertical curvature of the monochromator, the crystal thickness and, in the case of a sandwich, the number of wafers, are optimized during the simulation process.

The simulation process is sequential, which means that any cross-talk between different components is excluded. In practice, cross-talk effects are mediated by parasitic or incoherent scattering, which are anyway not processed by the program. Note that cross-talk between segments of a focusing crystal has to be taken into account since such an array is treated as a single component. As a result of the MC simulation, resolution and projections of 3-D intensity profiles of the beam of 'useful' neutrons between the monochromator and the sample as well as between the sample and the detector can be received [66–68].

For users and instrument scientists without experience in such calculations, it is recommended to first contact a scientist with ample experience in MC simulations in order to clarify necessary questions and requirements.

3.9.2. Matrix simulation technique

Another alternative of simulation of the experiment on a stress diffractometer is provided by the so called matrix technique developed by a Romanian group [69–71]. It appears to be a convenient procedure to compute the resolution and luminosity properties, to perform the configuration optimization, to compute the beam size or any properties defining an experimental configuration, as the normal

approximation is still acceptable. However, for more sophisticated purposes, when a correct description of the line profile is needed, a MC procedure should be used. The computation procedure of the matrix technique involves several steps (for details see Refs [70–72]). The first one is to choose the initial variables of the problem, which define the neutron trajectories between the source and the detector. For a crystal neutron diffractometer, the initial variables, which define the vector $\boldsymbol{R}$, are all the relevant spatial coordinates plus the variable of the reflectivity curve of the monochromator. The normal approximation of the probability distribution of the initial variables can be constructed with a known transmission matrix, S. This amounts to replacing the actual shape of the spectrometer elements with Gaussian distributions with the same second order moments. It is assumed that the neutrons are scattered with a probability given by the real geometrical shapes of the spectrometer elements; this approximation can be improved by defining probability distributions taking into account extinction and absorption.

The next step is to account for the presence of soller collimators, neutron guides, coarse collimators and slits (a slit is defined as a coarse collimator with zero length). The neutron guide is assumed to be a soller collimator with a wave length dependent angular divergence given by the total reflex critical angle; this approximates the actual rectangular transmission function of the guide with a triangular one, with the same second order moments.

The computational procedure then serves as a base for a computer program (DAX program) to evaluate the resolution and intensity properties of a given experimental configuration or to optimize the parameters defining such a configuration. The DAX program was realized some years ago [73] and since then it has been considerably improved to become a really powerful instrument for designing and optimizing experimental settings. It was intensively used in designing the focusing configurations in Bucharest and Piteşti, Romania, and at the MURR reactor in the USA for optimizing the already existing configuration according to experimental requirements.

The DAX program allows for obtaining the resolution function, line widths and intensities as well as the optimum values for some relevant parameters. The program can be used with configurations with a monochromator group of one or two crystals, conventionally with plane crystals but for focusing, curved crystals are used; with or without soller collimators (the former is the conventional set-up; the latter the focusing set-up) and with or without diaphragms or neutron guides. The crystals can be mosaic or perfect; an option for vibrating crystals is also included. The index in the program that corresponds to the experimental set-up is selected according to the ‘how to use’ instructions.

To reduce the involved matrix dimensions, the horizontal and vertical plane computations are separated at first and combined at the end. This is possible

owing to the lack of correlation between the corresponding variables. The experimental configuration optimization can be performed either analytically using the corresponding optimization conditions or numerically, by minimizing the optimization parameter $w_{1/2}^2/I_{max}$ ($w_{1/2}$ is the full line width and I_{max} is the maximum peak intensity). For Poisson statistics, a minimum value of this ratio assures the optimum conditions to separate two partially overlapping lines. For numerical optimization, the analytical conditions, when they really exist, are the zeroth order approximation. When the analytical condition does not exist, the input value for the numerically optimization process is chosen arbitrarily. For analytical optimization, the general focusing conditions [73] provide the optimum monochromator radius of curvature, sample monochromator distance and the optimum sample orientation. There are 12 parameters (14 for two crystal monochromators) for which numerical optimization can be performed, the radius (ii) of curvature, the cutting angle, the mosaic spread, the crystal thickness, the sample orientation or thickness, the soller collimators' divergences (if soller collimators are used as in the case of conventional configurations), the monochromator–sample and sample–detector distances and the detector window width. Though all 12 (or 14) parameters can be optimized together, this is not desirable because the computing time would be too long; for reasonable computing time the number of parameters to be optimized at the same time should not exceed six. A library with the relevant data concerning the most frequently used crystals is included in the program. If the crystal does not belong to this list, the corresponding data must be input by the user.

4. INSTRUMENTATION CONTROL AND DATA ACQUISITION

4.1. INTRODUCTION

Instrumentation control and data acquisition is a vast subject and a general treatment of it is probably best written from the point of view of an instrument scientist who is also a multiple user of several other neutron facilities and instruments. Instrumentation control and data acquisition logically take place prior to data analysis in the sequence of a measurement. However, with the development of more sophisticated hardware and software, these processes can now be organized in an interactive way, i.e. data analysis can take place while a measurement is running and can automatically influence its execution. For example, the regulation of the measurement duration is usually either based on a

preselected number of neutrons incident on the sample or on a preselected period of time. In more complex instrument control systems, where elements from the data analysis become part of the measurement control, the measurement duration can be regulated through the requirement of a minimum data quality to be reached before a new measurement is started at a different position.

For the purposes of this report, instrument control and data acquisition will be separated from data analysis. There are a variety of types of instruments in use (different types of detectors, motors, etc.) but also operating systems vary: e.g. Unix, Linux and Windows are currently used for controlling neutron instruments around the world. The software and sometimes also the hardware used are often non-standard custom solutions developed over many years by many people who have passed through various neutron source institutes. The general principle can be summarized, however, and a typical set-up of a system is shown schematically in Fig. 26.

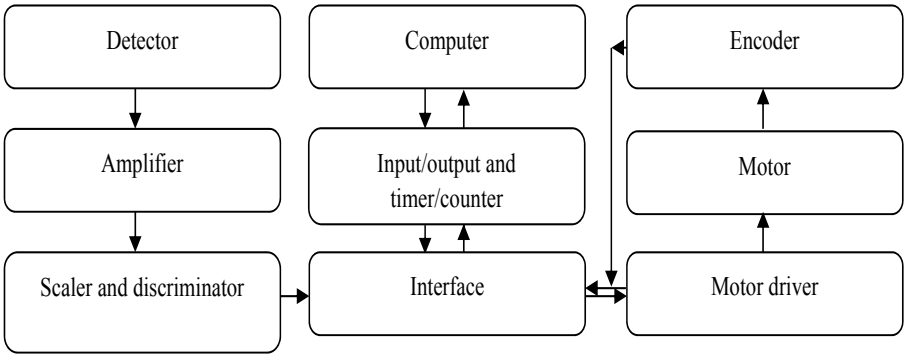

FIG. 26. General flow diagram of instrument control and data acquisition for a neutron instrument.

Data files and their formats also vary considerably between institutes, but there are concepts for harmonizing data formats, such as the NeXus format, which is already being used at a number of facilities [74].

The following sections describe briefly how a neutron signal on the detector is converted into a registered count for the output file of a measurement and how motors and encoders are used to implement the necessary motions of the specimen table and all other parts of the instrument that might need to be moved (e.g. the detector housing, the monochromator system, neutron optical elements).

4.2. SIGNAL TRANSFER FROM NEUTRON DETECTOR TO COUNTER

As described in Section 3.3.7, a neutron reaction generates an electronic pulse in the detector. Such electronic pulses need further processing before a neutron count can actually be registered by the instrument data recording system.

Signal processing mostly involves the amplification of the electronic signal and one or more steps of discrimination needed to separate neutron signals from signals of a different origin. For example, gas detectors pick up γ radiation in parallel to the neutrons and separation in this case is based on the amplitude of the amplified electronic signal.

The amplified and discriminated signal is then normally converted to a rectangular pulse that can be processed by the electronic system used for counting neutron signals. This system must be designed in such a way that independent neutron counting is facilitated for each position on the neutron detector.

At the end of each measurement, the recorded neutron counts versus detector position are stored in an appropriate data storage format and processing system.

In TOF instruments it is quite common that raw neutron count data are normalized with the information derived from prior detector sensitivity scans (see Section 3.5).When these steps are completed, the specimen can be moved to the next measurement position and the neutron counting process can be restarted.

4.3. ENCODERS AND MOTOR DRIVERS

The motor control system is required to accurately move the various motors e.g. for the x, y and z tables of the sample stage, the monochromator angle, the angular position of the detector assembly and the rotation of the sample stage. Encoders are often coupled into the instrument control chain in order to verify that requested motor movements have taken place.

Typical encoders used on the motor stages of a residual stress instrument are so-called rotary encoders. A rotary encoder, which is also known as a shaft encoder, is an electromechanical device that converts the angular position of a shaft to an analogue or digital code. An example of one that is widely used at the HZB can be seen in Fig. 27 in red. This is placed at the end of the rotating shaft of the motor.

Most of the motors used on E3 at the HZB are stepper motors. These are brushless, synchronous electric motors and a full rotation is divided into a large number of steps. This allows precise motion, where a certain number of steps correspond to a unit of measure, e.g. 1 mm for translation or 1° for rotation. Such stepper motors are also shown in Fig. 27.

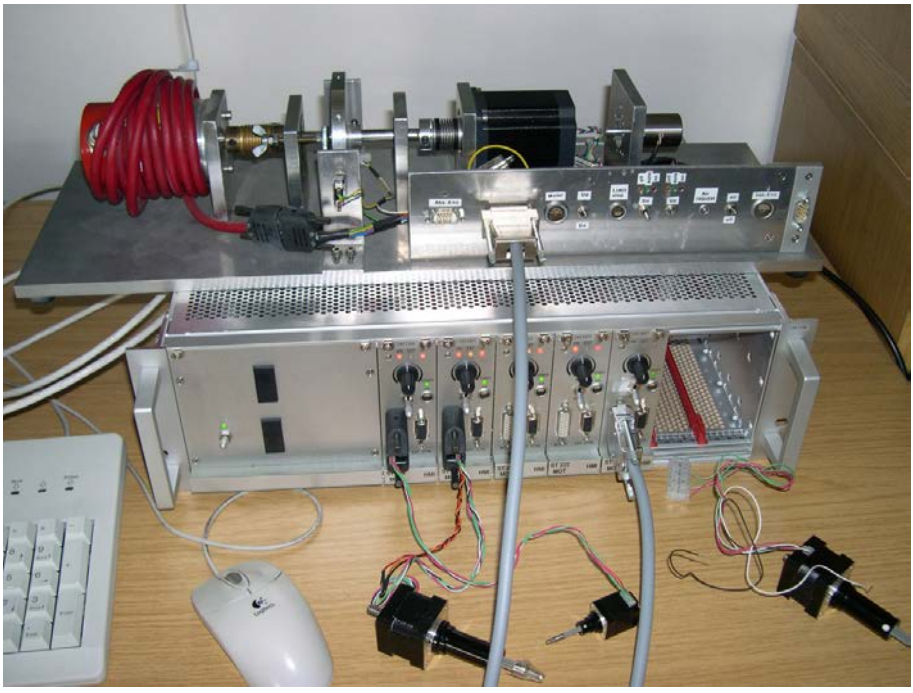

FIG. 27. ST 222 motor controller unit used at the HZB with an example of a stepper motor and rotary absolute encoder.

Figure 27 shows the motor controller unit ST 222, HZB's current custom solution for the position control of translators (x, y and z of a sample stage, for example) and rotation stages (such as the rotation motion of a detector and the rotation motion of the sample stage). Controller units — or motor drivers — are needed to translate the positioning commands provided from the instrument computer into the electrical signals needed for the motor to execute the requested motion.

Naturally, there is a trend for more sophisticated instrumentation, such as the use of a robot for sample manipulation (instead of a translation table and rotation stages) [75]. This is especially useful for texture analysis replacing the Eulerian cradles, which have been used up to now. This trend will continue and it is easy to envisage a complete robotization of instrument control in the future.

4.4. INTEGRATION INTO THE MEASUREMENT SYSTEM

Generally speaking, the entire iterative process of a neutron diffraction measurement of lattice strain is composed of specimen positioning and orientation, neutron counting and data recording, followed by specimen positioning and orientation and neutron counting. Details on how these steps work are given in the previous sections. These steps are repeated until all necessary measurements are done. Figure 26 illustrates how the components described in the previous sections are linked to a computer system.

The complete execution of a measurement is typically realized by means of dedicated software, which is often unique to a particular institute. These programs typically provide for the programming of measurement sequences of sample positioning and recording of neutron counts. For example, at the HZB, a program known as CARESS is currently used; at the Australian Nuclear Science and Technology Organisation, a software package called GumTree [76] has been developed, which is an open source scientific workbench. This is used for performing scientific experiments under a distributed network environment and provides a multiplatform graphical user interface for instrument data acquisition, on-line or off-line data visualization and analysis.

5. DATA ANALYSIS

5.1. INTRODUCTION

In common with all the other techniques for the experimental determination of residual stresses, neutron diffraction does not measure stresses directly. The measurement process itself renders a distribution of the intensity of scattered neutrons across a range of scattering angles for monochromatic instruments or across a range of travel times for TOF instruments. At angular positions where the combination of neutron wavelength and lattice spacing of the specimen material fulfils Bragg's law (Eq. (1) in Section 2.2.1.), a neutron peak is formed. Such a peak is shown for a monochromatic instrument in Fig. 3.2. In a typical TOF spectrum, the Bragg condition is fulfilled for multiple different lattice planes of the specimen material and such a spectrum therefore contains many neutron peaks. Figure 6 in Section 3.2 shows an example of a TOF spectrum.

Figure 5 shows that a neutron peak is characterized by a number of parameters that should be quantified in the process of data analysis. Those parameters are:

— The position of the peak in the spectrum;
— The shape of the peak;
— The amplitude of the peak;
— The width of the peak;
— The shape and magnitude of the neutron scattering background.

The most important profile parameters of diffraction peaks, which can be related to the stress field in a specimen, are the positions and widths. After comparison with the positions and widths of the same peaks of so called stress free or reference samples, in principle one, macro- and microstresses within the gauge (or sampling) volume can be calculated. If one single or several non-overlapping peaks are measured, their parameters are determined for each peak separately. If a diffraction pattern is measured over a wide range of peaks, the analysis of the whole spectrum using, for example, Rietveld, Pawley or Le Bail profile methods, can be performed [77], while single peak fitting would also be possible.

Next to the macro- and microstresses, there are other characteristics of the specimen that influence the above parameters in diffraction measurements and these characteristics can therefore be determined through analysis of the diffraction peak parameters. Such characteristics include:

— The plastic history of the material;
— Grain size and shape;
— Texture;
— Intergranular strains and stresses.

The type of data analyses that needs to be carried out to obtain the desired information on strains and stresses or any of the other characteristics mentioned depends on the type of measurement and the type of instrument that has been used. The complexity of the measurement and hence of data analyses can vary substantially. In this section, the basic principles of macroscopic stress analysis are presented first, as this corresponds to the most widely used application of neutron diffraction stress measurement. In addition, the ‘levels’ of complexity of the data analyses and the amount of potential information that can be extracted in each case will be indicated. Hence, in Section 5.3, a large amount of information on how neutron diffraction data are analysed is provided both for the case of single peak and for the case of multipeak analyses. Finally, Section 5.4 provides a brief account of the assessment of the uncertainties associated with neutron diffraction stress measurement.

Extraction of quantitative information on internal stresses from the diffraction data can be quite a complex task. The state of the art is described

in detail in the literature (e.g. Refs [78–81]) and is also discussed regularly at conferences [82]. Consequently, only a simplified overview is presented here.

5.2. MACROSCOPIC STRAIN AND STRESS DETERMINATION FROM DIFFRACTION DATA

5.2.1. Residual strain

At most instruments, the analysis of a single measurement renders the angular position of the observed neutron peak, 2θ, or — as the result of a profile refinement of multipeak data at a TOF instrument — the lattice parameter(s) a, b or c, associated with the location and direction of measurement. Together with the corresponding reference values, the (lattice) strain, ε_{hkl}, at that location within the specimen in that direction can be determined. In accordance with Bragg's law in a diffraction measurement the average lattice spacing d_{hkl} within the gauge volume can be derived from the scattering angle θ. In neutron diffraction, the angular position of the peak corresponds to 2θ. Section 5.3 describes the analysis of the neutron data that will render the peak position. Here, the focus is on the determination of macroscopic strains based on the peak positions measured.

Macroscopic strain inside the gauge volume results in a change of the average lattice spacings and consequently in the shift of diffraction peak(s) from nominally strain free position(s). The peak position is the average value of an experimentally measured variable, the scattering angle $2\theta_{hkl}$ for monochromatic instruments and travel time t_{hkl} for TOF instruments. From this value, the average strain in the direction normal to the reflecting planes can be calculated. Based on Eqs (10) and (11) below, lattice strain is derived for monochromatic instruments by:

$$\varepsilon_{hkl} = \frac{\sin\theta_{0,hkl}}{\sin\theta_{hkl}} - 1 \tag{10}$$

In single peak analysis applied to TOF data the lattice strain is obtained from:

$$\varepsilon_{hkl} = \frac{t_{hkl} - t_{0,hkl}}{t_{0,hkl}} \tag{11}$$

Finally, a profile refinement on multipeak data (see Section 5.3) allows the determination of (quasi-)engineering strains through the lattice parameter a:

$$\varepsilon = \frac{a - a_0}{a_0} \tag{12}$$

In the above equations, the index zero indicates the stress free or reference parameter.

5.2.2. Generalized Hooke's law

When strains have been measured in three mutually orthogonal directions for a given location, say x, y and z, the normal stress components in these directions can be obtained through the generalization of Hooke's law:

$$\sigma_i = \frac{E}{1+\nu}\varepsilon_i + \frac{\nu E}{(1+\nu)(1-2\nu)}\left(\varepsilon_x + \varepsilon_y + \varepsilon_z\right),\ i = x, y, \mathrm{z} \tag{13}$$

Note that in cases where the strains have been obtained from a single peak analysis, *hkl*-specific diffraction elastic constants must be used for this calculation. For full stress tensor determination, strain measurements at the same location in at least six independent directions are necessary. The applicable mathematics are described in the following section.

5.2.3. Measured *d* spacings and full stress tensor determination

In the following, some practical guidelines are given on the calculation of stress tensor components from measured lattice strains. The direction (φ, ψ) of a measured strain is defined in the specimen reference frame [1], as illustrated in Fig. 28.

The following system of equations expresses strain in terms of stress for a general direction (φ, ψ) of the scattering vector $\boldsymbol{q}$.

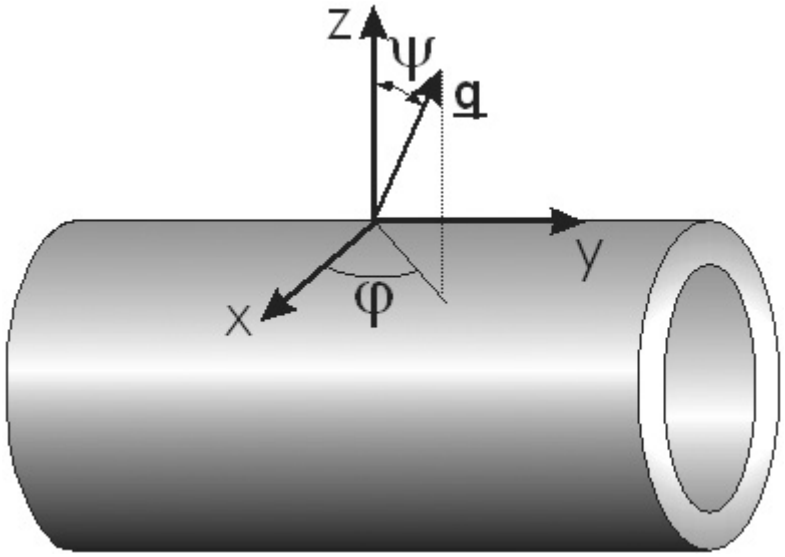

FIG. 28. Example for the definition of the sample reference frame.

$$\varepsilon(\varphi,\psi,hkl)=\frac{d(\varphi,\psi,hkl)-d_0}{d_0}=F_{11}\sigma_{11}+F_{22}\sigma_{22}+F_{33}\sigma_{33}+F_{23}\sigma_{23}+F_{13}\sigma_{13}+F_{12}\sigma_{12}$$

$$F_{11}(\varphi,\psi,hkl)=\frac{1}{2}s_2(hkl)\,\sin^2\psi\,\cos^2\varphi+s_1(hkl)$$

$$F_{22}(\varphi,\psi,hkl)=\frac{1}{2}s_2(hkl)\,\sin^2\psi\,\sin^2\varphi+s_1(hkl)$$

$$F_{33}(\varphi,\psi,hkl)=\frac{1}{2}s_2(hkl)\,\cos^2\varphi+s_1(hkl) \qquad (14)$$

$$F_{12}(\varphi,\psi,hkl)=\frac{1}{2}s_2(hkl)\,\sin^2\psi\,\sin 2\varphi$$

$$F_{13}(\varphi,\psi,hkl)=\frac{1}{2}s_2(hkl)\,\sin 2\psi\,\cos\varphi$$

$$F_{23}(\varphi,\psi,hkl)=\frac{1}{2}s_2(hkl)\,\sin 2\psi\,\sin\varphi$$

The system in Eq. (14) is written such that it forms a system of linear equations [1] which can be solved by freely available computer codes such as LAPACK [83] or Numerical Recipes [84]. It is by no means the only possible method but it has the advantage that stress constraints can be easily incorporated through the 'fixing' and 'freeing' of parameters. The factors F_{ij} are called stress factors. Equation (14) can be further transformed such that it expresses measured d spacings in terms of stress factors and d_0:

$$d(\varphi,\psi,hkl) = d_0^{(c)}F_{11}\sigma_{11} + d_0^{(c)}F_{22}\sigma_{22} + d_0^{(c)}F_{33}\sigma_{33} + d_0^{(c)}F_{23}\sigma_{23} + d_0^{(c)}F_{13}\sigma_{13} + d_0^{(c)}F_{12}\sigma_{12} + d_0 \quad (15)$$

Equation (15) can be approximated as a linear equation by keeping $d_0^{(c)}$ as a constant and d_0 as a variable. This is usually permissible because the approximation error of keeping $d_0^{(c)}$ as a constant is very small (of the order of $10^{-3}\sigma_{ij}$). A constraint on the stress tensor such as $\sigma_{33} = 0$ can be used to estimate d_0 through Eq. (15). This is particularly useful for measurement problems that do not allow the extraction of stress relieved coupons but where measurement locations involve close proximity to free surfaces or thin walled structures where one stress component (thickness direction) can be reasonably expected to be small.

It should be mentioned that another approach has been more frequently implemented recently. Known as the stress and strain orientation distribution function (SODF) [85, 86] these methods essentially determine the probable stress/strain tensors of single crystallites from the measurement of 'strain pole figures'. Strain pole figures are measurements of d spacing for a number of specimen orientations (hkl, φ, ψ) — hence the name pole figure which typically entails intensity measurements for many specimen orientations. By employing methods of texture analysis — where the goal is the estimation of the grain orientation distribution function ODF — the SODF is an estimation of the stress and strain tensor associated with each grain orientation. Because the SODF may contain orientation dependent microstresses, all six components of the stress/strain tensor are non-zero, which makes the number of unknown parameters in the SODF six times larger than in the ODF. As a result, the determination of the SODF requires a large number of measurements, both in terms of specimen directions (φ, ψ) and in the number of independent (hkl). Particularly the requirement of measuring several (hkl) makes TOF methods well suited for the determination of the SODF.

5.2.4. Elastic constants with and without texture

Because of plastic strain or recrystallization, preferred grain orientation is present to varying degrees in almost all engineering materials. The main effect of texture on neutron diffraction stress analysis is limited to materials with appreciable elastic anisotropy such as Cu, Fe, Ni, Ti and medium to strong texture [87]. In this case, the diffraction elastic constants are orientation dependent, and F_{ij} in Eq. (14) has to either be calculated in a different way [1, 87] or measured in a sufficient number of directions. Examples of the range of effects from weak to strong texture on the diffraction elastic constants in steel, both for neutron and X ray diffraction, can be found in Ref. [84]. In materials with

low elastic anisotropy such as aluminium and its alloys, the texture effect on the diffraction elastic constants is small regardless of the strength of the texture [88].

Generally, it can be said that TOF diffraction is the method that is the least sensitive to texture because of the averaging effect of having many (*hkl*) included in the data analysis. A single reflection (*hkl*) as obtained from a monochromatic instrument will be more sensitive to texture but even here the sensitivity to texture is limited if the measurement directions coincide with the principal axes of the specimen. Similar to X ray diffraction, off-axis neutron measurements can be severely affected by texture. For example, one should be careful in using the $\sin^2 \psi$ technique with neutrons because of the possibility of nonlinear $\varepsilon(\sin^2 \psi)$ behaviour. The estimation or calculation of such effects on diffraction stress measurements is rather complex. However, software has recently been made available for free download that accomplishes all the major steps involved. This includes calculations with and without texture, all grain elasticity models sensitive to texture, the input of texture information through the orientation distribution function, the calculation of bulk elastic constants and the calculation of stresses from measured *d* spacings [81, 89]. Also supplied are supplemental data such as single crystal elastic constants, pole figures, orientation distribution functions and diffraction elastic constants. Using these data, it is possible to decide if the effect of texture on the stresses needs further investigation.

The following examples illustrate how large the variation of diffraction elasticity constants in a single material can be. These data were taken from Ref. [90]. The values presented have been calculated for a material with no preferred orientation and based on an approach combining the Reuss [91] and Voigt [92] methods. Table 1 [89] shows values for five different crystallographic planes for an austenitic steel, which has the face centred cubic structure and Table 2 [89] shows values for a ferritic steel, which has a body centred cubic structure.

5.2.5. Helpful software

In general, neutron facilities use their own custom software for peak fitting and stress calculation. A notable exception is the software used at TOF diffractometers where Rietveld refinement programs play a central role. These programs can be generally obtained free of charge, and they cover a wide range of needs for obtaining strain/*d* spacings from diffraction data. Beyond peak fitting, it is often necessary to calculate elastic constants (see Section 5.2.4) or to measure texture in order to calculate the ODF. Without claiming completeness, the list in Table 3 [89, 93–97] provides a starting point for assembling software tools that satisfy reoccurring needs in diffraction stress analysis.

TABLE 1. DIFFRACTION ELASTIC CONSTANTS FOR FIVE DIFFERENT CRYSTALLOGRAPHIC REFLECTION PLANES IN AN AUSTENITIC STEEL

	Austenitic steel (face centred cubic structure)				
Crystallographic reflection plane	(111)	(200)	(220)	(311)	(331)
E_{hkl} [GPa]	247	139	207	175	217
υ_{hkl}	0.24	0.35	0.28	0.31	0.27

TABLE 2. DIFFRACTION ELASTIC CONSTANTS FOR FIVE DIFFERENT CRYSTALLOGRAPHIC REFLECTION PLANES IN A FERRITIC STEEL

	α iron (body centred cubic structure)				
Crystallographic reflection plane	(110)	(200)	(211)	(310)	(222)
E_{hkl} [GPa]	220	165	220	181	248
υ_{hkl}	0.28	0.33	0.28	0.32	0.25

TABLE 3. INDUSTRY SOFTWARE TOOLS FOR DIFFRACTION STRESS ANALYSIS

Name of software	Description	Download site
MAUD	Written in Java. Can run on Windows, Mac OSX, Linux and Unix. It is a general diffraction analysis program mainly based on the Rietveld method, but not limited to it. Works with X ray, synchrotron, Neutron, TOF. Texture and residual stress analysis using part or full spectra.	[93]
GSAS	A widespread used structure refinement and peak fitting program for TOF patterns. Available for a multitude of platforms. Actively maintained.	[94]

TABLE 3. INDUSTRY SOFTWARE TOOLS FOR DIFFRACTION STRESS ANALYSIS (cont.)

Name of software	Description	Download site
IsoDEC	Calculation of diffraction elastic constants (DECs) with and without texture, calculation of stress from *d* spacings, calculation of bulk elastic constants. Windows based program. Recent release and actively maintained.	[89]
DECCalc	Matlab based calculation of DEC without texture. Recent release.	[95]
popLA	DOS based texture analysis package, orientation distribution function estimation, pole figure plotting. Sporadically maintained.	[96]
MTEX	Matlab based texture analysis package, Contains a comprehensive list of analysis and visualization tools for texture analysis. Actively maintained.	[97]

5.3. METHODS FOR SINGLE PEAK AND MULTIPEAK ANALYSES

5.3.1. Determination of profile parameters of a single diffraction line

An elementary treatment assumes that the profile, $m(x)$, of a diffraction line can be described by an analytical function, which is dependent on three parameters: amplitude, position and width. For instance, if the diffraction profile is expressed in normalized Gaussian form, then

$$m_G(x) = A\exp(-x^2/2\sigma^2)/(2\pi)^{1/2}\sigma \quad (16)$$

where $x = \xi - \overline{\xi}$ is the difference between experimental variable and its mean value, A is the peak amplitude, σ is the standard deviation and $\sigma^2 = \overline{(\xi - \overline{\xi})^2}$ is the variance for $m_G(x)$. As the experimental variable ξ, the scattering angle 2θ or the TOF t, can be used for monochromatic or TOF instruments, respectively. The mean value $\overline{\xi}$ can be used as the peak position. The full width at half maximum (FWHM or w):

$$w = 2(2\ln 2)^{1/2}\sigma = 2.355\sigma \tag{17}$$

or the so-called integral width:

$$\Gamma = \int m(\xi)d\xi/m(0) = A/(A/(2\pi)^{1/2}\sigma) = (2\pi)^{1/2}\sigma = 2.507\sigma \tag{18}$$

are often used to describe the peak width. In Eqs (17) and (18) the numbers are indicated for the Gaussian distribution (16). Only the integral width is considered a parameter which should be used for microstress analysis, because it can be correctly connected (in a physical sense) with deformations in the material. However, from the point of view of numerical estimations, there is not much difference between w and Γ, and in practice, the FWHM is often applied.

Another often used analytical function for describing diffraction line shape is the Lorentz (also called Cauchy or Cauchy-Lorentz) distribution:

$$m_L(x) = A/[1 + (2x/w)^2] \tag{19}$$

where, as before, $x = \xi - \overline{\xi}$ and W is the FWHM. It can be shown that only this distribution correctly describes the broadening component attributable to finite crystallite size. If both strain and size effects are important, a diffraction line can be thought of as a convolution of a Gaussian and a Lorentzian distribution, which is called a Voigt function. Finally, the peak profile can also be described with a linear superposition of these functions, which is known as a pseudo-Voigt function.

In a general case the function $m(x)$ measured in an experiment is defined by the instrumental parameters and the sample microstructure and can be expressed as a convolution of the instrument resolution function $R(x)$ and the coherent neutron scattering cross-section $S(x)$:

$$m(x) = \int R(x' - x)\cdot S(x')dx' \tag{20}$$

where the integration limits are supposed to be infinite ($\pm\infty$). The function $R(x)$ can be determined by an experiment with a suitable standard powder sample, which diffracts with a coherent scattering cross-section with a discrete set of narrow δ like peaks. Alternatively, $R(x)$ can be simulated based on detailed information about the instrument. Usually the dependence of $R(x)$ on $\overline{\xi}$ is smooth and can be easily described by an analytical function with several parameters. All microstructural crystal properties (structural imperfections), i.e. finite size of coherently diffracting domains, lattice distortions, stacking faults, dislocations etc. should be included in $S(x)$ as a set of appropriate parameters.

The refinement of the parameters for the function $m(x)$ is performed by a least squares fit of the experimental data m_{exp}, measured as a set of discrete points, i.e. the sum of squares to be minimized is:

$$\chi^2 = \sum_i \omega_i (m_{\mathrm{exp},\,i} - m_{\mathrm{cal},\,i})^2 \tag{21}$$

where $m_{\mathrm{cal},\,i}$ is $m(x)$ calculated for the ith point and ω_i is the weight of the ith point. The sum is taken for all measured points.

For describing the background intensity a polynomial of the first or second degree should be added. To be sure of the separation of diffraction and background intensities, the boundaries of the measured range should be at a distance of at least ±2 W from the peak position (Fig. 29). The parameters obtained after the least squares fit can then be analysed from the point of view of the microstructure of the material. Apart from the profile parameters, the estimation of the corresponding statistical uncertainties can be obtained by a least squares fit, and in addition, correlations between parameters are also taken into account.

If the shape of diffraction lines cannot be described by any analytical function, the experimental profile m_{exp} is considered as a distribution function, which is used for the calculation of the position and breadth of the peak. The peak position is defined as its centre of gravity:

$$\bar{\xi} = \sum_i \xi_i \, m_{\mathrm{exp},\,i} \Big/ \sum_i m_{\mathrm{exp},\,i} \tag{22}$$

i.e. $\bar{\xi}$ is the mean value of the experimental variable (scattering angle, 2θ, or TOF, t), which can be recalculated into mean value of lattice spacing, d_{hkl}.

To calculate the width of a peak, Eqs (17) or (18) can be utilized, where the variance is defined as:

$$\sigma^2 = \sum_i \left(\xi_i - \bar{\xi}\right)^2 m_{\mathrm{exp},\,i} \Big/ \sum_i m_{\mathrm{exp},\,i} \tag{23}$$

The statistical uncertainties of the parameters obtained can be calculated in accordance with the usual rules that are described in textbooks.

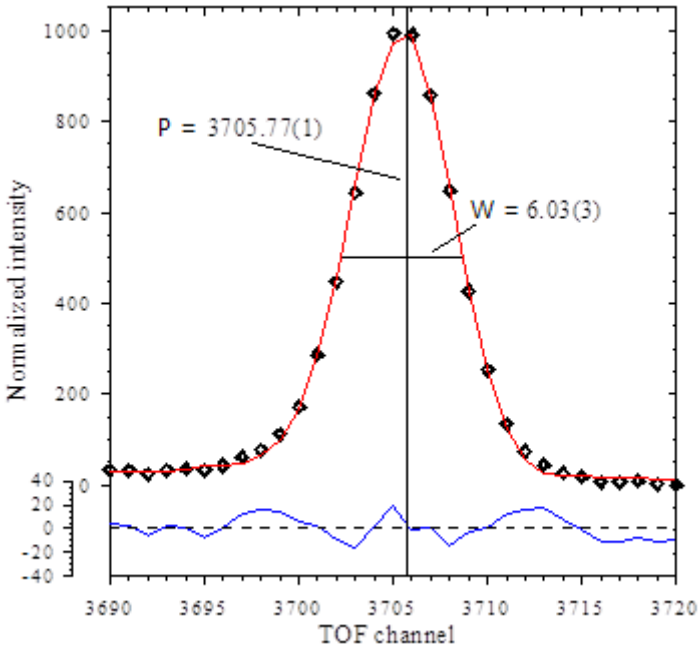

FIG. 29. Example of a least squares fit of a diffraction peak measured at a TOF diffractometer. The experimentally measured peak shape function was used. The smooth line through the points was calculated according to the fit results. The difference between the experimental and the calculated values is also shown (blue line). The uncertainty (of the last digit) of the refined parameters (position and width) is shown in parenthesis.

As neutron strain scanning becomes more effective, data from many positions in a specimen may be measured and under these circumstances it is common to fit the peak using automated scripted procedures so that the actual peak fitting is not closely inspected. To overcome this potential deficiency it is recommended that sufficient inspection is made of the data fitting to ensure the quality of the final strain distributions.

5.3.2. Material and measurement characteristics influencing the parameters of a neutron peak

To obtain an accurate and reliable determination of the position of a diffraction peak, it is important to have sufficient data in the 'wings' of the peak to adequately describe the background to the signal. This can only be achieved through the geometric set-up of the experiment, and the quality of the data should be checked throughout the experiment. This is important since changes in strain

from point to point within the specimen will, of course, cause the peak to shift. This may lead to the peak being insufficiently defined and the resulted fitted peak position being erroneous.

As well as a simple shift of the Bragg reflection, internal mechanical deformations in a material can also influence the shape of a profile (e.g. its width or whether it is more Gaussian or more Lorentzian in shape).

For a thorough so-called profile analysis the resolution function of the instrument has to be taken into account. Its influence on the diffraction peak should be well known, especially if stress effects are not strong. One of the most fundamental problems is the separation of the strain related diffraction line broadening effects from other contributions: A well known non-strain-related contribution to broadening caused by small particle size is called size broadening. Inhomogeneity of the material can also cause broadening effects. The statistical distributions regulating the magnitude of the impact of the different contributors are generally unknown. This means that their approximation by any analytical function (e.g. Gaussian function) could be incorrect and the combined effect is ambiguous. Another important fundamental problem is accounting of the coherency of diffraction in polycrystalline media. It is known that at least in certain cases the conventional simplified approach based on the kinematical diffraction theory could be insufficient for correct data processing.

5.3.3. Determination of crystal microstructure by the Rietveld method

At present, the most general and conventional approach for the refinement of structural and microstructural parameters of polycrystalline materials from multipeak diffraction data is the Rietveld method, introduced for the first time in the late 1960s. The detailed description of this method including special features of neutron diffraction data processing can be found in a textbook by Willis [98]. It should be emphasized that the Rietveld method can be used for the refinement of a structure rather than for its determination, i.e. the model of the atomic structure must be known beforehand.

In the Rietveld method the measured diffraction pattern and background intensities are described by an analytical function with a set of experimental and structural parameters, which are refined by the least squares fitting. Equation (21) is minimized, whereby $m(x)$ represents the whole intensity (many diffraction peaks) in the wide range of experimental variables (scattering angle, TOF, or d spacing). The set of refined parameters includes lattice parameters, occupancy factors, coordinates and thermal factors for all independent atoms in the unit cell, background and microstructural parameters. The latter describe crystallographic texture, lattice distortions and coherently diffracting domain size.

The theory and practice of the structural analysis of powder diffraction data by the Rietveld method show that there is no sense in including diffraction peaks higher than $(3R)^1$, where R is the resolution of a diffractometer (where it is supposed that R does not strongly depend on d_{hkl}). Taking into account that stable refinement is possible when the number of peaks exceeds the number of parameters by approximately a factor of five, one can conclude that for $R = 0.001$, up to 70 experimental, structural and microstructural parameters can be refined.

Two most important advantages of the Rietveld method are the possibility of analysis of diffraction patterns with strongly overlapping lines and patterns from multiphase materials. The correlations between parameters are minimal. In contrast to other methods of diffraction pattern profile refinement, the Rietveld method makes it possible to refine relative phase content in a multiphase sample (Fig. 30). The necessity of structural model knowledge should be mentioned as a disadvantage. However, the latter is not a serious drawback because the atomic structure of materials in which internal stresses are determined is in most cases well known.

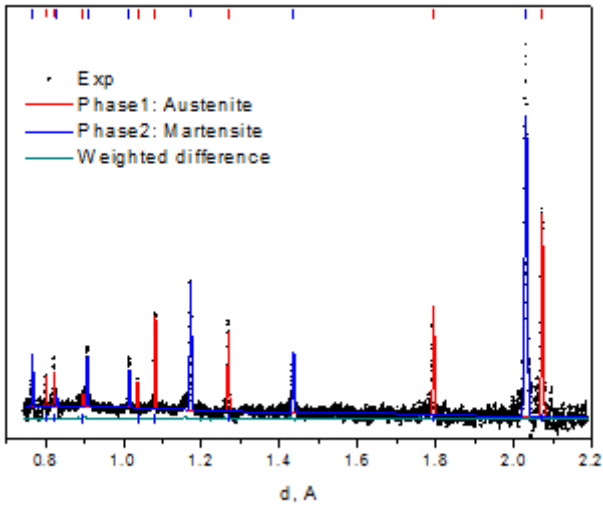

FIG. 30. Diffraction pattern of the austenitic steel after mechanical cycling, measured with a TOF diffractometer. Both phases, austenite and martensite, can be clearly seen. After data processing by the Rietveld method the following values were obtained for lattice parameters and volume fraction: $a_{Aust} = (3.588\ 21 \pm 0.000\ 05) \times 10^{-1}$ *nm,* $a_{Mart} = (2.871\ 39 \pm 0.000\ 05) \times 10^{-1}$ *nm,* $V_{Mart} = (52.4 \pm 1.9)\%$.

5.3.4. Relation between profile parameters and deformations

It should be noted that a single diffraction peak (*hkl*) measured with a fixed scattering geometry is a superposition of reflections from a particular set of crystallites with diffracting lattice planes d_{hkl} perpendicular to the scattering vector. Thus, for a single peak, Eq. (1) describes the deformation for the particular reflecting plane (*hkl*). On the contrary, a diffraction pattern measured with a TOF diffractometer over a wide range of *d* spacings consists of peaks originating from different sets of crystallites. If this pattern is processed by the Rietveld method, where all peaks are included, one obtains the average for the gauge volume lattice parameters. In this case by using Eq. (3) a and a_0, where a is a lattice parameter of the unit cell, the deformation averaged over many (*hkl*) planes is obtained (see, e.g., Ref. [99]).

The analysis of microstrains, which manifest themselves as diffraction peak broadening, is more complicated owing to a variety of reasons giving rise to broadening. Besides instrumental effects, there are several reasons with physical origins; the most important of them can be roughly classified as size and strain broadening. In a material without stresses the width of a peak, w_d, depends on the width of the resolution function, w_R. A contribution, w_s, connected with a small size of the diffracting domains can also exist (size effect). Microstresses produce a variance of lattice parameters and an additional contribution, w_ε, appears (strain effect). Usually it is supposed that statistical distributions containing w_R, w_s and w_ε are Gaussian distributions, and in this case:

$$w_d^2 = w_R^2 + w_\varepsilon^2 + w_s^2 \tag{24}$$

It can be shown that for an isotropic material $w_\varepsilon = \varepsilon d$ and $w_s = (k/L)d^2$, where $\varepsilon = \Delta a_s/a = \Delta d_s/d$, is the microstrain, L is the characteristic size of the coherently diffracting domains, $k \approx 1$ is a dimensionless coefficient depending on the domain shape. Owing to different dependences of w_ε and w_s on d, these can be easily determined if the width of the diffraction peaks is measured over a wide d spacing range and the relationship $w_R(d)$ for the resolution function is known.

For a conventional ($\lambda = \lambda_0 = \text{const}$) diffractometer it is convenient to express w_s and w_ε as functions of the Bragg angle: $w_\varepsilon = \varepsilon \tan\theta$, $w_s = (k\lambda_0/L)/\cos\theta$. It is possible to separate the size and the strain effects by combining these two equations and analysing the $w(\theta)$ dependence, which is known as the Hall-Williamson method [100]. For a TOF diffractometer, the d dependence is more natural.

Macro and microstrain determination by measuring positions and widths of diffraction peaks is as a rule not so simple. The strain effects are often very small and for their detection the instrument resolution must be high and the resolution

function must be well known. The Gaussian distribution is not correct for any effects; in particular, the size effect can be better described by a Lorentzian function, and therefore Eq. (24) is not valid. Both size and strain peak broadening effects can be anisotropic, i.e. dependent not only on the d_{hkl} value, but also on the direction in the lattice. Finally, both positions and widths of diffraction peaks can be influenced by some other types of structural imperfections besides internal mechanical deformation and finite size of diffracting domains. For instance, stacking faults and dislocations can shift diffraction peaks from nominal positions, while peak broadening can be connected with compositional inhomogeneity. A review of present day methods for diffraction line profile analysis can be found in Ref. [101].

5.4. ASSESSMENT OF THE UNCERTAINTIES

Reference [3] states that "the uncertainty in a measured parameter is an estimate of the lack of knowledge in the true value of the parameter". Providing an appropriate estimate of the uncertainty of a measured strain or stress is therefore of equal importance to the measurement result itself, as this provides an indication for the reliability of the measurement.

In accordance with Refs [102, 103] all potential contributors (x_i) to the uncertainty in a measurand (say, ε) need to be taken into consideration in the determination of the uncertainty $u(\varepsilon)$ through:

$$u^2(\varepsilon) = \sum_{i=1}^{N} \left(\frac{\partial \varepsilon}{\partial x_i} \right)^2 u^2(x_i) \tag{24}$$

When analysing the data, the following main potential contributors to the uncertainty in strain measurement should always be taken into consideration.

— The uncertainty in the measurement of θ, d or t and their respective stress free (θ_0, d_0, or t_0) values is the most import contribution to strain uncertainty from a diffraction measurement in accordance with Eqs (25) and (26) and should always be taken into consideration. These figures and their uncertainties are derived from the fitting of the neutron count data.
— The uncertainty in the wavelength of the incident beam is derived from the calibration of the instrument set-up following Section 3.5. On a properly calibrated instrument, this contribution is usually small. Nevertheless, if the possibility of mechanical instabilities or temperature variations at the

monochromator position exists, such contributions need to be estimated and included in the uncertainty assessment.

— When variations in temperature or chemical composition of the specimen as a function of position or time can possibly occur, these need to be considered because both influence the lattice spacing of the material under investigation.

— Section 3.6.5 states that it is often possible to determine the measurement position within the specimen to within 0.1 mm. In complicated set-ups this accuracy may not be achievable. When strain measurements are performed in regions with steep strain gradients, the uncertainty in measurement position within the specimen directly translates into an uncertainty in strain.

A simple example for a monochromatic instrument that in practice is often applied is a case where only the fitting uncertainty in the diffraction angles (θ, θ_0) is considered as a contributing factor; Eq. (25) becomes:

$$u(\varepsilon)^2 = \cot^2 \theta_0 \cdot (\Delta\theta^2 + \Delta\theta_0^2) \tag{26}$$

Although other contributors to uncertainty are often neglected, this is not always appropriate and should only be done after ensuring that these contributions would really be negligible.

Based on Eq. (13) in Section 5.2.2, the magnitude of a normal stress tensor component depends on the lattice strains measured in three orthogonal directions and corresponding diffraction elasticity constants.

In combination with Eq. (25), this translates into an estimation of the uncertainty for the stress tensor component in the *x* direction as follows:

$$\begin{aligned} u^2(\sigma_x) = & \left(\frac{(1-\nu_{hkl})E_{hkl}}{(1+\nu_{hkl})(1-2\nu_{hkl})} \right)^2 \cdot u^2(\varepsilon_x) \\ & + \left(\frac{\nu_{hkl}E_{hkl}}{(1+\nu_{hkl})(1-2\nu_{hkl})} \right)^2 \cdot \left(u^2(\varepsilon_y) + u^2(\varepsilon_z) \right) \\ & + \left(\frac{\partial \sigma_x}{\partial E_{hkl}} \right)^2 u^2(E_{hkl}) + \left(\frac{\partial \sigma_x}{\partial \nu_{hkl}} \right) u^2(\nu_{hkl}) \end{aligned} \tag{27}$$

For the determination of the uncertainty in the stresses, the practice of neglecting the contributions of the elastic constants is also frequently applied. It is admittedly not always easy to quantify the uncertainties of the elastic constants themselves, but one should keep in mind that the uncertainty contributions

related to the elasticity constant are growing with the absolute values of strain at the measurement location concerned, i.e. the larger the strains are, the larger these contributions become.

In summary, it should be kept in mind that the assessment of the uncertainty is an integral part of the strain and stress determination and its importance can hardly be underestimated.

6. EXAMPLES OF APPLICATIONS

Typical samples that are successfully investigated by neutron diffraction to determine residual stress states are crankshafts, pistons, turbine blades, wheels, impellers, shot peened components, welds and composite materials.

Real life specimens are often of a complicated shape or material, making the measurements challenging. For example, aluminium components often have large grains, which necessitates either the use of a large gauge volume or specimen rocking during measurement in order to mitigate the effect of the grain size on the measurements. Thus the spatial or angular resolution can be significantly reduced. Titanium is also a difficult material to measure due to its large incoherent scattering, which increases the background.

The determination of the strain free reference value is often the most challenging part of an investigation. A number of approaches to this challenge are described in Section 3.6.4.

6.1. MEASUREMENTS OF STRESS/STRAIN STATE INDUCED BY A WELD DEPOSITED PASS

Using the strain diffractometer installed at the reactor LVR-15 in Řež, Czech Republic, the macrostrain distribution was measured in the vicinity of two different welds from Inconel 52 deposited on steel plates from 15Ch2MFA. This steel is used for the construction of reactor vessels. The thickness of the plates was 7 mm and the welds were deposited in form of a single bead or six beads in two layers. The single and the six bead welds had a height of 1 mm and 3.5 mm and width of 5 mm and 12 mm, respectively (see Fig. 31).

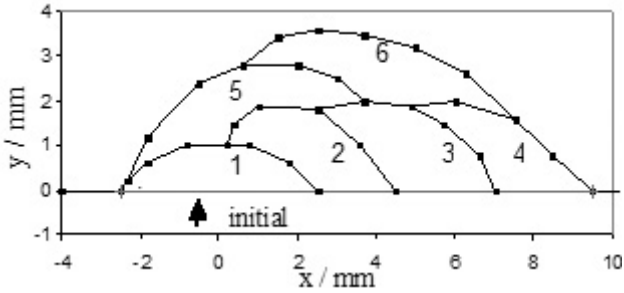

FIG. 31. Diagram displaying the sequence of welding.

The extent of the fusion zone in the strain scanning direction was approximately 0.3 mm. The gauge volume of 2 × 2 × 3 mm^3 was located in the middle of the plate, i.e. at a depth of 3.5 mm, and the scanning was carried out along a line going orthogonally across the weld. Measurements were performed using the α-Fe (110) reflection plane. Figure 32 displays a photograph of one of the plates with the single bead (the welding direction is indicated by an arrow) and the results of the macrostrain scanning for both samples. Axes x, y and z are parallel to the longest edge of the plate, the medium wide edge and the shortest edge, respectively. For calculation of the macrostrain values, the strain free Bragg angle position was measured at the corner of the plate.

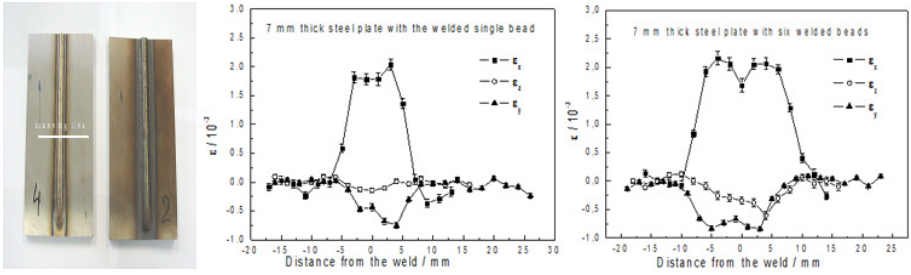

FIG. 32. Photo of the plate of 15Ch2MFA with a single bead weld and the measured strain components vs. the distance from the weld passes for both samples.

6.2. RESIDUAL STRESSES IN A BIMETALLIC STAINLESS STEEL ZIRCONIUM ADAPTER

A bimetallic stainless steel zirconium adapter [104] is used in some structures of RBMK reactor channels. This adapter is a complex cross-section cylinder (Fig. 33) with a steel outer layer and a zirconium alloy inner layer. It is manufactured by vacuum sintering at a temperature of 900°C. The thermal expansion of steel is three times larger than that of zirconium. The steel shell compresses the zirconium part when the adapter is being cooled down, which introduces residual stresses inside the bimetallic joint. These stresses could be a reason for crack nucleation or adapter failure. The aim of this work is to investigate the residual stress state of the stainless steel near the steel–zirconium alloy splice. The investigated regions are shown in Fig. 33 as cross-section A-B, cross-section 2 and cross-section 3. Experience shows that cross-section A-B is the most critical in view of fatigue failure where the so-called first zirconium screw tooth exists.

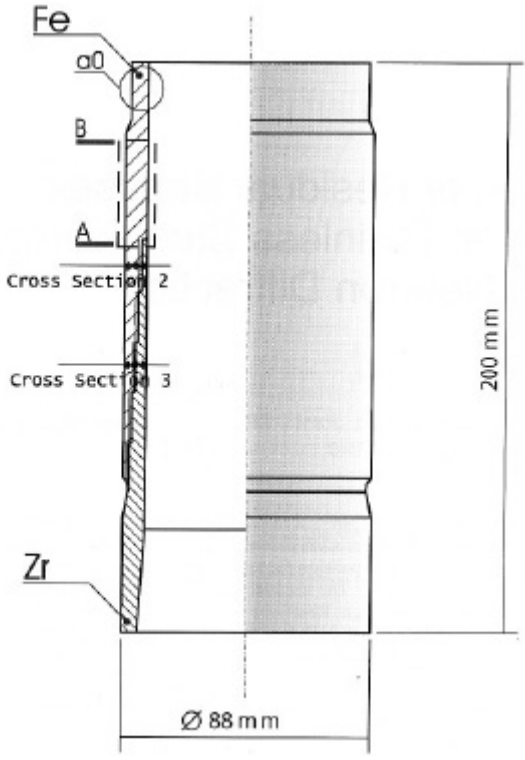

FIG. 33. An adapter in an RBMK reactor.

The study was performed using neutron diffraction on an FSD at the IBR-2 pulsed reactor in Dubna, Russian Federation, and on a high resolution neutron diffractometer at the LVR-15 reactor in Řež, Czech Republic. The measured results are shown in Fig. 34, from which it can be seen that residual stresses in all three cross-sections are compressive and therefore should have a beneficial influence on the fatigue performance of the adapter, which works under tensile load conditions. The important factor is the presence of a stress concentrator in cross-section A-B, close to the junction of the steel and zirconium parts of the adapter. In Fig. 34 this location is indicated by a thin circle.

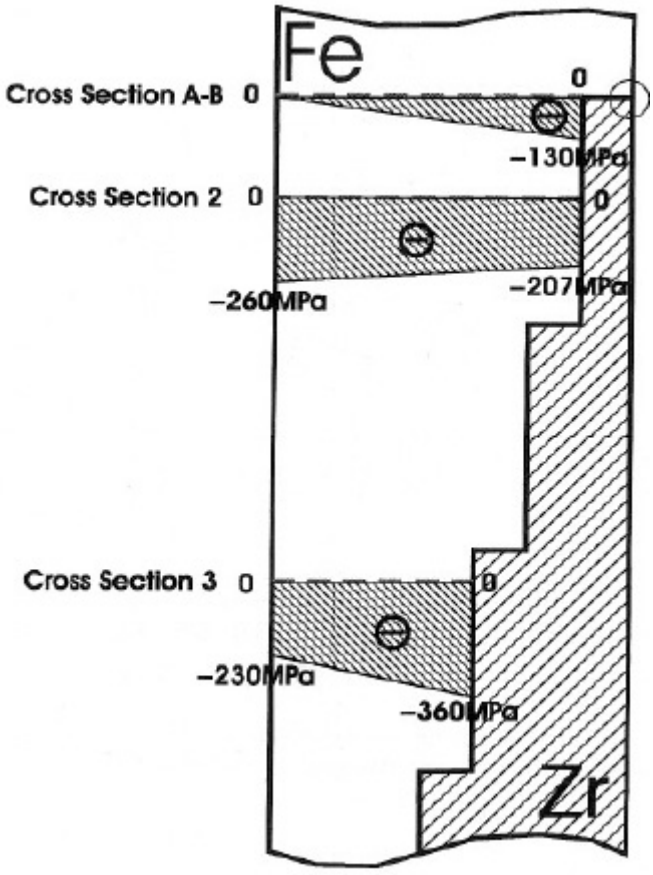

FIG. 34. The measured residual stresses in the stainless steel part in the various cross-sections of the adapter. The wall of the adapter is shown in the region of the critical cross-sections. The thin circle indicates the location of the stress concentrator.

6.3. MEASUREMENT OF RESIDUAL STRESSES IN A BIMETALLIC NUCLEAR PIPING WELD

Numerous light water reactors for nuclear power production in existence in the world operate with a primary piping system made from stainless steel components. Such stainless steel piping is welded to pressure vessel nozzles that are made of low alloy ferritic steels in virtually all cases. In such dissimilar metal — or bimetallic — welds, the residual stresses do not only originate from the welding process, but they are also generated through the thermomechanical mismatch of the different materials involved.

On the HB4 Large Component Neutron Diffraction Facility at the High Flux Reactor in Petten, the Joint Research Centre has performed a series of measurements in a reduced size mock-up of such a bimetallic piping weld. In this particular experiment, the specimen was made of a ferritic steel grade A508 welded to a stainless austenitic steel grade 304L by applying a buttering layer and subsequently a multipass V groove circumferential weld. The specimen was 168 mm in diameter, ~400 mm in length and had a wall thickness of 25 mm. Figure 35 shows the specimen on the diffractometer during measurements in the piping circumferential direction, i.e. the hoop direction. The interface between the low alloy steel and the stainless steel buttering layer can be easily recognized. A hole was cut into the specimen for these measurements in order to reduce the neutron path length through the material. In the picture the incident neutron beam duct is positioned inside this hole so that the incident beam aperture is close to the measurement position.

Many of the measurement locations for this specimen were actually within the weld material. Welded regions often exhibit inhomogeneities and variations of the free-of-stress parameter in diffraction experiments. For this reason, dedicated reference specimens have been used here in order to account for such variations as much as possible. One of the reference specimens can be seen in Fig. 35 at the bottom, in front of the piping specimen.

The main aim of such measurements, in particular in relation to nuclear applications, is to provide for the validation of numerical predictions of the residual stresses. Figure 36 shows the measured residual stresses, along a line 3 mm from the outer surface of the pipe parallel to its axis, in comparison to the corresponding residual stress data derived from two different approaches for prediction. The blue line has been derived from a simplified approach where the welding process itself has not been modelled at all. In this case only a simple cooling from an elevated temperature of about 500–600°C has been modelled, whereby the residual stresses were generated by the mismatch of the materials during cooling [105]. The green line stems from a detailed bead by bead two dimensional simulation process [106].

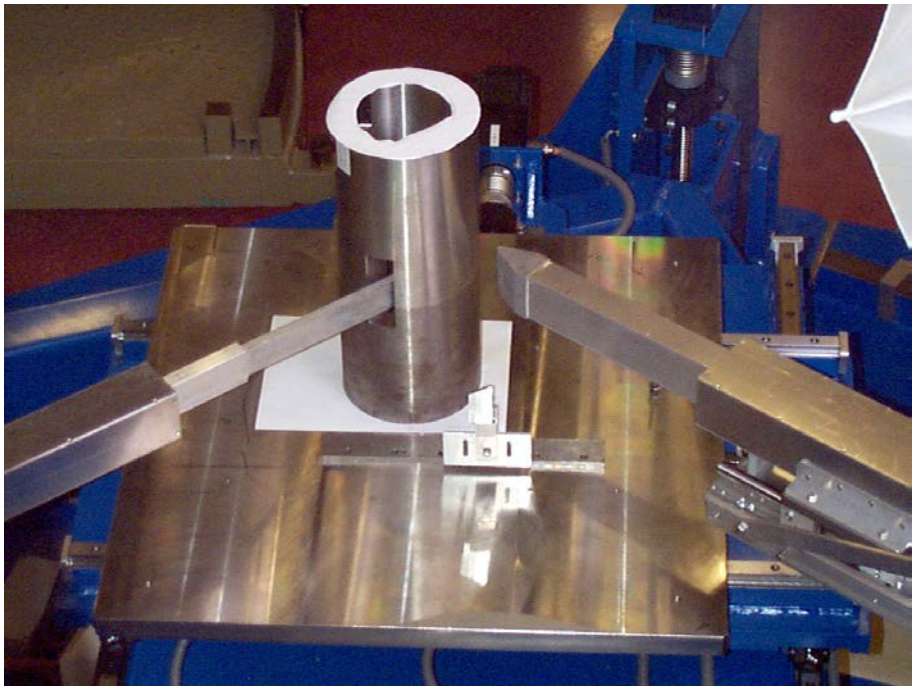

FIG. 35. Bimetallic piping weld specimen during hoop direction measurements at the HB4 Large Component Neutron Diffraction Facility at the HFR Petten. The incident neutron beam duct is on the left and the diffraction neutron beam duct is on the right. At the front end of the diffracted beam duct, the cadmium mask providing for the beam aperture can be seen.

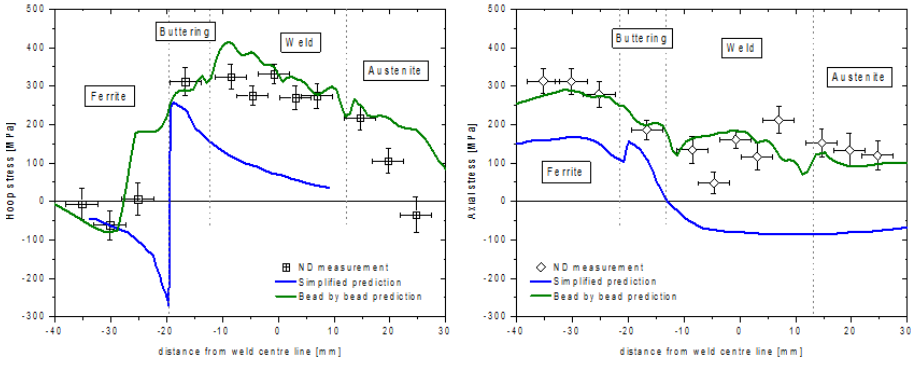

FIG. 36. Hoop (left) and axial (right) residual stresses near the outer wall of a 25 mm thick bimetallic piping weld. The data points correspond to the neutron diffraction measurements (horizontal error bars indicate gauge volume dimension); the blue and green lines correspond to the simplified and detailed numerical predictions, respectively.

It can be seen that, in this case, the results produced by the more detailed simulation compare much better to the measurement results than those from the simplified analysis do. The simplified analysis has also produced a significant underprediction of the residual stresses, which means that this approach should definitely not be used for component integrity analyses.

7. FUTURE TRENDS IN RESIDUAL STRESS MEASUREMENTS

7.1. INSTRUMENTS AT STEADY STATE SOURCES

The neutron stress/strain scanner evaluates the variations of lattice spacing within a sample with a spatial resolution of the order of millimetres given by the dimensions of the gauge volume. It is, in fact, a powder diffractometer equipped with a position sensitive detector (PSD) optimized with respect to luminosity and resolution in a limited range of scattering angles $2\theta_S$ [4, 107]. The preferred scattering geometry for the strain measurements is at $2\theta_S \approx 90^o$ when the investigated gauge volume has a rectangular form (see Fig. 37). As the strains $\varepsilon = \Delta d/d$ (d is the lattice spacing) in the material are usually of the order of 10^{-4}, a sufficiently high resolution in $\Delta d/d$ of the instrument is required.

A higher resolution of a conventional powder diffractometer equipped with a mosaic monochromator can be achieved when using a large monochromator take-off angle, $2\theta_{M,}$ (usually larger than 90°) in combination with an acceptable mosaicity of the monochromator. Figure 38 shows an example of the resolution function of the conventional powder diffractometer for two strongly different values of the take-off angles [98, 108]. On the other hand, using a larger take-off angle means that a lower neutron flux is delivered to the sample as the angle is proportional to the monochromatized wavelength spread $\delta\lambda_M = \lambda\Delta\theta \cot \theta_M$ ($\Delta\theta$ is the angular divergence of the beam) [109]. Therefore, some compromise in the choice of $2\theta_M$, the mosaicity of the monochromator and the dimensions of the gauge volume has to be made. Typically, stress/strain diffractometers equipped with mosaic monochromators operate at $2\theta_M \approx 90°$ and with a scattering angle $2\theta_S \approx 90°$ and with a resolution FWHM ($\Delta d/d$) of approximately $(5 – 10) \times 10^{-3}$. The resolution is influenced by the mosaicity of the monochromator, the $\Delta\lambda/\lambda$ value of the monochromatized beam, any collimations of the beam before and after the monochromator and of course, by the value of the monochromator take-off angle $2\theta_M$ [99, 108]. For a given diffractometer setting, the resolution can be improved by decreasing the beam divergence by using finer soller collimators

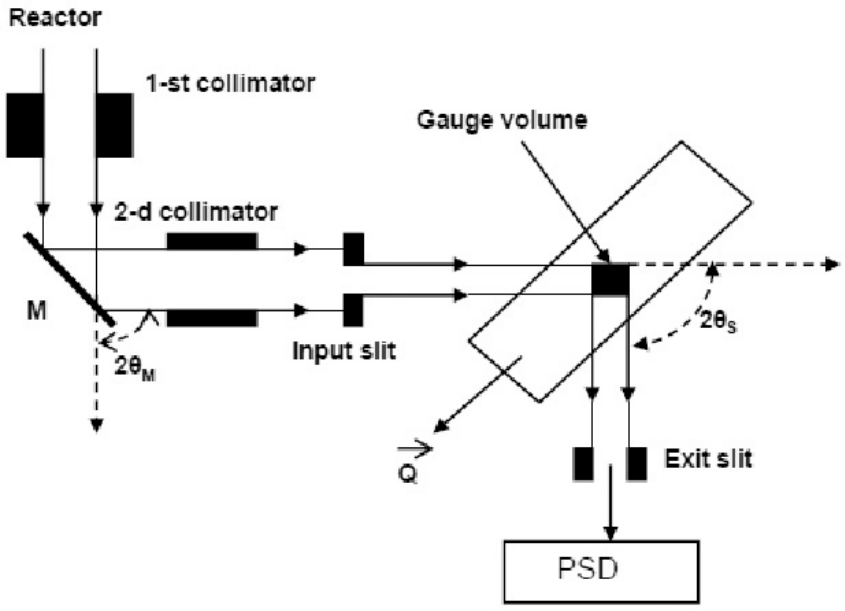

FIG. 37. Diagram of the neutron diffraction stress/strain scanner.

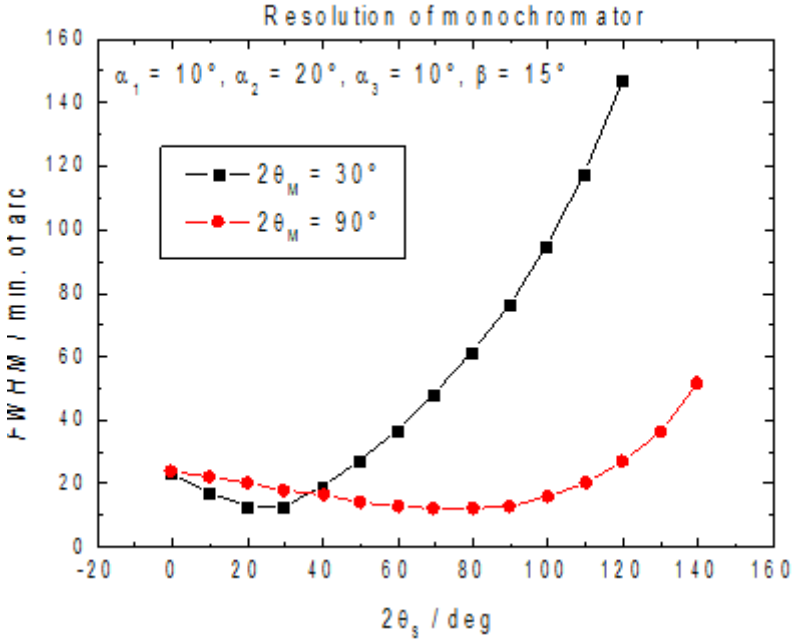

FIG. 38. Example of the resolution function of the powder diffractometer for two monochromator take-off angles.

in combination with a mosaic monochromator with a rather low mosaic spread. However, this results in a considerable limitation of the monochromatized neutron flux delivered to the sample [109].

Concerning future trends in residual stress and strain measurements, two goals can be mentioned:

(a) The possibility of measuring at a greater depth, e.g. up to 5–10 cm in steel samples. At present, the dedicated stress/strain scanners installed at high flux neutron sources can effectively carry out measurements in steel samples at depths of approximately 3 cm.
(b) The possibility of measuring near the surface in the range of 0.01–0.1 mm. At present, the dedicated stress/strain scanners installed at high flux neutron sources (e.g. at the ILL) can effectively carry out near surface measurements in steels in the range of 0.1–0.5 mm [26].

Achievement of these goals always requires a sufficient increase of the neutron flux so as to deliver suitable properties to the sample. It can be done by installing dedicated instruments at high flux neutron sources (existing and yet to be built sources) fully employing neutron optics (focusing guide tubes, focusing lenses, focusing mirrors, focusing monochromators, focusing in scattering). The simplest way of increasing the neutron flux delivered on the sample is to use a vertically focusing monochromator with mosaic as well as focusing crystals. It is well known that vertical focusing (perpendicularly to the scattering plane) has practically no influence on the resolution of an instrument. Depending on experimental conditions, vertical focusing can increase the monochromatic neutron flux by a factor of 2–5. This section deals with Bragg diffraction based on the use of cylindrically bent perfect crystal focusing monochromators. A big step towards the improvement of the properties of neutron diffraction stress/strain scanners was the employment of bent perfect crystal monochromators, which are discussed in the following subsections.

7.1.1. Horizontally focusing monochromator at a large take-off angle

The situation differs considerably when using horizontally focusing bent crystal monochromators instead of mosaic ones (see Fig. 39) [44, 45, 50], which has several advantages for optimized focusing performance. First of all, this kind of monochromator works with open beams without any soller collimators. All parameters — effective mosaicity, collimation α_2, $\Delta(2\theta_S)$ and FWHM of the diffraction profile — can be predicted. Details of this performance and the related formulas necessary for the optimization of the instrument performance have been already discussed in Section 3.8.1. It should be pointed out that the

effective mosaicity of the bent perfect crystal is typically smaller than the mosaic counterpart by a factor of 5–10. However, in this case the same property is also valid related to the instrument luminosity, i.e. using larger monochromator take-off angles leads to lower neutron flux due to the smaller wavelength spread $\delta\lambda_M$ delivered to the sample according to $\delta\lambda_M/\lambda = \Delta\theta \cot \theta_M$. This is due to the focusing of the monochromatic beam on the sample as well as the scattering angles from the sample (quasi-parallel beam $\Delta(2\theta_S)$. This type of focusing is mostly used for neutron stress and strain scanners installed at neutron sources with constant neutron flux (reactors). In the case of $2\theta_M \approx 2\theta_S \approx 90^o$ the optimized diffractometer performance with the sample at the focal distance f of the bent monochromator ($f = L_{MS} = (R_{opt}/2) \sin \theta_M$) has a very interesting property, namely that those neutrons which are diffracted by the sample also have quasi-parallel trajectories before the monochromator ($\alpha_1 \approx 0°$). However, this is not valid when $2\theta_M \neq 2\theta_S$.

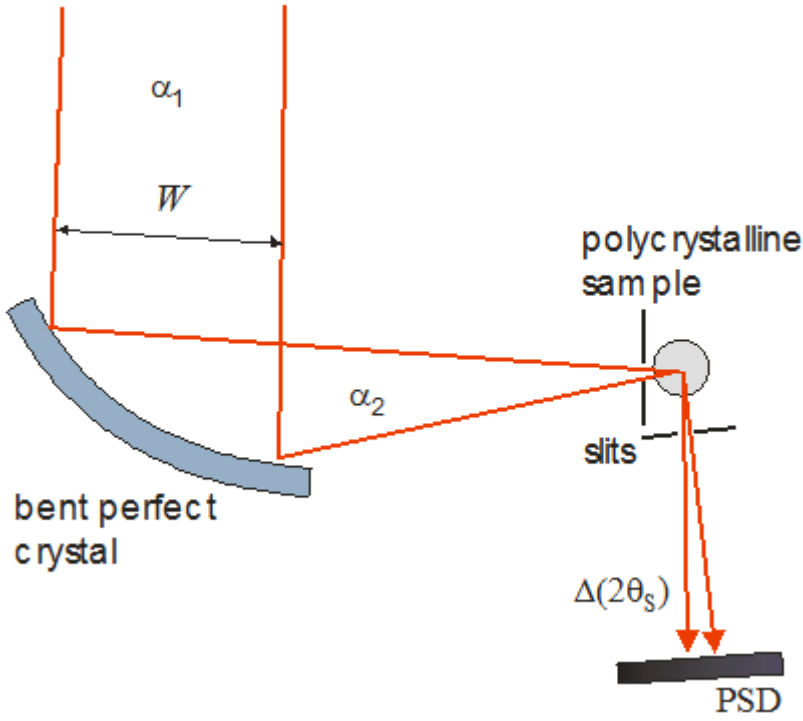

FIG. 39. Sketch of the focusing performance for $2\theta_M \approx 2\theta_S \approx 90°$.

7.1.2. Horizontally focusing monochromator at a small take-off angle

Although it could deliver a high neutron flux to the sample ($\delta\lambda_M/\lambda = \Delta\theta \cot \theta_M$), a small monochromator take-off angle is not usually used because it is supposed that the resolution in $\Delta d/d$ is much worse for larger scattering angles (see Fig. 38). As in the case of the stress/strain scanner, the instrument is optimized for one reflection at the scattering angle in the vicinity of 90°, and when used with the bent perfect crystal monochromator, there are several free parameters influencing angular resolution which can be easily manipulated. In addition to the radius of curvature of the bent monochromator R_M, its thickness t_M is also such a parameter. The thickness of the bent monochromator together with its curvature determines its effective mosaicity and consequently the uncertainty $\Delta\alpha_{2t}$ (see Eq. (9) in Section 3.8.1). Let us suppose the following parameters for the optimized performance schematically displayed in Fig. 40: L_{MS} = 2 m, w = 1 mm, 2tan θ_S/tan θ_M = 7, t_M = 4 mm and R_M = 8 m. Then, the formulas from Section 3.8.1 are used to obtain $\Delta(2\theta_S)_w = 3 \times 10^{-3}$ and $\Delta(2\theta_S)_t = 1.4 \times 10^{-2}$. The value of the former uncertainty is acceptable even for an instrument with very good resolution, while the latter is rather large.

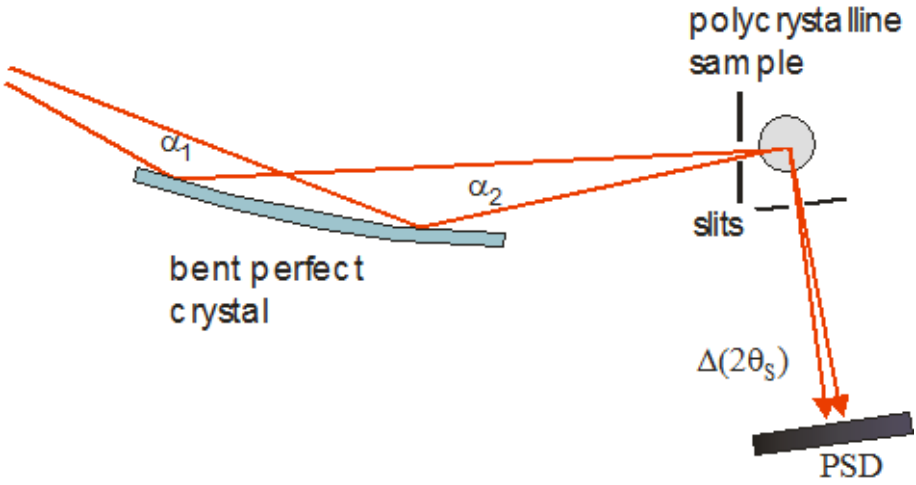

FIG. 40. Diagram of the optimized focusing performance for $2\theta_M \approx 30°$ and $2\theta_S \approx 90°$.

However, as can be seen from Eq. (6) in Section 3.8.1 the crystal thickness t_M can be exploited for manipulation. Of course, by setting a thinner bent perfect crystal, a correspondingly smaller integrated reflectivity is obtained, which is, however, compensated for by the larger monochromatized wavelength spread $\delta\lambda_M$ delivered to the sample. Recently, comprehensive experimental studies on

the possible use of a diffractometer with a small monochromator take-off angle for stress/strain measurements have been carried out at the HANARO reactor at KAERI, investigating the use of different diffraction geometries (symmetrical, asymmetrical, transmission, reflection) of the focusing bent perfect Si(111) crystals in order to find the most suitable performance alternative [110]. It has been found that symmetrical reflection geometry of the focusing monochromator is best providing a very good figure of merit. In these experiments the signal to background ratio was rather high (>20), therefore the figure of merit, *F*, for accuracy in peak position determination is with very good approximation proportional to the integral intensity in the peak, *I*, divided by the square of FWHM as $F \infty I/(FWHM)^2$. Figure 41 shows one example of the optimization experimental procedure with two Si(111) monochromators of different thicknesses, both in the symmetrical reflection geometry, when the lattice planes (111) are parallel to the largest surface of the crystal slab.

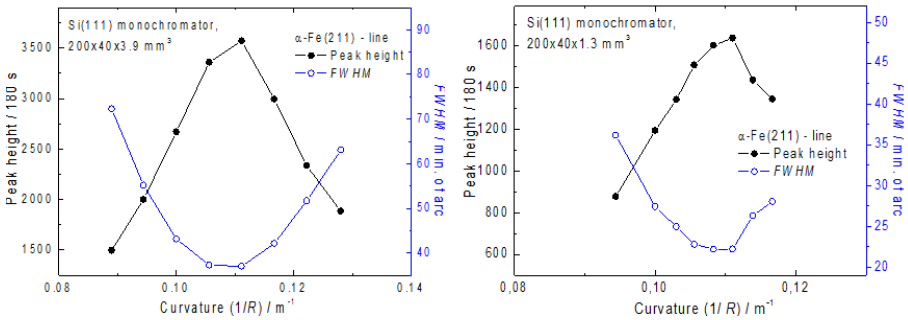

FIG. 41. The luminosity and resolution characteristics of the stress and strain diffractometer performance with the bent perfect Si(111) monochromator of the thickness of 3.9 mm and 1.3 mm taken using α-Fe(112) pin of 2 mm diameter and 40 mm height as a sample.

As can be seen from Fig. 41, the focusing arrangement achieves a maximum peak height and a minimum FWHM, simultaneously by setting the optimum radius of curvature the diffraction profile. As is shown in Fig 41, in the case of the 3.9 mm thick monochromator, a very good intensity related to the α-Fe(211) diffraction profile is obtained, but the 1.3 mm thick monochromator provides still good intensity (the peak height is smaller by a factor of 2.2) with very good FWHM and with only a slightly smaller value of the figure of merit *F*. However, in many cases (e.g. in steels), when the gauge volume is situated deeper in the material, the peak intensity of the diffraction profile becomes comparable with the level of the background. In such a case, for a successful stress/strain measurement a maximum possible detector signal related to the

chosen diffraction line is preferable. It should also be pointed out that according to Eq. (80 in Section 3.8.1, the radius of curvature R_{opt} is optimized just for a particular scattering angle $2\theta_S$ related to the chosen reflection $(hkl)_S$, which in the presented case was (112) of α-Fe. Since the FWHM in the resolution function for a fixed radius of curvature R_{opt} has a sharp minimum only for the chosen $2\theta_{hkl}$ and strongly increases with a changing $2\theta_S$, a different scattering angle $2\theta_S$ will require a different R_{opt}. In comparison with the previous performance with a large monochromator take off angle ($2\theta_M \approx 2\theta_S \approx 90°$, the trajectories of the neutrons contributing to the quasi-parallel diffracted beam have a large divergence α_1 at the monochromator (see Fig. 40). Due to this fact, it is necessary to work with the open primary beam collimation because the use of a soller collimator would result in a strong reduction of the detector signal. A major advantage of focusing diffractometer performance in comparison with that employing a mosaic monochromator is that the detector signal is roughly proportional to the size of the irradiated volume of the bent perfect crystal. However, the smaller the monochromator take-off angle that is used, the larger the volume of the focusing monochromator that is irradiated and the higher the neutron flux delivered to the sample. Very good luminosity with a small take-off angle is shown in Fig. 42 where three diffraction profiles for different collection times are introduced.

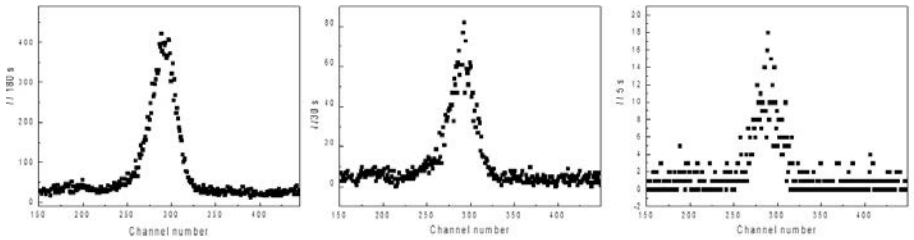

FIG. 42. Diffraction profiles of an α-Fe(112) pin of 1 mm diameter and 40 mm height for different measurement times.

An α-Fe(112) pin of 1 mm diameter and 40 mm height was used as a sample. The PSD was situated at a distance of 120 cm from the sample. The small diameter of the sample had practically no influence on the FWHM of the diffraction profile, because the spatial resolution of the detector, 2.5 mm, as well as the uncertainty, $\Delta\alpha_{2t}$, were much larger. It is clear that a PSD with a better spatial resolution could be set closer to the sample, which would lead to a further increase of the collected detector signal. In this case, investigations were concentrated on the value of the detector signal and the error in the determination of the peak position. It should be pointed out that approximately 40 channels in Fig. 42 correspond to an angular range similar to the FWHM. After fitting the

diffraction profiles, it was found that even with a measurement time of 5 s, the peak position can be determined with a relative error of about 10^{-4} (the angular width of one channel was 0.0095°) which is sufficient for most residual stress/strain measurements [111, 112].

Some further improvements to the presented performance optimization are still possible, e.g. by the installation of a PSD with a better spatial resolution and by the employment of a horizontally and vertically focusing monochromator. As the vertical focusing has little influence on the angular resolution of the instrument, its future installation could further improve luminosity by a factor of 2–3. Finally, with the tested diffractometer alternative, very good luminosity and resolution of the dedicated stress and strain instrument can be achieved even at medium power research reactors. It enables not only effective macrostress and strain scanning but also effective microstress and strain studies and even the study of some kinetic processes in polycrystalline materials with a duration of only a few seconds. For in situ experiments with samples subjected to an external thermomechanical load the use of this diffractometer can be attractive as such experiments usually use much larger gauge volumes, whereas smaller volumes enable the shortening of the measurement time of the diffraction profile.

7.1.3. Exploitation of the effect of wavelength dependent attenuation on neutron diffraction stress measurements for large depths in metals

Most neutron diffractometers have difficulty measuring strains in steel components with thicknesses of greater than 40 mm. Withers [113] provided a detailed analysis of depth capabilities in neutron strain measurements based on the Chalk River National Research Universal reactor LR3 instrument and estimated the maximum penetration path length (l) at which the strain can be measured with 10^{-4} accuracy in 1 h with a 40 mm^3 sampling volume. The value of l was approximately 40 mm with the 211 reflection of a body centred cubic ferritic steel at a scattering angle ($2\theta_S$) of 90°. Figure 43 shows the reflection (a) and transmission geometry (b) of the sample for the measurements of the normal (N) and the transverse (T) or longitudinal (L) components, respectively.

The maximum penetration path length (l) is the sum of the incident (l_i) and diffracted (l_d) beam path lengths. It increases with depth in the case of a reflection geometry (see Fig. 43(a)), while it is the same for all depths in transmission geometry (Fig. 43(b)). The gauge volume is defined by a number and type of mechanical slits in the incident and diffracted beams. The analyses have shown that the maximum feasible penetration depths are 15 and 30 mm in the reflection and transmission geometries, respectively. Thus, it is suggested that the stress distribution could be appropriately measured in a 30 mm thick steel plate; basically, the maximum available path length depends on the performance of

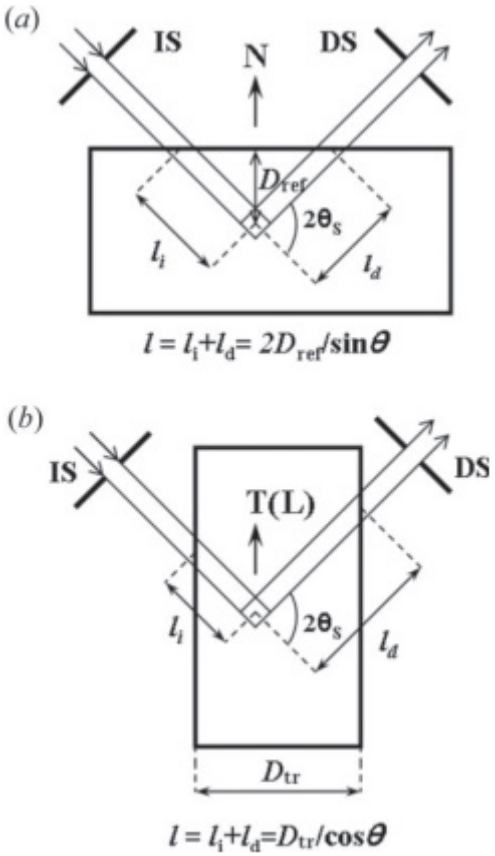

FIG. 43. The geometries of neutron beam penetration in (a) reflection and (b) transmission geometry.

the instrument and the intensity of the neutron source. In general, the maximum achievable path increases as the acquisition time or sampling volume increases for a given instrument. As has been mentioned above, there is a growing need for residual stress measurements in thicker components, often which are often those made from steel. It is clear that the principal problem is the neutron attenuation of the investigated material because the detector signal decreases exponentially with the beam path length [3]. Of course, this problem could be overcome to a certain extent by using a highly luminous dedicated instrument, or by using a rather large gauge volume, or both. However, the luminosity of the instrument is limited by the neutron flux provided by the neutron source where the instrument is installed. Therefore, it would help to use a neutron wavelength for which the neutron attenuation factor of the material is rather small. That is, to use the sharp

variation in total neutron cross-section with neutron wavelength to optimize the experiment. As this variation exhibits a saw tooth structure (Bragg diffraction edges) the attenuation factor is substantially smaller for an incident wavelength just under the edge than for a wavelength just above the edge. For ferritic and austenitic steels, this is illustrated in Fig. 44.

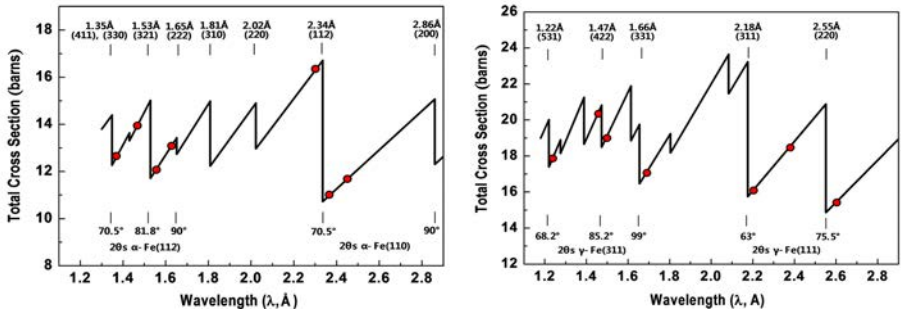

FIG. 44. Calculated total neutron cross-section of ferrite (α-Fe) and austenite (γ-Fe) as a function of neutron wavelength. The wavelengths at which the maximum penetration depth was measured are shown with closed black circles.

In order to investigate this new opportunity, the test experiments carried out for the neutron wavelength are marked in Fig. 44 by black dots. An example of the obtained results is shown in Fig. 45. By using the neutron wavelength of 2.39×10^{-1} nm and 2.19×10^{-1} nm and focusing a bent perfect crystal Si(111) monochromator, it was observed that the achievable total beam path length is approximately 85 mm in both ferritic and austenitic steels. The usefulness of the described instrument performance optimization has been demonstrated through residual stress mapping in the vicinity of a weld joint in a 50 mm thick plate (see Fig. 46) [114].

Finally, the above mentioned results have been achieved at a medium power research reactor using only a horizontally focusing monochromator, and there are parameters that can be still improved. An additional option is a vertically focusing monochromator and the collection of neutrons from a much higher beam tube. This could increase the monochromatic neutron flux delivered to the sample by a factor of 3–5.

7.1.4. Flux increase through other focusing techniques

Double focusing perfect crystal monochromators have brought about significant improvements in the figure of merit. However, most monochromators at modern reactor sources are already operating at their optimum, and further

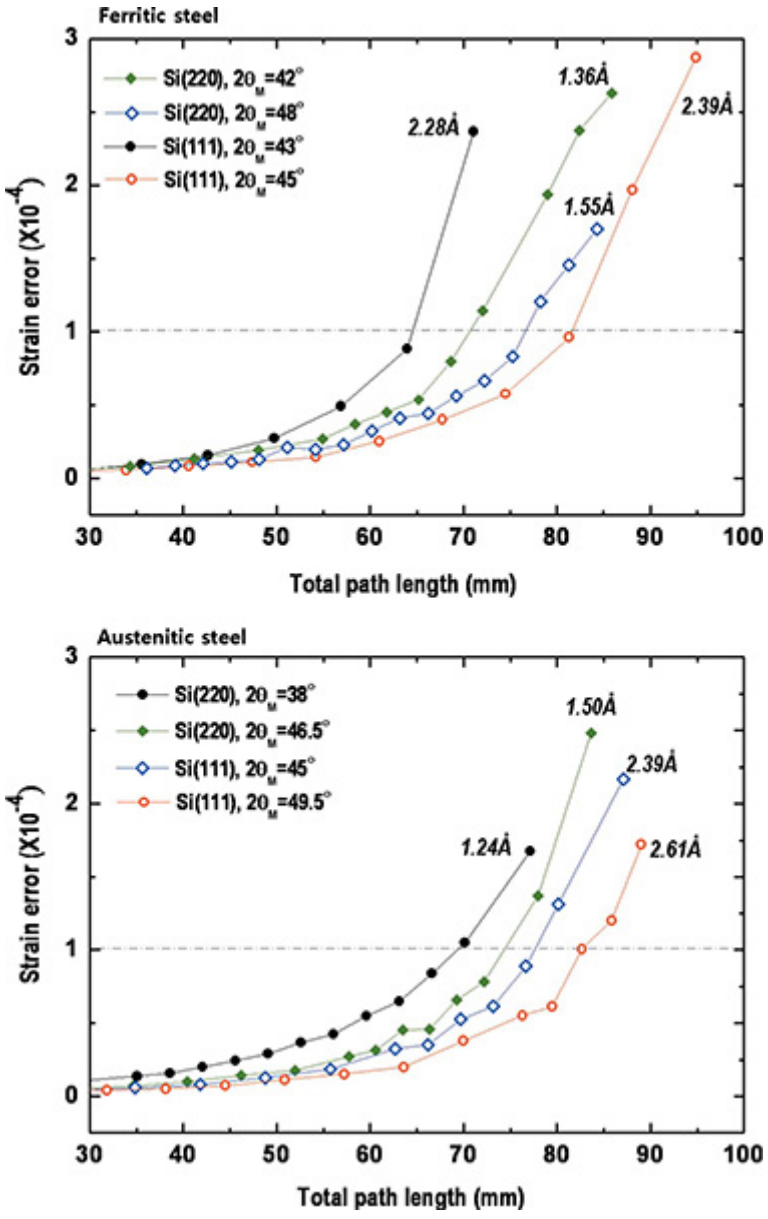

FIG. 45. The dependence of the strain error on the total penetration path length in α-Fe and γ-Fe steels. The depth scan was carried out in reflection geometry (1 h measurement, 80 mm³ gauge volume) by measuring: α-Fe: the 211 reflection for 1.36 × 10^{-1} nm and 1.55 × 10^{-1} nm and the 110 reflection for 2.28 × 10^{-1} nm and 2.39 × 10^{-1} nm; γ-Fe: the 311 reflection for 1.24 × 10^{-1} nm and 1.5 × 10^{-1} nm and the 111 reflection for 2.39 × 10^{-1} nm and 2.61 × 10^{-1} nm.

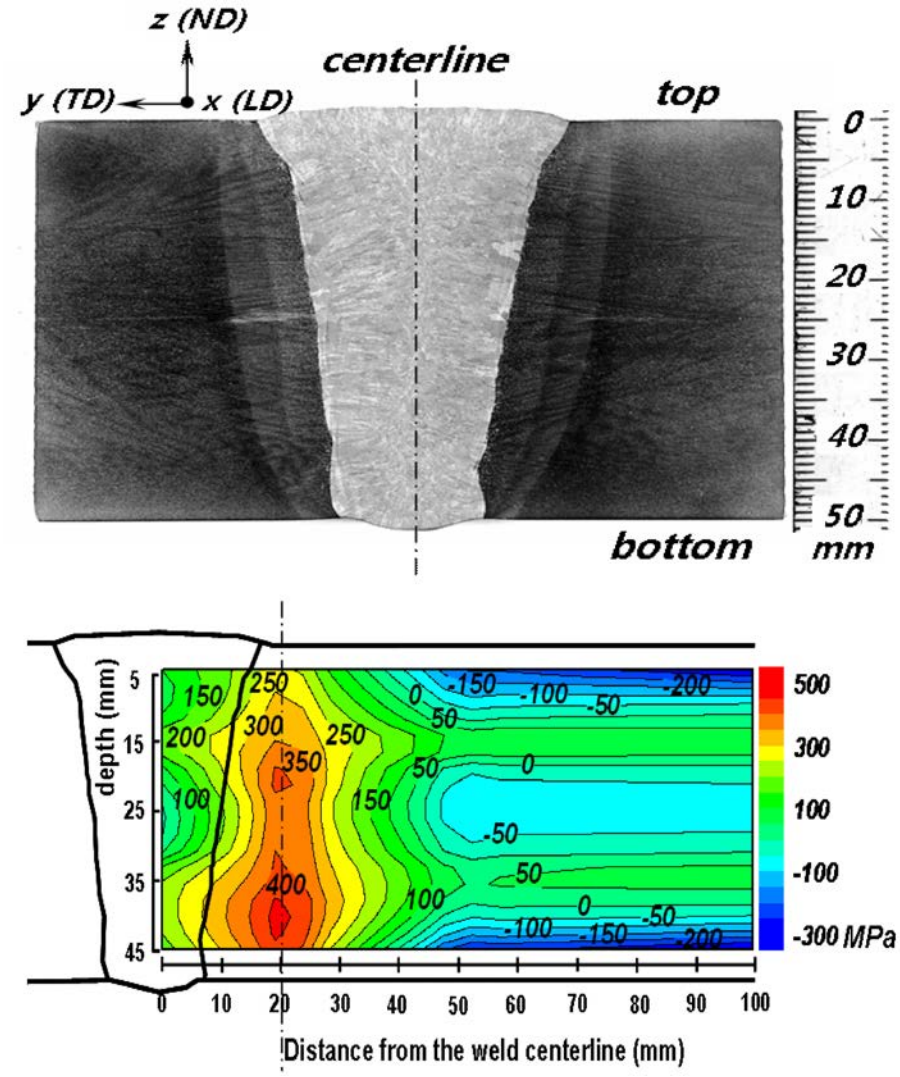

FIG. 46. (a) Macrostructure of the 50 mm thick low carbon steel weld. Note the LD (longitudinal, x), TD (transverse, y) and ND (normal, z) directions of the weld plate. (b) Two dimensional mapping of the longitudinal residual stress (σ_x) in the 50 mm thick weld plate.

gains through design improvements are likely to be small compared with their current performance. An exception maybe the sandwich or multiwavelength concept [45, 52] discussed in Section 3.8.1. In this approach, a second wavelength at a similar intensity is used, which allows the measurement of two sample reflections in reasonable proximity to each other. Other concepts based

on the total reflection of neutrons at glancing angles are actively explored, some of which are discussed in the following subsections.

(a) Fibre-optical lens

Figure 47 shows a diagram (left) of a fibre-optical lens and a photograph to illustrate scale (right) . A fibre-optical lens was tested for possible application in small sample crystallography, and, by extension, for small gauge volumes [115, 116] of the order of $0.5 \times 0.5 \times 0.5$ mm^3. Real intensity gains of up to a factor of 3 were found. However, the lens performs best at longer wavelengths with a quasi-parallel input beam, both of which instrument settings are often less desirable at reactor sources.

(b) Kirkpatrick–Baez mirrors

Kirkpatrick–Baez mirrors are elliptically bent, grazing incidence (super) mirrors for X ray and neutron focusing. Gains of up to a factor of 100 have been reported for neutrons at spot sizes of $0.1 \times 0.1 \times 0.1$mm. The required length of the mirrors (≈0.5 m) is a drawback. Also, it is not yet clear whether a Kirkpatrick–Baez mirror can work in conjunction with a double focusing perfect crystal monochromator. A diagram of a Kirkpatrick–Baez mirror is shown in Fig. 48.

(c) Wolter optics

Wolter optics for neutron focusing is a rather recent, very promising concept [118]. Illustrations for the Wolter optics concept are provided in Fig. 49.

In a tubular assembly of concentric conical sections, neutrons are reflected twice though combinations of surfaces consisting of three possible types: paraboloid–ellipsoid, confocal hyperboloid–paraboloid or hyperboloid–paraboloid. In a recent test at NIST with a single mirror (single tube, no nesting) with cold neutrons ($\lambda = 6 \times 10^{-1}$ nm) a flux gain on the focal point of approximately 18 was reported for a focal diameter of ≈ 1 mm. While lower gains should be expected for thermal neutrons, the possibility of nesting more mirrors should compensate for the decrease. Nonetheless, similar to Kirkpatrick–Baez mirrors, questions remain about how Wolter optics will work downstream from a double focusing monochromator.

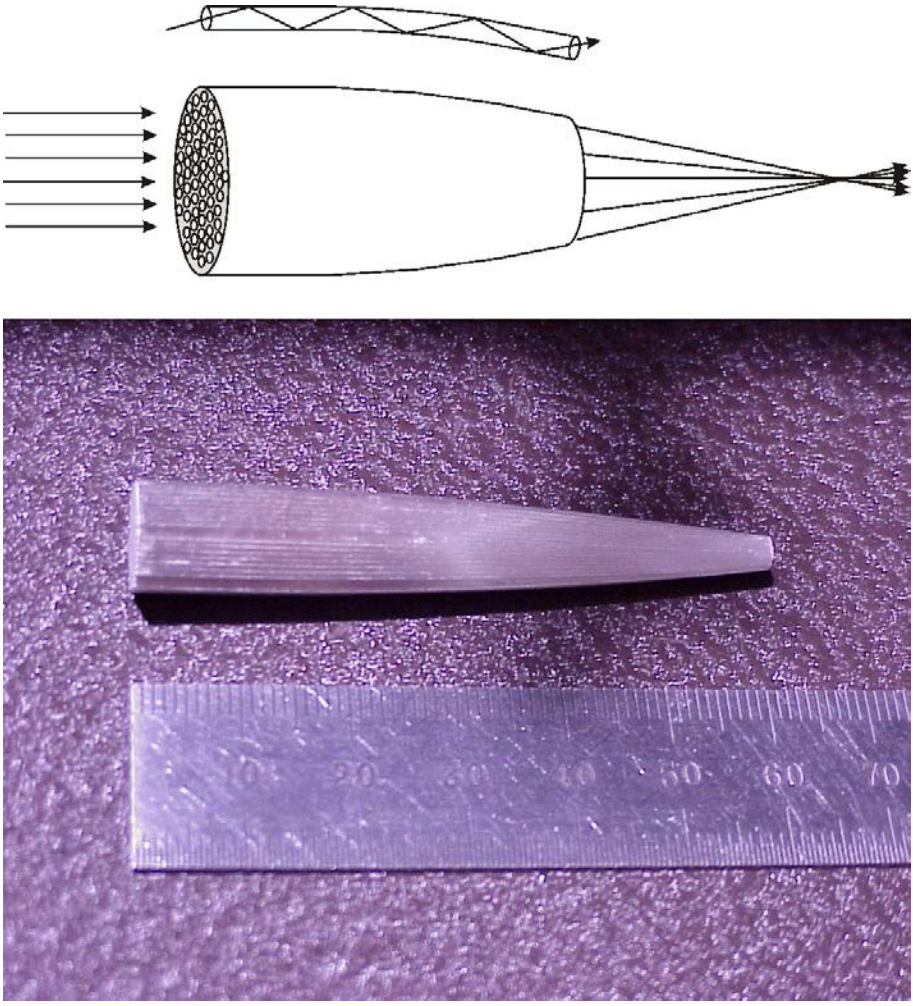

FIG. 47. Fibre-optical lens for neutron focusing [115, 116].

7.2. INSTRUMENTS AT PULSED NEUTRON SOURCES

In Section 3.1 it was noted that only three pulsed neutron sources (ISIS, LANSCE and IBR-2) currently operate at the nominal parameters, and a further two (SNS and J-PARC) are in the startup phase. The most advanced of the stress diffractometers constructed at these sources are ENGIN-X (ISIS) and VULCAN (SNS), the so-called third generation neutron strain scanners. Their configuration is an exemplary embodiment of the trends in the development of this experimental technique.

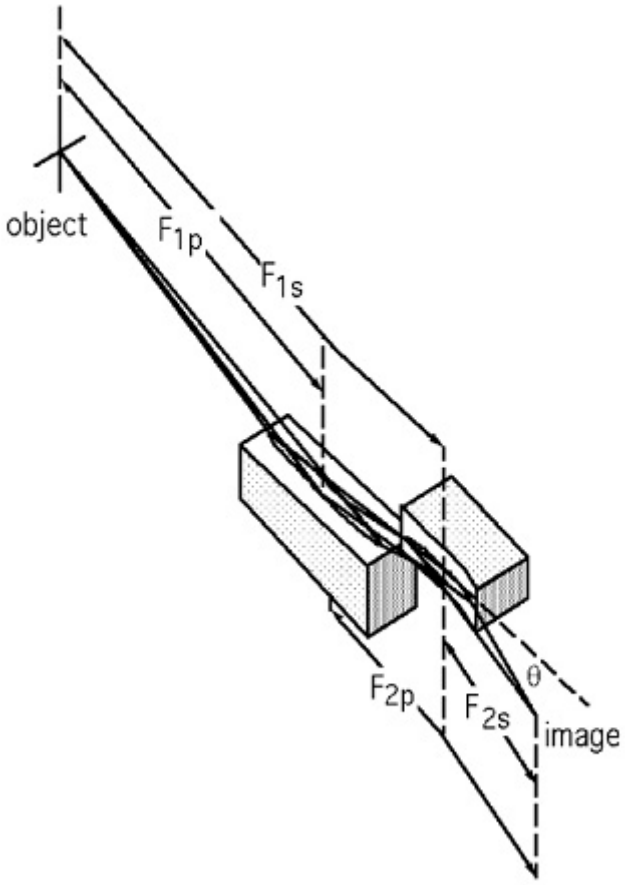

FIG. 48. Diagram of a Kirkpatrick–Baez mirror [117].

The main objectives set during the construction of these instruments were: to reduce the gauge volume to ~1 mm^3; to reduce data acquisition time during 3-D scanning to less than 1 h; to improve the spatial resolution, at least along one direction in the sample, to about 0.1 mm; to extend the accessible d_{hkl} range in order to simultaneously register 10 diffraction peaks or even more; and finally to combine other procedures and techniques with neutron diffraction which are useful or necessary for better characterization of the samples.

A diagram of the ENGIN-X stress diffractometer [119] at ISIS, which was described in Section 3.9, is shown in Fig. 50. The instrument features a relatively large flight path from the source to the sample position (50 m) providing good $\Delta d/d$ resolution; two detectors placed at scattering angles $2\theta_0 = \pm 90°$, which facilitates strain measurement in two perpendicular directions simultaneously,

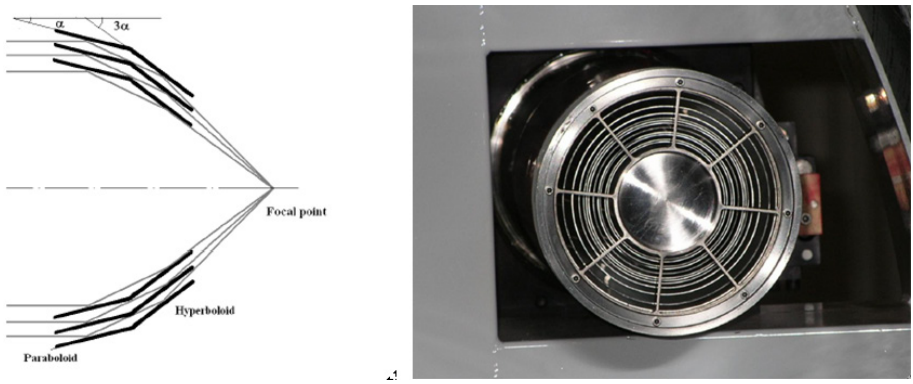

FIG. 49. Left: Schematic of a nested Wolter optics. Right: HERO nested X ray optics illustrating the concept of nested mirrors for large gains [118].

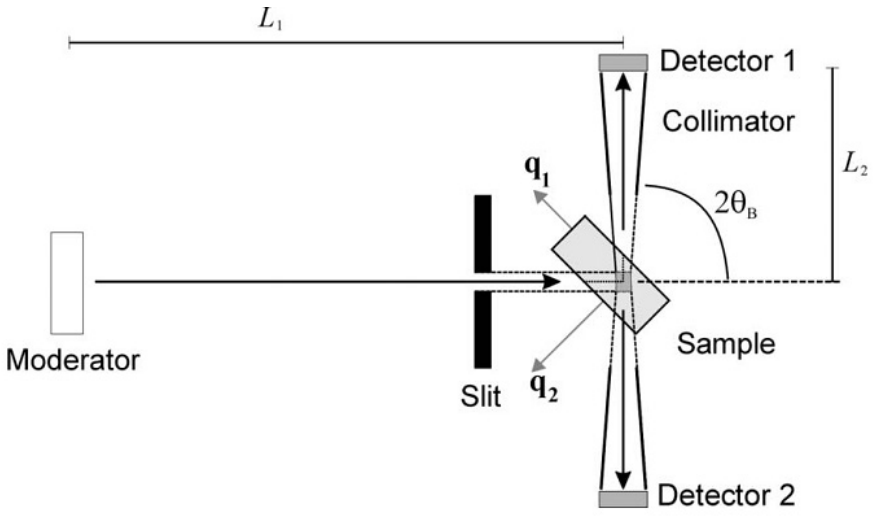

FIG. 50. Diagram of a TOF neutron strain scanner. The elastic strain is measured along the directions of the momentum transfer vectors $\boldsymbol{q}_1$ and $\boldsymbol{q}_2$. The gauge volume is given by the intersection of incident and diffracted beams defined by slits and collimators. Figure and descriptions are from Ref. [120].

and radial collimators in front of the detectors, which are used to accurately define the gauge volume.

Placing detectors at ±90° provides the most favourable shape for the gauge volume, and in addition, allows for large angular coverage in the vertical plane, as the divergence perpendicular to the diffraction plane does not affect the resolution. Thus, the convergence of scattering angles at ENGIN-X is ±14°

in the horizontal and ±21° in the vertical plane. For the selection of the gauge volume size, a set of radial collimators with the same angle of divergence is used (Fig. 51). The current set of collimators allows gauge volume selection from 0.5–4 mm in the horizontal plane.

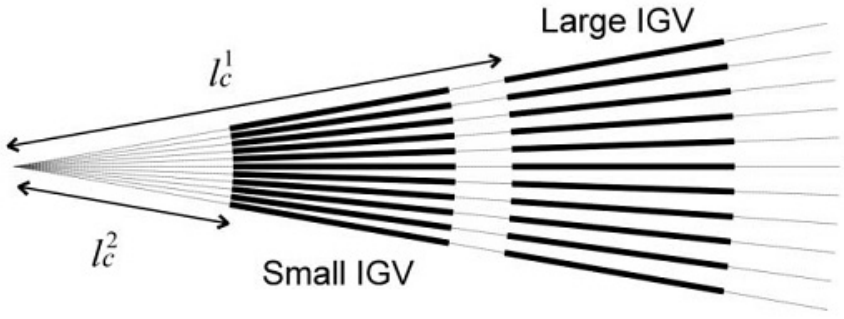

FIG. 51. Design of two radial collimators with the same divergence but different spatial resolutions. Figure and descriptions are from Ref. [119].

The design of the VULCAN stress diffractometer [121] at the SNS pulsed source differs in some details only: a little shorter flight path (43.5 m), a larger scattering angle range in the horizontal plane (2θ = 60–150°). Vulcan has a larger flux of neutrons from the source as the average power (~1 MW) at SNS is approximately 5 times higher than the power at ISIS, and an advanced neutron guide system [120], which includes focusing sections of logarithmic form (Fig. 52), also leads to improved spatial resolution, reduced measurement time and an expanded range of applications. In particular, VULCAN is widely used for in situ measurements [122]; a large range of scattering angles and the presence of a small angle scattering detector allow good control of the microstructure changes during the experiment. An additional feature is a large degree of flexibility for intensity resolution optimization, which is provided by an interchangeable focusing section (3 m) of the neutron guide system.

The available wavelength range on both diffractometers ranges from 0.5–6 × 10^{-1} nm. This allows the recording of d_{hkl} between 0.4 and 4 × 10^{-1} nm, i.e. ~20 individual peaks of α-Fe are visible simultaneously, supporting a detailed analysis of microstresses and anisotropic effects.

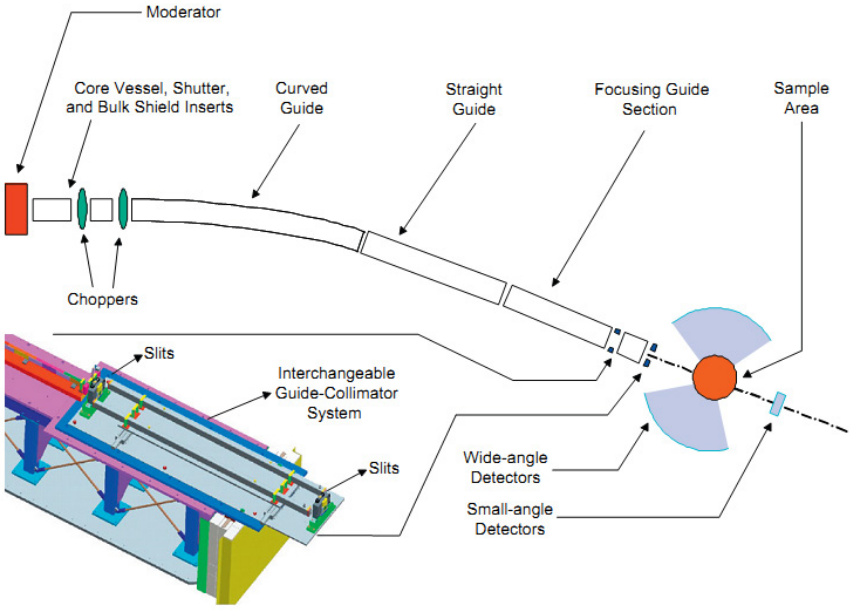

FIG. 52. Diagram of the VULCAN diffractometer at the SNS. Figure and descriptions are from Ref. [120].

7.2.1. Trends in analysis of experimental data measured on a TOF stress diffractometer

One of the main features of TOF stress diffractometers is the ability to measure a large number of diffraction peaks simultaneously and, consequently, the possibility of using the Rietveld method for characterization of the crystalline state. In the simplest implementation, this method enables the averaging of the lattice parameters in the crystal lattice over the gauge volume. In addition, one of the possibilities of this method is the analysis of anisotropy effects that influence the position and width of the diffraction peaks, as well as the effects of texture on the intensity of the peaks. Another important task is a separation of different factors that determine the diffraction line broadening. An effective solution of both these tasks has been found, but has not yet been widely implemented.

An overview of new approaches to the analysis of the diffraction peak shape, which increase the reliability of the extraction of strain contribution to anisotropic broadening, can be found in Ref. [101]. In particular, anisotropic broadening of the diffraction lines caused by a spatially varying scalar variable, such as variations in the composition of the bulk material, has recently been

analysed [123]. The method was adapted for all crystal systems, embedded in a program for Rietveld refinement and tested on a model object with a hexagonal lattice (ε-$FeN_{0.433}$). Analysis of the diffraction data based on the proposed model by fitting individual lines and by using the Rietveld profile refinement gave a comparable result.

It is interesting to note that the measurement of a large number of peaks at a TOF stress diffractometer facilitates (at least in principle) the determination of a stress free lattice parameter by using the algorithm proposed in Ref. [124], which is based on the elastic anisotropy of the material. The most consistent account of the elastic properties of textured material is provided by the Material Analysis Using Diffraction (MAUD) software package [93]. In the literature there are already good examples of joint quantitative analysis of both the texture and the residual stress tensor (see, e.g., Refs [125, 126]).

7.2.2. Neutron diffraction and other modes of neutron scattering at pulsed sources

At TOF stress diffractometers the study of internal stresses can be easily coupled with additional capabilities such as small angle neutron scattering (SANS) neutron radiography and tomography (neutron imaging) or both. SANS allows the determination of the geometrical characteristics of large scale inhomogeneities, which have a coherent scattering length different from that of the matrix. SANS is actively used, for example, to analyse the precipitation of nanoclusters in ODS steels [127]. For the simultaneous analysis of internal stresses and microstructural characteristics with the VULCAN stress diffractometer, a special detector is placed at small scattering angles for data acquisition of momentum transfers in the range from 0.01 to 0.2×10^{-1} nm^{-1}. Through this, the identification of irregularities in the material with sizes from several to several tens of nm is possible. The combined analysis of diffraction and SANS data is particularly useful for in situ studies of processes in materials under the influence of external factors such as temperature, loading, etc.

In recent years the neutron imaging technique has been considerably developed, which is primarily due to advances in 2-D detectors which have provided the required spatial resolution (better than 0.1 mm). Like diffraction, neutron imaging is a non-destructive method for the analysis of the internal structure of complex objects and any changes to the structure with time. The combination of diffraction analysis of internal stresses with neutron imaging opens new possibilities for the in-depth characterization of materials. It is especially promising for pulsed neutron sources, where energy selective transmission imaging can easily be implemented. In the first experiments, effective contrast enhancement and contrast variation of neutron imaging

exploiting Bragg edge effects have been demonstrated (see, e.g., Fig. 53 from Ref. [128]). Good wavelength resolution at TOF stress diffractometers offers the possibility of obtaining 3-D information on the distribution of internal stresses that, in principle, allows the reconstruction of tomographic images of the stresses [129].

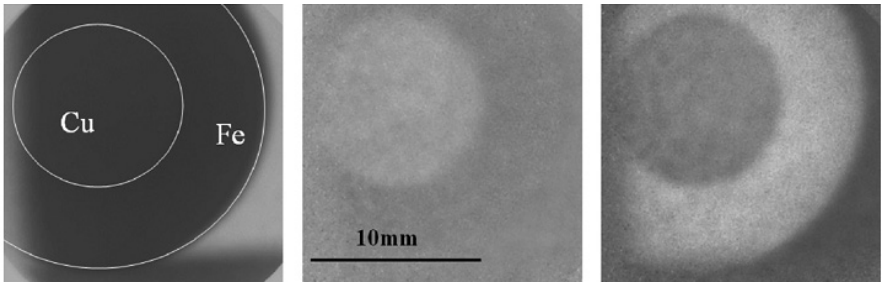

FIG. 53. Radiographic images of an iron and copper cylinder. Left: The direct image obtained for a wavelength above 4×10^{-1} nm shows no significant contrast between Fe and Cu. The white rings are guides to the eye to mark the phase boundaries. Centre: Ratio of two images taken for λ above a Bragg edge of copper. Right: Ratio of two images taken for λ above a Bragg edge of ferrite.

7.3. THE FUTURE DEVELOPMENT OF INSTRUMENT CONTROL

All aspects of instrument control, data acquisition and analysis are expected to merge in the future, and it might become difficult to draw the line between the different concepts. For instance, real time data analysis will feed back, influencing the instrument control in order to optimize the measurement time. Also, planning, the most time consuming aspect of a measurement, is in need of optimization, and this too will become a crucial aspect of instrument control. Table 4 [130] shows how each aspect of a measurement might potentially be interrelated in the future.

With ever increasing computer power, the concept of using simulations to execute a measurement (involving a detailed description of the instrument and sample) becomes more realistic. The advantage of this is not only the efficient use of beam time but also the confidence in the results obtained. With a more thorough description of the instrument and especially of the sample, many influencing factors for a measurement could be described and quantified. The factors that can strongly influence a neutron strain measurement include: texture, sample surfaces and interfaces, grain size, multiphase materials, areas of plastic deformation, the distribution of neutrons within the gauge volume, absorption

of neutrons in the sample, types of neutron optics and noise or background. A realistic description and simulation of the sample is crucial. As it is often desirable to verify finite element models with measurements such as neutron strain scanning, such a model could in future be input directly into the simulation before the measurement begins. Progress has already been made in making more complex virtual sample descriptions for neutron simulations [131]. With future advances in computing power, it can easily be seen that more complex and realistic descriptions of instruments and samples will ensue. The concepts of simulation and measurement and instrument control will thus come together, bringing forth more confidence in measurement results.

TABLE 4. POSSIBLE MEASUREMENT DESIGN AND INSTRUMENT CONTROL IN THE FUTURE

Step	Possible mechanism
Input model with description of the problem and sample	Uploading of a finite element model of the specimen into a web based tool is one possibility.
Web site output	Web site gives all possible stress/strain measuring options (possibly also including methods other than neutron diffraction). Shows by visualization why some methods work and some do not. Important to show potential new users how the method works, hence speeding up learning process.
Simulation of measurement	The same web based tool could make the complete simulation for a particular instrument and hence perform the optimization of the measurement. This step would show what is and is not possible and could also produce an optimized experimental protocol.
Experimental protocol	This protocol from the simulation together with a training programme could be used to control the instrument and to perform the measurement itself.
Actual measurement	The simulation can also be used to correct possible aberrations in real time, interacting with data acquisition and data analysis tools.

8. SUMMARY

The use of neutron diffraction for the characterization of residual stress has now matured into a technique that provides unique insights into stress fields deep within engineering components and structures. As such, it has become an increasingly important tool within engineering and has led to improved manufacturing processes to reduce stress and distortion as well as to the definition of more precise structural integrity procedures. The continuing drive to optimize performance and minimize weight in many applications in order to maximize competitiveness will ensure that this field continues to grow. Furthermore, for many situations it is the only non-destructive means of measuring the stress state deep within engineering components and structures under certain conditions (temperature, stress, atmosphere, etc.) representative of those which might be experienced in-service.

REFERENCES

[1] HAUK, V., Structural and Residual Stress Analysis by Nondestructive Methods, Elsevier, Amsterdam (1997).

[2] ALLEN A.J., HUTCHINGS M.T., WINDSOR C.G., ANDREANI C., Neutron diffraction methods for the study of residual stress fields, Adv. Phys. **34** (1985) 445–473.

[3] INTERNATIONAL ORGANIZATION FOR STANDARDIZATION, Non-Destructive Testing — Standard Test Method for Determining Residual Stresses by Neutron Diffraction, ISO/TS 21432:2005, ISO, Geneva (2005).

[4] LORENTZEN, T., HUTCHINGS, M.T., WITHERS, P.J., HOLDEN, T.M., Introduction to the Characterization of Residual Stress by Neutron Diffraction, CRC Press, Boca Raton, FL (2005).

[5] FITZPATRICK, M.E., LODINI, A., Analysis of Residual Stress by Diffraction Using Neutron and Synchrotron Radiation, Taylor and Francis, London, New York (2003) 171.

[6] NOYAN, I.C., COHEN, J.B., Residual Stress Measurement by Diffraction and Interpretation, Springer, New York (1987).

[7] INTERNATIONAL ATOMIC ENERGY AGENCY, Measurement of Residual Stress in Materials Using Neutrons (Proc. Tech. Mtg. Vienna 2003), IAEA-TECDOC-1457, IAEA, Vienna (2005).

[8] REIMERS, W., PYZALLA, A.R., SCHREYER, A.K., CLEMENS, H. (Eds), Neutrons and Synchrotron Radiation in Engineering Materials Science: From Fundamentals to Material and Component Characterization, Wiley-VCH, Weinheim (2008).

[9] SHULL, C.G., WOLLAN, E.O., The diffraction of neutrons by crystalline powders, Phys. Rev. **73** (1948) 830–841.

[10] BROCKHOUSE, B.N., HURST, D.G., Energy Distribution of Slow Neutrons Scattered from Solids, Phys. Rev. **88** (1952) 542–547.

[11] INSTITUT LAUE-LANGEVIN, Rapport Transparence et Sécurité Nucléaire 2010 (2011), http://www.ill.eu/reactor-environment-safety/high-flux-reactor/

[12] CARPENTER, J.M., Pulsed spallation neutron sources for slow neutron scattering, Nucl. Instr. Methods **145** (1977) 91–113.

[13] TECHNICAL UNIVERSITY OF MUNICH, FRM II Reactor, http://www.frm2.tum.de/en/technik/reactor/index.html

[14] INSTITUT LAUE-LANGEVIN, Instruments & Groups, http://www.ill.eu/instruments-support/instruments-groups/

[15] INTERNATIONAL ATOMIC ENERGY AGENCY, Research Reactor Database, http://nucleus.iaea.org/RRDB/

[16] SCIENCE AND TECHNOLOGY FACILITIES COUNCIL, ISIS, http://www.isis.stfc.ac.uk/

[17] INTEGRATED INFRASTRUCTURE INITIATIVE FOR NEUTRON SCATTERING AND MUON SPECTROSCOPY, The NMI3 Information Portal, http://neutron.neutron-eu.net/n_ess/

[18] PAUL SCHERRER INSTITUT, Spallation Neutron Source Division ASQ, http://asq.web.psi.ch/facility/

[19] FRANK, I.M., PACHER, P., First experience on the high intensity pulsed reactor IBR-2, Physica B & C **120** (1983) 37–44.
[20] RANDAU, C., Implementierung und Bewertung des Kontinuierlichen Neutronendiffraktometrischen Texturanalyse-Experiments, Diploma Thesis, Univ. of Applied Sciences, Berlin (2007).
[21] RANDAU, C., GARBE, U., BROKMEIER, H.-G., StressTextureCalculator: a software tool to extract texture, strain and microstructure information from area-detector measurements, J. Appl. Cryst., **44** (2011) 641–646.
[22] KRAWITZ, A.D., The early history of neutron stress measurements, Mater. Sci. Forum **571–572** (2008) 3–11.
[23] ALLEN, A.J., ANDREANI, C., HUTCHINGS, M.T., WINDSOR, C.G., Measurement of internal stress within bulk materials using neutron diffraction, NDT Int. **14** (1981) 249–254.
[24] DE BROGLIE, L.V., Recherches sur la théorie des quanta, Ann. de Phys., 10e série, **t. III** (1925) 22–128.
[25] TECHNICAL UNIVERSITY OF MUNICH, Beam guidance of the Neutrons, http://www.frm2.tum.de/en/technik/beamguidance-of-the-neutrons/
[26] TECHNICAL UNIVERSITY OF DELFT, "IRI Cursus Neutronenverstrooiing Onderzoek Vaste Stof en Vloeistof met Behulp van Neutronen", lecture material for a course given at TU Delft, Netherlands, 1996.
[27] PIRLING, T., Neutron strain scanning at interfaces: An optimised beam optics to reduce the surface effect, Materials Science Forum, **347–349** (2000) 107–112.
[28] GITLIN, J.N., National Security Driving a Helium-3 Shortage, Hurting Physics, Ars Technica (2011), http://arstechnica.com/science/news/2011/02/national-security-driving-a-helium-3-shortage-hurting-physics.ars
[29] BRANDT, P.C., Stress Measurement by Means of Neutron Diffraction, PhD thesis, Univ. of Twente (1991).
[30] OHMS, C., et al., "The European Network on Neutron Techniques Standardization for Structural Integrity – NeT", ASME Pressure Vessels and Piping Conference (Proc. Conf. Chicago, IL, 2008), American Society of Mechanical Engineers, New York (2009).
[31] INTERNATIONAL ORGANIZATION FOR STANDARDIZATION, Polycrystalline Materials — Determination of Residual Stresses by Neutron Diffraction. ISO/TTA 3, ISO, Geneva (2001).
[32] OHMS, C., Residual Stresses in Thick Bi-metallic Fusion Welds: A Neutron Diffraction Study, PhD thesis, Tech. Univ. Delft (2013).
[33] OHMS, C., KATSAREAS, D.E., WIMPORY, R., HORNAK, P., YOUTSOS, A.G., "Residual stress analysis in a thick dissimilar metal weld based on neutron diffraction", ASME/JSME 2004 Pressure Vessels and Piping Conference (Proc. Conf. San Diego, CA, 2004), American Society of Mechanical Engineers, New York (2004) 85–92.
[34] EIGENMANN, B., MACHERAUCH, E., "Röntgenographische Untersuchung von Spannungszuständen in Werkstoffen", Mat.-wiss. u. Werkstofftech. **26** 3 (1995) 148–160.

[35] WITHERS, P.J., PREUSS, M., STEUWERB, A., PANG, J.W.L., Methods for obtaining the strain-free lattice parameter when using diffraction to determine residual stress, J. Appl. Cryst. **40** (2007) 891–904.
[36] JAMES, J., SANTISTEBAN, J.R., EDWARDS, L., DAYMOND, M.R., A Virtual Laboratory for Neutron and Synchrotron Strain Scanning, Physica B, Condensed Matter **350** (2004) 743–746.
[37] WEBSTER, P.J., et al., Impediments to efficient through-surface strain scanning, J. Neutron Res. **3** (1996) 223–240.
[38] NEOV, D., OHMS, C., WIMPORY, R.C., YOUTSOS, A.G., Residual stress analyses by neutron diffraction in irradiated double-V butt welded steel plates, Mater. Sci. Forum **571–572** (2008) 381–386.
[39] DANN, J.A., et al., A comparison between Engin and Engin-X, a new diffractometer optimized for stress measurement, Physica B **1–3 Suppl.** (2004) E511–E514.
[40] ANDERSON, I.S., GUÉRARD, B., (Eds), Advances in Neutron Scattering Instrumentation (Proc. Conf. Society of Photo-Optical Instrumentation Engineers, Seattle, WA, 2002), SPIE, Bellingham, WA (2002) 64–74.
[41] BROKMEIER, H.G., et al., The robot concept at STRESS-SPEC for the characterization of semi-finished products, Materials Science Forum **652** (2010) 197–201.
[42] VRÁNA, M., MIKULA, P., LUKAS, P., SAROUN, J., STRUNZ, P., High esolution diffraction Techniques for strain/stress measurements at a steady state reactor, Act. Phys. Hung. **75** (1994) 305–310.
[43] MIKULA, P., SAROUN, J., VRÁNA, M., LUKAS, P., WAGNER, V., High-resolution neutron powder diffractometry on samples of small dimensions, Mater. Sci. Forum **228–231** (1996) 269–274.
[44] MIKULA, P., et al., Bragg diffraction optics in neutron diffractometry, Physica B **283** (2000) 289–294.
[45] VRÁNA, M., MIKULA, P., LUKAS, P., WAGNER, V., Two-wavelength sandwich monochromator for materials research experiments, Physica B **241–243** (1998) 231–233.
[46] VRÁNA, M., LUKAS, P., MIKULA, P., KULDA, J., Bragg Diffraction Optics in High Resolution Strain Measurements, Nucl. Instrum. Meth. A **338** (1994) 125–131.
[47] MIKULA, P., et al., "Neutron Diffractometer Exploiting Bragg Diffraction Optics — A High Resolution Strain Scanner", The 5th International Conference on Residual Stresses (Proc. Int. Conf. ICRS-5 Linköping, Sweden, 1997), ERICSSON T., ODEN A., ANDERSSON M., (Eds), Vol. 2, University of Linkoping, Sweden (1998) 721–725.
[48] MIKULA P., WAGNER, V., Strain Scanning Using a Neutron Guide Diffractometer, Mater. Sci. Forum **347–349** (2000) 113–118.
[49] MOON, M.K., et al.,Optimization of bent perfect Si(3 1 1)-crystal monochromator for a residual strain/stress instrument at the HANARO Reactor — Part I, Physica B **369** (2005) 1–7.
[50] MOON, M.K., et al., Optimization of bent perfect Si(2 2 0)-crystal monochromator for residual strain/stress instrument — Part II., Physica B **368** (2005) 70–75.

[51] MIKULA, P., LUKÁŠ, P., VRÁNA, M., High resolution neutron diffraction for non-destructive analysis of residual stresses in polycrystalline materials, Applied Mechanics and Materials **3–4** (2006) 331–336.
[52] TANAKA, I., AHMED, F.U., NIIMURA, N., Application of a stacked elastically bent perfect Si monochromator with identical and different crystallographic planes for single crystal and powder neutron diffractometry, Physica B **283** (2000) 295–298.
[53] STUHR, U., et al., Time-of-flight diffraction with multiple pulse overlap, Nucl. Instrum. Meth. A, **545** (2005) 319–329 (Part I) and 330–338 (Part II).
[54] BOKUCHAVA, G.D., et al. "Neutron Fourier diffractometer FSD for internal stress analysis: first results", Appl. Phys. A-Mater. **74** (2002) S86–S88.
[55] SEEGER, P.A., DAEMEN, L.L., The neutron instrument simulation package, NISP, Advances in Computational Methods for X-Ray and Neutron Optics (Proc. Conf. Society of Photo-Optical Instrumentation Engineers, Denver, Co, 2004) (SANCHEZ DEL RIO, M., Ed.), SPIE, Bellingham, WA (2004) 109–123.
[56] PARIZZI, A.A., LEE, W.T., KLOSE, W., Modeling the Neutron Spin-Flip Process in a Time-Of-Flight Spin-Resonance Energy Filter, Appl. Phys. A **74** Supplement (2002) S1502–S1504.
[57] WILLENDRUP, P., FARHI, E., LEFMANN, K., McStas 1.7 — a new version of the flexible Monte Carlo neutron scattering package, Physica B **350** 1–3 Suppl. (2004) E735–E737.
[58] ZSIGMOND, G., et al., A survey of simulations of complex neutronic systems by VITESS, Nucl. Instrum. Meth. A **529** (2004) 218–222.
[59] ŠAROUN, J., KULDA, J., RESTRAX — a program for TAS resolution calculation and scan profile simulation, Physica B **234–236** (1997) 1102–1104.
[60] HIESS, A., CURRAT, R., SAROUN, J., BERMEJO, F.J., ILLs renewed thermal three-axis spectrometer IN8C, Physica B, **276–278** (2000) 91.
[61] ŠAROUN, J., KULDA, J., WILDES, A., HIESS, A., Monte Carlo simulation of neutron fluxes on an absolute scale — comparison to experiments, Physica B **276–278** (2000) 148–149.
[62] GILLES, R., ARTUS G., SAROUN, J., BOYSEN, H., FUESS, H., The new structure powder diffractometer at the FRM-II in Garching, Physica B **276–278** (2000) 87–88.
[63] ŠAROUN, J., PIRLING, T., Optimisation of Focusing Monochromator for the Neutron Strain Scanner at a Supermirror Guide, Internal report, Institut Laue-Langevin, Grenoble (2000).
[64] KULDA, J., et al., IN20 — The ILL high-flux polarised-neutron three-axis spectrometer, Appl. Phys. A **74** (2002) S246–S248.
[65] KEMPA, M., et al. The FlatCone multianalyzer setup for ILL's three-axis spectrometers, Physica B **385–386** (2006) 1080–1082.
[66] WIMPORY, R.C., et al., Efficiency boost of the materials science diffractometer E3 at BENSC: One order of magnitude due to a horizontally and vertically focusing monochromator, Neutron News **19** (2008) 16–19.
[67] ŠAROUN, J., Focusing monochromator optimisation for the residual stress diffractometer, KAERI Daejeon, personal communication, 2009.

[68] LIU, Y., Ray tracing simulation of the residual stress diffractometer, CIAE, personal communication, 2008.
[69] FREUND, A., Cross-sections of materials used as neutron monochromators and filters, Nucl. Instrum. Meth. A **213** (1983) 495–501.
[70] STOICA, A.D., On the resolution of slow-neutron spectrometers. I. A general method to calculate resolution functions, Acta Cryst. A **31** (1975) 189–192.
[71] POPOVICI, M., STOICA, A.D, BAJOREK, A., On the resolution of slow-neutron spectrometers. III. Experimental test of the time-of-flight diffractometer resolution-function calculations, Acta Cryst. A, **31** (1975) 197–200.
[72] IONITA, I., STOICA, A.D., The crystal neutron diffractometer resolution function, spatial effects included, J. Appl. Cryst. **33** (2000) 1067–1074.
[73] POPOVICI, M., Progress Report on IAEA Research Project 3496/1982, 3496/RB/1984, unpublished.
[74] KONNECKE, M., The state of the NeXus data format, Physica B **385–386** (2006) 1343–1345.
[75] JAMES, J. A., EDWARDS, L., Application of robot kinematics methods to the simulation and control of neutron beam line positioning systems, Nucl. Instrum. Meth. A **571** (2006). 709–718.
[76] LAM, T., et al., GumTree — An integrated scientific experiment environment, Physica B **385–386** 2 (2006) 1330–1332.
[77] KRIVOGLAZ, M.A, X-ray and Neutron Diffraction in Nonideal Crystals, Springer, Berlin (1996).
[78] HUTCHINGS, M.T., KRAWITZ, A.D., Measurements of Residual and Applied Stress Using Neutron Diffraction, Kluwer Academic, Dordrecht, Netherlands (1992).
[79] DAVID, W.I.F., et al., Structure Determination from Powder Diffraction Data, Oxford Univ. Press (2002).
[80] MITTEMEIJER, E.J., SCARDI, P., Diffraction Analysis of the Microstructure of Materials, Springer, Berlin (2004).
[81] GNÄUPEL-HEROLD, T., IsoDEC: A software for the calculation of diffraction elastic constants, J. Appl. Cryst. **45** 3 (2012) 111–113.
[82] MITTEMEIJER, E.J., SCARDI, P. (Eds.), Diffraction Analysis of the Microstructure of Materials, Springer, Berlin (2004)
[83] LAPACK — Linear Algebra PACKage. Netlib. Retreived from http://www.netlib.org/lapack/
[84] PRESS, W.H., FLANNERY, B.P., TEUKOLSKY, S.A., VETTERLING, W.T., Numerical Recipes in Pascal: the Art of Scientific Computing, Cambridge University Press, Cambridge (1996).
[85] BEHNKEN, H., Direct Evaluation of Intergranular Strains and Stresses, Phys. Stat. Sol. A, **177** (2000) 401–417.
[86] WANG, Y.D., WANG, X.-L., STOICA, A.D., RICHARDSON, J.W., LIN PENG, R., Determination of the stress orientation distribution function using pulsed neutron sources, J. Appl. Cryst. **36** (2003) 14–22.
[87] GNÄUPEL-HEROLD, T., CREUZIGER, A., IADICOLA, M.A., A model for calculating diffraction elastic constants, J. Appl. Cryst. **45** 2 (2012) 197–206.

[88] IADICOLA, M.A., GNÄUPEL-HEROLD, T., Effective X-ray elastic constant measurement for in situ stress measurement of biaxially strained AA5754-O, Mat. Sci. Eng. A-Struct. **545** (2012) 168–175.
[89] NATIONAL INSTITUTE OF STANDARDS AND TECHNOLOGY, Calculation of Diffraction Elastic Constants,
www.ncnr.nist.gov/xtal/software/isodec/
[90] EIGENMANN, B., MACHERAUCH, E., Röntgenographische Untersuchung von Spannungszuständen in Werkstoffen, Mat.-wiss. u. Werkstofftech, **27** 3 (1996) pp. 426–437.
[91] REUSS, A., Berechnung der Fliessgrenze von Mischkristallen aufgrund der Plastizitätsbedingung für Einkristalle Z., Angew. Math. Mech. **9** (1929) 49–58.
[92] VOIGT, W., Lehrbuch der Kristallphysik, Teubner, Leipzig (1928).
[93] LUTTEROTTI, L., MATTHIES, S., WENK, H.R., Materials Analysis Using Diffraction (2011),
http://www.ing.unitn.it/~maud/
[94] GSAS, Homepage on CCP14
http://www.ccp14.ac.uk/solution/gsas/.
[95] "A software for the calculation of diffraction elastic constants from single crystal coefficients"
http://www.uni-kassel.de/maschinenbau/en/institute-einrichtungen/ifw/fachgebiete/metallische-werkstoffe/deccalc.html.
[96] A. ROLLETT, Web Pages
http://neon.materials.cmu.edu/rollett/texture_subroutines/popLA/
[97] MTEX — A MATLAB Toolbox for Quantitative Texture Analysis. Retrieved from: http://code.google.com/p/mtex/
[98] WILLIS, B.T.M. (Ed., Thermal Neutron Diffraction (Proc. Summer School, Harwell, UK, 1968), Oxford, Oxford University Press (1970) 14–33.
[99] DAYMOND, M.R., BOURKE, M.A.M., VON DREELE, R.B., CLAUSEN, B., LORENTZEN, T., Use of Rietveld refinement for elastic macrostrain determination and for evaluation of plastic strain history from diffraction spectra, J. Appl. Phys. **82** (1997) 1554–1562.
[100] WILLIAMSON, G. K., HALL, W. H., X-ray line broadening from filed aluminium and wolfram, Acta Metall. **1** 1 (1953) 22–31.
[101] MITTEMEIJER, E.J., WELZEL, U., The "state of the art" of the diffraction analysis of crystallite size and lattice strain, Z. Kristallogr. **223** (2008) 552–560.
[102] INTERNATIONAL BUREAU OF WEIGHTS AND MEASURES, INTERNATIONAL ORGANIZATION FOR STANDARDIZATION, Guide to the Expression of Uncertainty in Measurement, 1st edn, ISO, Geneva (1993).
[103] TAYLOR, B. N., KUYATT, C.E., Guidelines for Evaluating and Expressing the Uncertainty of NIST Measurement Results, NIST Technical Note 1297, National Institute of Standards and Technology, Gaithersburg, MD (1994).
[104] TAMONOV, A.V., SUMIN, V.V., Investigation of residual stresses in a bimetallic stainless steel-zirconium adapter by neutron diffraction, J. Neutron Res. **12** (2004) 69–73.

[105] FAIDY, C., BIMET – Synthesis Report, Summary Report on the FP4 Nuclear Fission Safety Project "BIMET", Électricté de France, Paris (2001).
[106] KEPPAS, L., KATSAREAS, D.E., ANIFANTIS, N.K., "Finite Element Simulation and Residual Stress Prediction in Multi-Pass Joint Welds of Bi-Metallic Pipes", in Report on Detailed 2D Bead-by-Bead Simulations of Bimetallic Multipass Welded Joints, Technical Report, JRC, Petten, Netherlands (2007).
[107] PINTSCHOVIUS, L., JUNG, V., MACHERAUCH, E., VÖHRINGER, O., Residual Stress Measurements by Means of Neutron Diffraction, Mater. Sci. Eng. **61** (1983) 43–50.
[108] CAGLIOTI, G., PAOLETTI, A., RICCI, F.P., Choice of Collimator for a Crystal Spectrometer for Neutron Diffraction, Nucl. Instrum. Methods **3** (1958) 223–228.
[109] BACON, G.E., Neutron Diffraction, Oxford, Clarendon Press (1975).
[110] SEONG, B.S., EM, V., MIKULA, P., SAROUN, J., KANG, M.-H., Optimization of a bent perfect Si(111) monochromator at a small take-off angle for use in a stress instrument, J. Appl. Cryst. **43** (2010) 654–658.
[111] SEONG, B.S., EM, V., MIKULA, P., SAROUN, J., KANG, M.-H., Unconventional performance of a highly luminous strain/stress scanner for high resolution studies, Mater. Sci. Forum **681** (2011) 426–430.
[112] SEONG, B.S., EM, V., MIKULA, P., SAROUN, J., KANG, M., Optimized Strain/Stress Diffractometer Equipped with Focusing Bent Perfect Crystal Monochromator Would Permit Some Kinetic Processes in Polycrystalline Materials (Proc. 10th European Conf. on Non-Destructive Testing, Moscow, 2010), NDT.net, Bad Breisig (2010).
[113] WITHERS, P.J., Depth capabilities of neutron and synchrotron diffraction strain measurement instruments, J. Appl. Cryst. **37** (2004) 596–606.
[114] WOO, W., et al., Effect of wavelength-dependent attenuation on neutron diffraction stress measurements at depth in steels, J. Appl. Cryst. **44** (2011) 747–754.
[115] MILDNER, D.F.R., et al., A monolithic polycapillary focusing optic for polychromatic neutron diffraction applications, Rev. Sci. Instrum. **73** (2002) 1985–1993.
[116] GIBSON, W. M., et al., "Polycapillary focusing optic for small-sample neutron crystallography", J. Appl. Crystallogr. **35** (2002) 677–683.
[117] ICE, G.E., et al., High-performance Kirkpatrick-Baez supermirrors for neutron milli- and micro-beams, Mater. Sci. Eng. A-Struct. **437** (2006) 120–125.
[118] MILDNER, D., "Wolter Optics for Neutron Imaging", presentation at NOP2010, International Workshop on Neutron Optics, Alpe d'Huez, France, 2010.
[119] SANTISTEBAN, J. R., DAYMOND, M.R., JAMES, J.A., EDWARDS, L., ENGIN-X: a third-generation neutron strain scanner, J. Appl. Cryst. **39** (2006) 812–825.
[120] WANG X.-L., STOICA. A.D., Focusing neutron guides for VULCAN—Design aspects, estimated performance, and detector deployment, Nucl. Instr. Meth. A, **600** (2009) 309–312.
[121] OAK RIDGE NATIONAL LABORATORY, The Engineering Materials Diffractometer at SNS,
http://neutrons.ornl.gov/vulcan/
[122] AN, K., et al., First in situ lattice strains measurements under load at VULCAN, Metall. Trans. A **42** (2011) 95–99.

[123] LEINEWEBER, A., MITTEMEIJER, E.J., Diffraction line broadening due to lattice-parameter variations caused by a spatially varying scalar variable: its orientation dependence caused by locally varying nitrogen content in ε-$FeN_{0.433}$, J. Appl. Cryst. **37** (2004) 123–135.
[124] DAYMOND, M.R., JOHNSON, M.W., The determination of a stress-free lattice parameter within a stressed material using elastic anisotropy, J. Appl. Cryst. **34** 3 (2001) 263–270.
[125] WENK, H.R., LUTTEROTTI, L., VOGEL, S.C., Rietveld texture analysis from TOF neutron diffraction data, Powder Diffr., **25** (2010) 283–296.
[126] SUMIN, V.V., PAPUSHKIN, I.V., VASIN, R.N., VENTER, A.M., BALAGUROV, A.M., Determination of the residual stress tensor in textured zirconium alloy by neutron diffraction, J. Nucl. Materials **421** (2012) 64–72.
[127] RATTI, M., LEUVREY, D., MATHON, M.H., DE CARLAN, Y., Influence of titanium on nano-cluster (Y, Ti, O) stability in ODS ferritic materials, J. Nucl. Materials **386–388** (2009) 540–543.
[128] KOCKELMANN, W., FREI, G., LEHMANN, E.H., VONTOBEL, P., SANTISTEBAN, J.R., Energy-selective neutron transmission imaging at a pulsed source, Nucl. Instr. Meth. A , **578** (2007) 421–434.
[129] ABBEY, B., ZHANG, S.Y., VORSTER, W.J.J., KORSUNSKY, A.M., Feasibility study of neutron strain tomography, Procedia Engineering **1** 1 (2009) 185–188.
[130] WIMPORY, R.C., "Multipurpose instrument for strain, stress, texture and more" and "Simultaneous Measurement and Simulation in Neutron Strain Scanning", presented at workshop on Current State and Future of Neutron Stress Diffractometers' workshop, Sydney, 2012.
[131] BOIN, M., et al., Validation of Bragg edge experiments by Monte Carlo simulations for quantitative texture analysis, J. Appl. Crystallogr. **44** (2011) 1040–1046.

ACRONYMS AND ABBREVIATIONS

BER-II	Berliner Experimentier-Reaktor II
BPC	bent perfect crystal
DEC	diffraction elastic constants
FRM II	Forschungsreaktor München II (Research Reactor Munich II)
FSD	Fourier stress diffractometer
FWHM	full width at half maximum
HANARO	high flux advanced neutron application reactor
HFIR	high flux isotope reactor
HFR	High Flux Reactor
IBR-2	Russian acronym for “Pulsed fast reactor 2”
JINR	Joint Institute for Nuclear Research
LCNDF	Large Component Neutron Diffraction Facility
LVR-15	Light Water Reactor 15
MAUD	material analysis using diffraction
NBSR	neutron beam split-core reactor
NRU	national research universal reactor
ODF	orientation distribution function
OPAL	Open Pool Australian Light Water Reactor
POLDI	pulse-overlap diffractometer
PSD	position sensitive detector
RBMK	high power channel reactor
RTOF	reverse time of flight
SANS	small angle neutron scattering
SNS	spallation neutron sources
TOF	time of flight
TRIGA	Training, Research, Isotopes, General Atomic
TWA 20	Technical Working Area 20
VAMAS	Versailles project on Advanced Materials and Standards

Annex I

ROUND ROBIN TESTS

I–1. INTRODUCTION

In the experimental sciences, a round robin test is a comparison of the determination by measurement of the magnitude of a certain observable at different facilities by different experimenters. Round robin testing facilitates the benchmarking of a laboratory's equipment and procedures, but also provides for the estimation of the scatter band with which an applied test method should be associated. New laboratories and new test methods can be verified against the results obtained at established facilities or by existing methods.

The IAEA CRP 1314 on the Development and Application of the Technique of Residual Stress Measurement in Materials Using Neutrons facilitated the mutual support of institutions from several member states in the conception and further development of their neutron diffraction facilities for residual stress measurement. The structure of this report was in fact agreed upon at the end of this CRP.

As individual residual stress measurement facilities were developed, upgraded or both at the various participating institutions in the course, but also in the aftermath, of this CRP, it was agreed that benchmarking exercises in the form of round robin measurements should be performed in order to verify the performance of new and upgraded equipment, and also to familiarize experimenters with techniques that are possibly new to them.

Facilities in the following countries were originally considered for participation in the exercises:

— Czech Republic;
— Germany;
— Hungary;
— India;
— Indonesia;
— Netherlands;
— Pakistan;
— Romania;
— Russian Federation;
— South Africa.

This annex represents the status of the round robin exercises at the time of drafting of this report. Not as many facilities as originally foreseen were able to perform the measurements as in several cases the neutron source, the diffraction equipment, or both, were in operation during the relevant period.

I–2. DESCRIPTION OF THE ROUND ROBIN EXERCISES

Two round robin exercises were agreed to by the participating organizations on their — in many cases new — neutron diffractometers:

- In the first exercise the VAMAS TWA 20 aluminium ring and plug specimen from the late 1990s was to be reused.
- In the second exercise the objective would be to demonstrate the ability to measure a straight line of increasing strain in a specimen subjected to 4 point bending.

Two specimen sets had been manufactured for the VAMAS TWA 20 exercise [I–1] and the same specimens were used for the first round robin. Prior to the start of the first round robin, the JRC had performed a new series of measurements in the specimen hoop and radial directions. A comparison between these results and the 1997 results is presented in Fig. I–1.

For the second round robin, the JRC, with the support of the JINR, Russian Federation, has developed a suitable 4 point bending device that could provide a strain range of ±1000 μm/m in 10 mm thick steel specimens.

The first round robin was based on an identical exercise performed in the course of the 1996–1999 VAMAS TWA 20 activity [I–1]. The specimen set for this round robin is shown in Fig. I–2. It is an interference fit between an aluminium ring and a slightly oversized aluminium plug inserted into it. The specimen is 50 mm long and 50 mm in diameter. A second identical plug, 25 mm in diameter and from the same batch of material, is shown in the picture to the left of the ring and plug specimen. This second plug was to be used for the free of stress measurements.

The photograph also shows a fiducial mark — a line — engraved across the visible flat surfaces of the cylindrical specimens. This line ensured that the same orientations of the ring and plug specimen and the reference plug with respect to one other are maintained for the measurements, and it also represented the diametric line, along which the measurements were to be taken. The detailed requirements for measurement execution and reporting in this round robin exercise are given in the technical information, Section I–4.

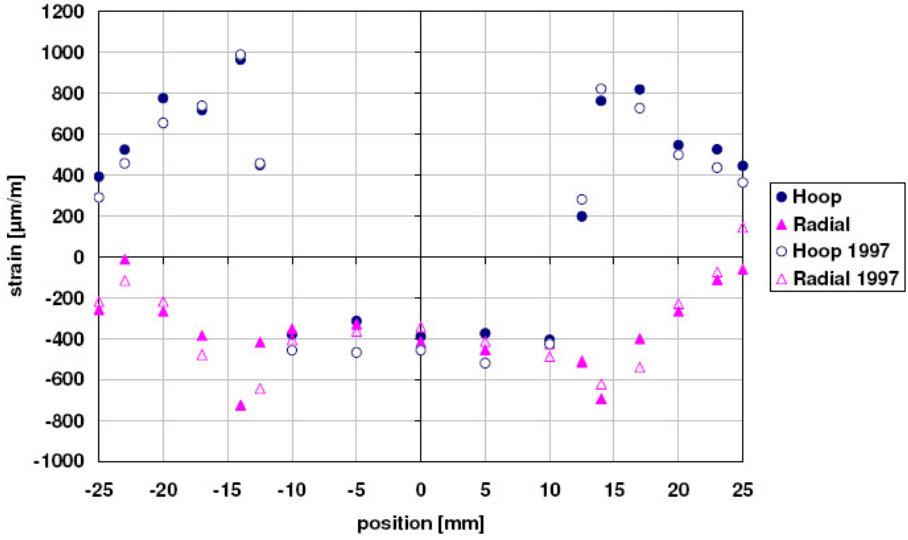

FIG. I–1. Round robin No. 1: hoop and radial strains measured at JRC in 1997 and in 2009 (see legend for details).

FIG. I–2. Round robin No. 1: aluminium ring and plug interference fit specimen set.

Measurements of strain in the hoop and radial directions were requested; measurements in the axial direction were optional in this exercise. The free of stress references were to be measured from the simple plug specimen in the same orientations (based on the fiducial mark) and with the same measurement settings as for the strain measurements.

As mentioned above, the JRC had performed the first measurement series at its High Flux Reactor in April 2009 (see data presented in Fig. I–2). Based on these measurements, an amendment to the existing protocol for this round robin was devised, which is also given in Section I–4. The instructions given in this section were given to the participants together with the specimens so that the measurements were executed along the same lines by all the laboratories.

For the second round robin, it was agreed that the specimens to be considered would be steel strips, one of carbon steel and one of stainless steel, with a 10 × 20 mm^2 cross-section of a length to match the dedicated 4 point bending device provided (see Fig. I–3). The strain range desired was agreed to be ±1000 μm/m. This range was considered to be fully within the elastic regime for normal steels, so that the experiments would not result in any permanent deformation of the specimens.

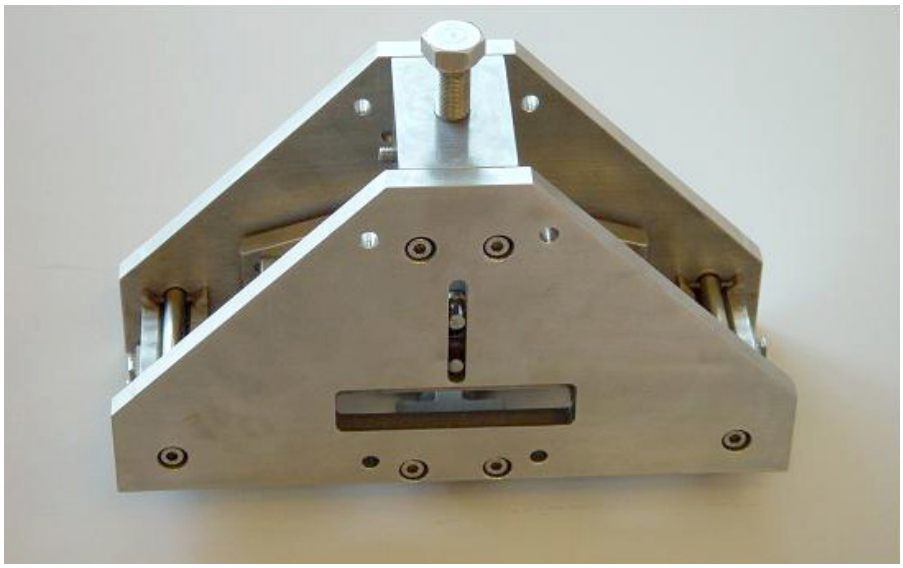

FIG. I–3. Four point bending device for round robin No. 2.

For the purpose of this round robin exercise, a four point bending device was designed at the JRC, based on information received from the JINR. This purpose based design fulfilled the following general requirements:

— To facilitate the desired bending strain range in 10 mm thick steel as specified above;
— To provide openings for incident and diffracted neutron beam access in a diffraction angle range from 70° to 110°;
— To provide for this access in two — or preferably three —specimen orientations;
— To allow for a limited range of specimen rocking during measurements.

The design of the 4 point bending device and the dimensions of the specimen should allow for measurements at 8–10 locations through the thickness of the steel beams, with a reasonable strain gradient of up to 200 $\mu m \cdot m^{-1} \cdot mm^{-1}$ depending on the setting of the bending. It should be possible for all the participating facilities to resolve a strain gradient of this magnitude. Sampling volume cross-sections of up to 2×2 mm^2 should be usable for this exercise.

For the stainless steel — the exact material remains to be selected — it is considered possible that measurements will be influenced by grain size effects. Where possible, the instrument operators should try to mitigate such effects through specimen rocking during measurements.

The device shown in Fig. I–3 had been manufactured to the design of JRC; however, careful inspection of the parts led to the conclusion that many of the requested tolerances in manufacturing had not been respected. In fact, the functioning of the device was compromised to such a degree that JRC had to return it to the manufacturer. At the time of reporting, JRC had not obtained new devices from a new supplier. Nevertheless, the Institute for Solid State Physics and Optics (SZFKI), Hungary, had produced in the meantime a 4 point bending device following the JRC design which was fully functional. Despite this achievement, it was not possible to begin the second round robin exercise before the drafting of this report. It is nevertheless the intention to pursue both round robins and to report on the final outcome in a different context in the future.

I–3. RESULTS OF ROUND ROBIN No. 1

The ring and plug round robin has been ongoing since Spring 2009. The detailed instructions for the execution of the measurements were largely copied from the corresponding exercise in VAMAS TWA 20 [I–1]. These instructions, amended by additional information based on earlier experience, can be found

in Section I–3. All the participating laboratories were requested to perform measurements and to report the resulting data in accordance with the instructions.

At the time of reporting, the following laboratories have executed the ring and plug measurements for this round robin:

— JRC, Netherlands;
— HZB, Germany;
— SZFKI, Hungary;
— NPI, Czech Republic;
— BATAN, Indonesia.

In addition, independently of the current round robin, ANSTO in Australia and ORNL in the USA, at their facilities at OPAL, HFIR and at the SNS, performed these measurements in the context of the benchmarking of their new facilities. They agreed to also contribute their data to the present IAEA round robin data comparison.

The following CRP participants did not have residual stress diffractometers operational during the years 2009 and 2010 and will foreseeably contribute measurements to this round robin exercise at a later stage:

— FLNP, Russian Federation;
— SAFARI, South Africa;
— INR Piteşti, Romania.

Measurements in India and Pakistan will be scheduled when both specimen sets are available for this round robin, based on the availability of the facilities there.

Figures I–4 and I–5 show the hoop and radial strains, respectively, that have been reported by the participating laboratories, including the respective uncertainties derived from the fitting errors of the data. At this point, data are available from five laboratories. The data present in the plot illustrate the situation nicely. The measurement agreement between the laboratories for the hoop direction is very good, with the majority of the data points agreeing to within the uncertainty that is based on the fit errors of the measurements. NPI has measured substantially more measurement locations than requested. On the average the data sets from JRC, NPI, HZB and BATAN agree well in the amount of strain measured. The deviating trend of the SZFKI data on the right hand side of the plot cannot be easily explained.

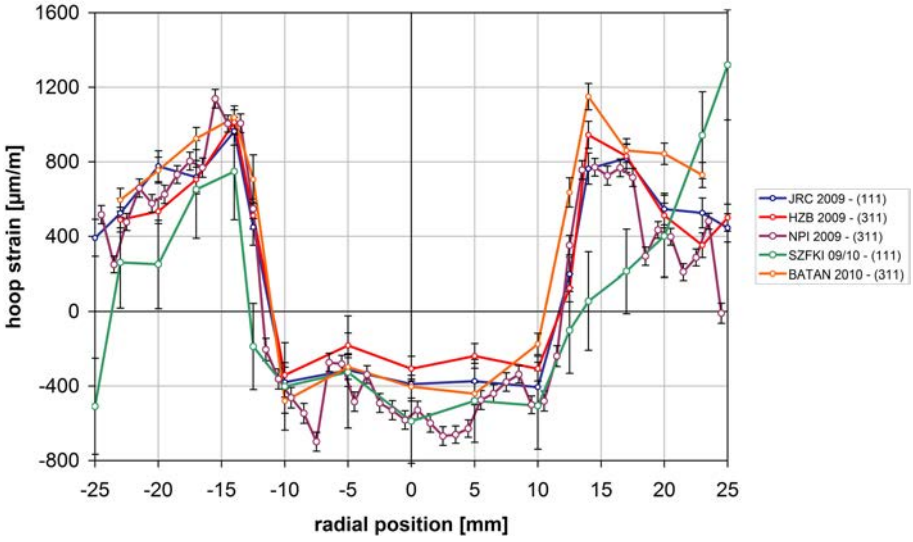

FIG. I–4. Round robin No. 2: Hoop strains reported by the participating laboratories.

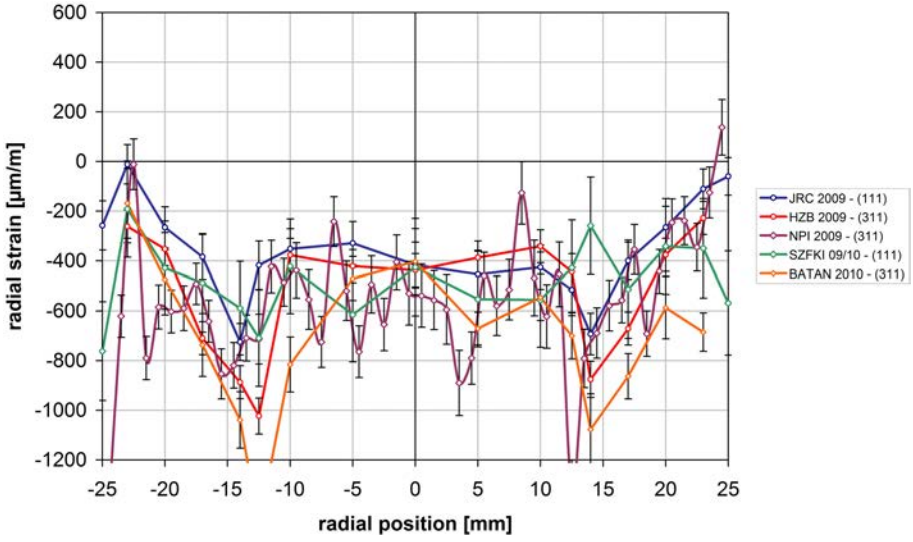

FIG. I–5. Round robin No. 2: Radial strains reported by the participating laboratories.

The amount of scatter of the results varies between the laboratories. It is actually highest for the NPI data. This observation can obviously not be explained with the number of individual measurements; it must also be related to

the measurement geometry, the sampling volume used and the angular resolution of the instrument. In fact, one item that directly contributes to the data is the sampling volume used. Some laboratories have used a 3 mm beam width and others only 2 mm. The material apparently exhibits a grain size where the size of the sampling volume makes a difference to the data scatter. Actually, the JRC, having used a 3 mm beam width, obtained the data with the lowest overall scatter. In almost all cases, the data scatter for the radial direction was higher than for the hoop direction.

Experimental data such as these provide information on the accuracy of specimen positioning in the beam, and they also give an indication of possible differences in the reference measurements. In this case, there is a very small apparent positioning difference between the data sets that can be seen from the results obtained at the positions +12.5 mm and −12.5 mm. A detailed analysis would show a deviation for the other data sets more or less within the fitting uncertainty of the data.

The SZFKI data have more than twice the fitting uncertainty compared to the other data sets. This appears to be mainly related to the use of a PG monochromator and its (002) diffraction plane. This type of monochromator provides a lower measurement resolution than those used at the other facilities and the peak widths observed are consequently two to three times larger, resulting in the relatively high fitting uncertainties.

For the radial direction measurements (Fig. I–6), the agreement between the data sets is a little worse than in the hoop direction. The number of data points not agreeing within the error is bigger, and there seems to be, at least for the data points within the ring, a reference offset between the results. For the NPI data, again a higher scatter is observed, and in the case of the radial direction measurements, this scatter obscures the steep strain gradient at the ring and plug interface that can still be identified in the JRC and HZB data. The SZFKI do not reproduce the strain gradient at the ring and plug interface well either. In the left half of the plot, the strain gradient in the ring seems to be similar to what has been observed by the other laboratories, but again this is not the case for the right hand side of the plot. Also here the measurement uncertainties are substantially higher for the SZFKI data. For the BATAN and NPI data there seems to be a slight offset of the reference measurements with respect to an ‘educated average’ of the other data sets. On the other hand, the strain gradients in the ring, left and right, are in reasonably good agreement with the other data sets and the strain gradient at the ring–plug interface is present as well.

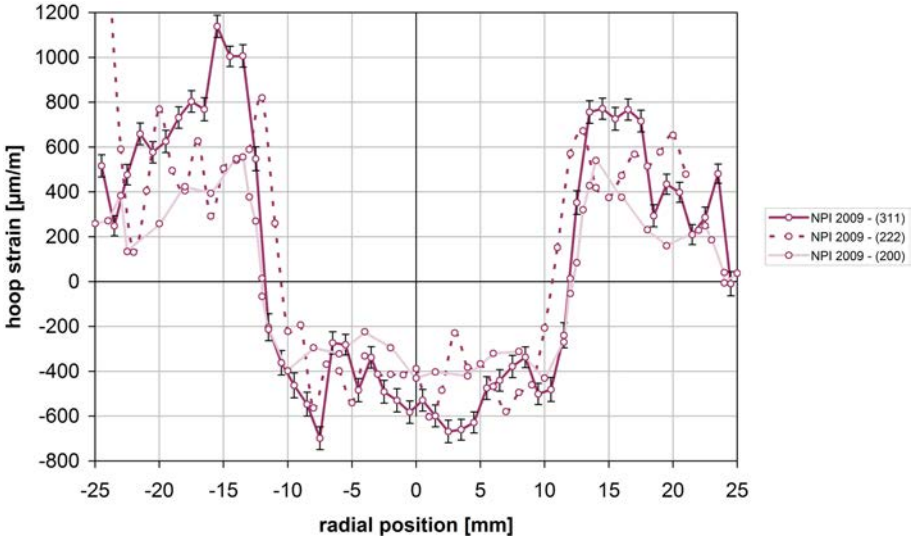

FIG. I–6. Round robin No. 2: hoop strains measured by NPI on the (311), (222) and (200) crystallographic planes.

In addition to the required measurements, NPI have used three different crystallographic reflection planes, namely the (311) included in Figs I–4 and I–5, and the (222) and the (200) planes. As aluminium alloys are normally considered elastically isotropic materials, the choice of diffraction plane should not have a significant influence on the strains measured. Figure I–6 shows the hoop strains that have been observed by NPI in these measurements.

While there are, in this case, small differences between the strains observed on the different diffraction planes, the results are largely in reasonable agreement, as expected. It is noticed that the measurements from the (200) reflection plane exhibit significantly less scatter than those from the other two planes. While slightly different instrument settings have been used for the (200) measurements, it is not directly obvious what the reason for this is.

The NPI measurements, in some cases, also exhibit pronounced surface effects, which are, for example, completely missing in the JRC data presented in Fig. I–5. Surface effects are instrument specific and, in turn, depend on scattering angle, gauge volume and neutron optics (e.g. type of monochromator and type of slits, collimators used).

More comprehensive round robin data analyses will be provided and reported within a separate publication when data have been made available by the remaining participants.

I–4. TECHNICAL INFORMATION FOR THE RING AND PLUG ROUND ROBIN EXERCISE

Ring and plug measurements — experimental protocol[1]

Introduction

Two sets of aluminium alloy ring and plug and reference plug samples are supplied and designated as samples 1 and 2. A photograph of the ring and plug is provided in Fig. I–7. The details below are meant to provide the technical requirements that should be complied with in the measurements and the technical information that should be recorded and supplied. The instructions are written for a conventional monochromatic instrument. Those with pulsed sources or other types of instruments should make changes as necessary, but should try to ensure that their data will be as comparable as is reasonably possible. The complementary information given is based on experience with the VAMAS ring and plug round robin exercise.

Technical details

(1) The reference plug is a cylinder of 25 mm diameter and 50 mm length.
(2) The ring and plug sample is a cylinder of 50 mm diameter and 50 mm length.
(3) A line with an arrow, to indicate a common direction, has been marked across an end face diameter on each component — the ring, the plug and the reference plug. The lines on the ring and plug sample should be aligned but may be a few degrees off. (In sample 1 the misalignment is approximately 6° and the arrows on the ring and the plug are in opposite directions, but this should make little difference to the results). To reduce uncertainty, the plug line should always be taken as the common direction and be the line along which measurement points are located. The head of the arrow on the plug defines the positive radial direction.
(4) Measurements on the reference plug should be made at its centre in with radial (defined by the arrow), hoop (normal to the arrow) and axial orientations.
(5) Measurements on the ring and plug should be made across the central diameter at selected locations in radial (defined by the arrow on the plug), hoop (normal to the arrow) and axial orientations.

---

[1] This experimental protocol was drafted for the VAMAS TWA20 activity by P.J. Webster, University of Salford, United Kingdom.

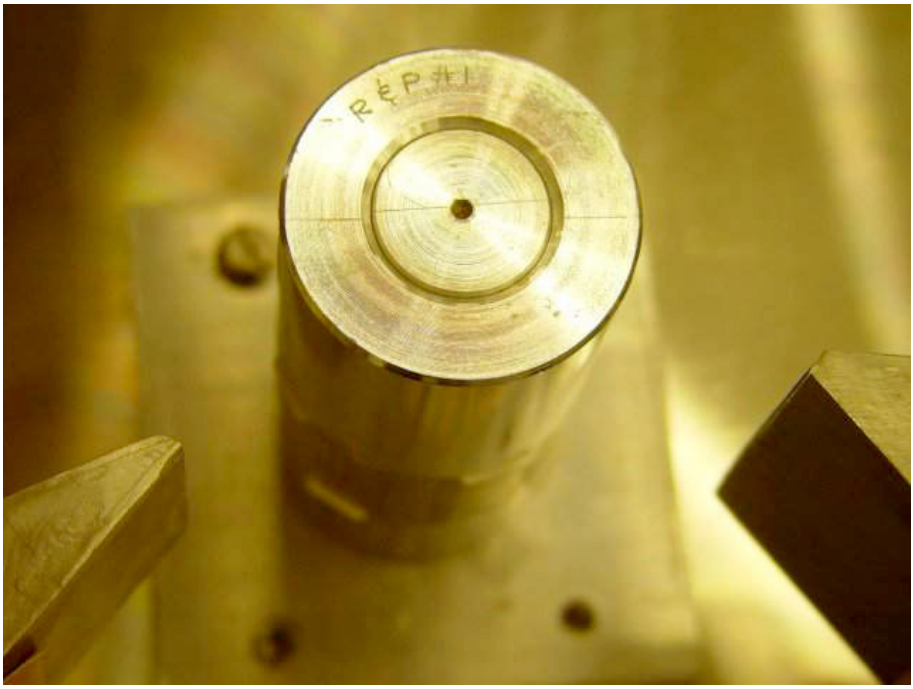

FIG. I–7. Round robin No. 2: Aluminium ring and plug specimen at neutron diffractometer, measurements in hoop direction (normal to the engraved fiducial mark).

(6) Gauge heights should not be greater than 20 mm for hoop and radial measurements and not greater than 5 mm for axial measurements.

(7) Slit widths should be not greater than 3 mm and should be the same for all measurements.

(8) Measurements should be made at 15 (as agreed), or (preferably) 17, specified locations (as defined by the position of the centre of the geometrically defined gauge volume).

(9) Five of the specified locations are at the centre of the plug, at the interface of the ring and the plug and at the surface of the ring, i.e. $r = 0$, ±12.5 mm and ±25 mm. These measurements should enable instrument characteristics such as spatial resolution and surface effects to be evaluated. The remaining ten or twelve locations have been chosen so as to best define the residual stress fields in the ring and plug, clear of the interface and surface. The specified locations are $r = \pm 5$ mm, ±10 mm, ±14 mm, ±17 mm, ±20 mm and ±23 mm.

(10) The choice of reflection(s) is open. At the Deep River meeting it was stated that (111) and (200) were preferred but (220), (311) and (222) are also acceptable. It should be noted that the samples are textured and, in some directions, some reflections are relatively very weak, and it is unlikely to be practicable to make all three orthogonal measurements with some of the reflections. Members are advised to check reflection intensities for orthogonal orientations at the start of their experiments so that counting times for the different orientations may be estimated.
(11) Counting times should be chosen such that the minimum statistical strain accuracy is 10^{-4}.
(12) Absolute and relative data are both acceptable.
(13) Appropriate changes should be made as necessary for pulsed and special instruments.

Measurement record requirements

— Type of instrument;
— Instrument name and location;
— Date and time measurements were taken;
— Monochromating crystal/reflection;
— Type of detector;
— Monochromator to reference point distance;
— Detector to reference point distance;
— Absolute or nominal wavelength and calibration procedure;
— Incident slit width (ISW);
— Detector slit width (DSW);
— Incident slit height (ISH);
— Detector slit height (DSH);
— Incident slit to reference point distance (ISD);
— Detector slit to reference point distance (DSD);
— Detector angle;
— Actual gauge intensity profile (if possible);
— Sketch of experimental arrangement showing beam and sample positions (with defining arrow) for each measurement orientation;
— Radial, hoop and axial peak positions with estimated uncertainties;
— Radial, hoop and axial strains with estimated uncertainties;
— Radial, hoop and axial stresses with estimated uncertainties;
— Elastic constants and Poisson's ratios used.

Remarks for the 2009/2010 exercise complementary to the protocol from 1998

— For the purpose of this round robin, measurements in the specimen hoop and radial directions are considered the most relevant. These can be completed in a very short time. Axial direction measurements facilitate stress calculation, but are less important for the interlaboratory comparisons. Moreover, measurements in the axial direction have been found to be very challenging in these specimens because of their strong texture. Axial measurements would probably be possible in the (220) reflection plane only.
— Accurate specimen alignment is of paramount importance. It is strongly encouraged to invest the time necessary for this (for all directions). As stated above, the measurements themselves can be made quickly. At the JRC, Petten, 15 minutes per measurement point were sufficient in April 2009.
— For the radial and hoop directions, the (111) or (311) reflection planes are preferred in view of the choices made by the participants of the VAMAS TWA 20 round robin in the late 1990s.
— Concerning the sampling volume, it is suggested to use beam sizes of 2–3 mm width; the beam height should be 20 mm or less as indicated in the 1998 protocol. Higher measurement resolution, although certainly possible at many facilities, could have an impact on the comparison of results.
— Try to complete the attached reporting template as much as possible. For this purpose, a lot of data will have to be recorded with respect to the measurement set-up and the analysis of the data. Please review the template carefully prior to your measurements.

Other notes

(a) Because of intergranular strains, it is necessary to measure the reference plug in the three symmetry directions (most importantly in the radial and hoop directions).
(b) For axial measurements — if performed — the line marked on the ring and plug should be horizontal. Likewise for the reference measurements on the plug.
(c) For radial and hoop measurements, the axis should be vertical. For radial measurements, the arrow should be along the scattering vector. For hoop measurements, it should be perpendicular.
(d) When measuring across the diameter in a specified orientation (radial, hoop or axial), the sample orientation should be kept constant. It should not be rotated 180° at $r = 0$ when changing from negative to positive radial locations to reduce beam attenuation effects.

(e) All original data should be stored so that they may be reanalysed if necessary.

REFERENCES TO ANNEX I

[I–1] WEBSTER, G.A. (Ed.), Neutron Diffraction Measurements of Residual Stress in a Shrink-Fit Ring and Plug, Versailles Project on Advanced Materials and Standards, Report No. 38, National Physical Laboratory, Teddington (2000).

Annex II

EXAMPLES OF RESIDUAL STRESS FACILITIES

This annex provides an overview of some neutron diffractometers for residual stress measurement in operation throughout the world. The authors do not guarantee the completeness of the following lists. Indeed, there was no intent to include instruments that are not in operation yet or no longer in operation at the time of drafting this report. Furthermore, no instruments have been considered where residual stress measurement is not the primary application of the installation.

Table II–1 presents an overview of operational instruments in different regions, while Tables II–2 to II–12 contain more detailed technical information for some neutron diffractometers for residual stress measurement that has been provided by the scientists responsible for these instruments.

TABLE II–1. OVERVIEW OF NEUTRON DIFFRACTOMETERS FOR RESIDUAL STRESS MEASUREMENT

Country	Facility	Source/Institute	Type
		Europe	
Czech Republic	SPN-100	LVR-15/NPI	Monochromatic
Czech Republic	TKSN-400	LVR-15/NPI	Monochromatic
France	SALSA	HFR/ILL	Monochromatic
France	DIANE	Orphee/LLB	Monochromatic
Germany	E3	BER-II/HZB	Monochromatic
Germany	STRESS-SPEC	FRM II/TU Munich	Monochromatic
Hungary	ATHOS	BRR/BNC	Monochromatic
Netherlands	HB4-LCNDF	HFR/JRC	Monochromatic
Netherlands	HB5-V.I.S.A.	HFR/JRC	Monochromatic
Romania	DIR 1	TRIGA/INR	Monochromatic

TABLE II–1. OVERVIEW OF NEUTRON DIFFRACTOMETERS FOR RESIDUAL STRESS MEASUREMENT (cont.)

Country	Facility	Source/Institute	Type
Russian Federation	FSD	IBR-2/JINR	Reverse TOF
Russian Federation	EPSILON	IBR-2/JINR	TOF
Switzerland	POLDI	SINQ/PSI	TOF
UK	ENGIN-X	ISIS/RAL	TOF
	North America		
Canada	L3	NRU-II/NRC	Monochromatic
USA	SMARTS	LANSCE/LANL	TOF
USA	VULCAN	SNS/ORNL	TOF
USA	NRSF2	HFIR/ORNL	Monochromatic
USA	BT8-DARTS	NBSR/NCNR	Monochromatic
	Africa		
South Africa	Residual Stress Diffractometer	SAFARI-1 /NECSA	Monochromatic
	Asia-Pacific		
Australia	KOWARI	OPAL/ANSTO	Monochromatic
China	Residual Stress Diffractometer	CARR/ CIAE	Monochromatic
India	PD-3	Dhruva/BARC	Monochromatic
Indonesia	DN1	RSG-GAS/ BATAN	Monochromatic
Pakistan	Residual Stress Diffractometer	PARR/PINSTECH	Monochromatic
Republic of Korea	HRPD	HANARO/KAERI	Monochromatic
Japan	TAKUMI	J-PARC/ JAEA and KEK	TOF

TABLE II–2. HIGH RESOLUTION STRESS/STRAIN DIFFRACTOMETER TKSN-400, CZECH REPUBLIC

Source	LVR-15, 15 MW research reactor
Name of instrument	High Resolution Stress/Strain Diffractometer TKSN-400
Web link	Reactor: http://www.cvrez.cz/web/en/reactor-lvr-15 Instrument: http://neutron.ujf.cas.cz/en/hk9
User facility?	Yes
If yes, where are the users from?	Central European Region
Experiment proposal deadlines	Continuously during the year
Time from application to beam time for normal users	2–3 months
Measurement principle (monochromatic, TOF, RTOF, etc.)	Monochromatic
Wavelength (range)	0.13–0.22 nm
Take-off angle (range)	40–70°
Monochromator type and reflection(s)	Si(220)
Resolution (intrinsic peak width, $\Delta d/d$, etc.)	$\Delta d/d = 2 \times 10^{-3}$
Neutron flux on specimen	$5 \times 10^{5} \cdot \mathrm{cm}^{-2}\mathrm{s}^{-1}$
Specimen weight capacity	Up to 50 kg
Movement ranges of positioning stages	x 100 mm y 100 mm z ±50 mm
Additional sample movement possibilities (Eulerian cradle, Hexapod, Robot arm, etc.)	Yes, Eulerian cradle
Available sample environment furnace, load frame, irradiated samples, etc.)	Tension compression rig equipped with the heating system up to 1000°C
Description of detector	1d-PSD 200 mm length, 2 mm spatial resolution
Beam opening: sizes, horizontal/vertical	30 mm × 60 mm

TABLE II–2. HIGH RESOLUTION STRESS/STRAIN DIFFRACTOMETER TKSN-400, CZECH REPUBLIC (cont.)

Source	LVR-15, 15 MW research reactor
Beam defining optics (slits, radial collimators)	Slits
Software packages	Custom
Data formats	ASCII
Typical applications	In situ structure and phase studies influenced by an external load; stress scanning around the welds
Operation (days/year)	Depends on reactor, typically 180
Industrial users	Yes
Iron pin data	In process

TABLE II–3. SPN-100, CZECH REPUBLIC

Source	LVR-15, 15 MW research reactor
Name of instrument	SPN-100
Web link	Reactor: http://www.cvrez.cz/web/en/reactor-lvr-15 Instrument: http://neutron.ujf.cas.cz/en/hk4
User facility?	Yes
If yes, who are the users?	Central European Region
Experiment proposal deadlines	Continuously during the year
Time from application to beam time for normal users	2–3 months
Measurement principle (monochromatic, TOF, RTOF, etc.)	Monochromatic
Wavelength (range)	0.15–0.23 nm
Monochromator type and reflection(s)	Bent Si(111) and Si(220)
Take-off angle (range)	30–60°

TABLE II–3. SPN-100, CZECH REPUBLIC (cont.)

Source	LVR-15, 15 MW research reactor
Resolution (intrinsic peak width, $\Delta d/d$, etc.)	$\Delta d/d =$
Neutron flux on specimen	$2 \times 10^5 cm^{-2} \cdot s^{-1}$
Specimen weight capacity	Up to 50 kg
Movement ranges of positioning stages	x 100 mm y 100 mm z ±50 mm
Additional sample movement possibilities (Eulerian cradle, Hexapod, Robot arm, etc.)	Yes
Available sample environment (furnace, load frame, irradiated samples, etc.)	Tension compression rig equipped with the heating system
Description of detector (with details)	1d-PSD 200 mm length, 2 mm spatial resolution
Beam opening: sizes, horizontal/vertical	30 mm × 60 mm
Beam defining optics (slits, radial collimators)	Slits
Software packages	Own
Data formats	ASCII
Typical applications	Stress scanning around the welds
Operation (days/year)	Depecnds on reactor, typically 180
Industrial users (yes/no, examples if possible)	Yes
Iron pin data	In process

TABLE II–4. E3, GERMANY

Source	BER-II, 10 MW research reactor
Name of instrument	E3
Web link	www.helmholtz-berlin.de
User facility?	Yes
If yes, where are the users from?	International

TABLE II–4. E3, GERMANY (cont.)

Source	BER-II, 10 MW research reactor
Experiment proposal deadlines	1 March and 1 September
Time from application to beam time for normal users	3–6 months
Measurement principle (monochromatic, TOF, RTOF, etc.)	Monochromatic
Wavelength (range)	0.1486 nm
Take-off angle (range)	65°
Monochromator type and reflection(s)	Vert. foc. horizont. bent Si
Resolution (intrinsic peak width, $\Delta d/d$, etc.)	1.4×10^{-3}
Neutron flux on specimen	$\approx 5 \times 10^{6}$ cm$^{-2}\cdot$s^{-1}
Specimen weight capacity	300 kg
Movement ranges of positioning stages:	x 100 mm y 100 mm z 0–300 mm
Additional sample movement possibilities (Eulerian cradle, hexapod, robot arm, etc.)	Eulerian cradle
Available Sample Environment (furnace, load frame, irradiated samples etc.)	Furnace, cryostat
Description of Detector (with details)	300 × 300 mm^2 Denex detector (PSD)
Beam opening: sizes, horizontal/vertical	Typically 1–20 mm^2
Beam defining optics (slits, radial collimators)	Slits and radial collimator to be added soon
Software packages	TvTueb, stress-tex, peak fit
Data formats	Caress
Typical applications	Crankshafts, pistons, combustion chambers, impellers, welds
Operation (days/year)	220
Industrial users	Yes

TABLE II–5. ATHOS, HUNGARY

Source	10 MW Budapest Research Reactor (BRR)
Name of instrument	ATHOS
Web link	www.bnc.hu
User facility?	Yes
If yes, where are the users from?	Central European Region
Experiment proposal deadlines	May 15, Oct 15
Time from application to beam time for normal users	3–6 months
Measurement principle (monochromatic, TOF, RTOF, etc.)	monochromatic,
Wavelength (range)	0.2–0.6 nm
Take-off angle (range)	37–120°
Monochromator type and reflection(s)	PG 002/004
Resolution (intrinsic peak width, $\Delta d/d$, etc.)	$\Delta d/d =$
Neutron flux on specimen	$\sim 10^6\ \mathrm{cm^{-2} \cdot s^{-1}}$
Specimen weight capacity	Up to 10 kg
Movement ranges of positioning stages	x 100 mm y 100 mm z ±50 mm manually
Additional sample movement possibilities (Eulerian cradle, hexapod, robot arm, etc.)	No
Available sample environment (furnace, load frame, irradiated samples etc.)	Furnace and load frame in development
Description of detector	200 mm × 200 mm 1.8 mm resolution delay line type
Beam opening: sizes, horizontal/vertical	30 mm × 60 mm
Beam defining optics (slits, radial collimators)	Slits and radial collimator
Software packages	Custom
Data formats	ASCII
Typical applications	—

TABLE II–5. ATHOS, HUNGARY (cont.)

Source	10 MW Budapest Research Reactor (BRR)
Operation (days/year)	Depends on reactor, typically 80–160
Industrial users	—
Iron pin data	In process

TABLE II–6. LARGE COMPONENT NEUTRON DIFFRACTION FACILITY — HB4 LCNDF, THE NETHERLANDS

Source		45 MW High Flux Reactor, HFR
Name of instrument		Large Component Neutron Diffraction Facility — HB4 LCNDF
Web link		http://ie.jrc.ec.europa.eu/ http://www.nrg.eu/product/irradiat/hfr/index.html
User facility?		No
Experiment proposal deadlines		—
Time from application to beam time for normal users		—
Measurement principle (monochromatic, TOF, RTOF, etc.)		monochromatic
Wavelength (range)		0.19–0.65 nm
Take-off angle (range)		30–135°
Monochromator type and reflection(s)		PG (004) or PG(002)
Resolution (intrinsic peak width, $\Delta d/d$, etc.)		unknown
Neutron flux on specimen		$<10^6$ cm$^{-2}\cdot$s^{-1}
Specimen weight capacity		1000 kg
Movement ranges of positioning stages:	x y z	200 mm 200 mm 300 mm manually

TABLE II–6. LARGE COMPONENT NEUTRON DIFFRACTION FACILITY — HB4 LCNDF, THE NETHERLANDS (cont.)

Source	45 MW High Flux Reactor, HFR
Additional sample movement possibilities (Eulerian cradle, hexapod, robot arm, etc.)	ω rocking during measurement possible
Available sample environment (furnace, load frame, irradiated samples, etc.)	Heavy container for measurements in irradiated materials, limited purpose furnaces up to 1400°C
Description of detector	AECL 32 wire multidetector, 2 mm wire spacing corresponding to 0.1° of angle per wire, surface area 63 mm × 127 mm, ^{3}He gas detector
Beam opening: sizes, horizontal/vertical	1–8 mm horizontal 1–35 mm vertical
Beam defining optics (slits, radial collimators)	Slits
Software packages	Custom made software based on LabVIEW for instrument operation, PEAKFIT for data analysis
Data formats	ASCII, binary
Typical applications	Mainly residual stress measurements on welds in steel
Operation (days/year)	Normally >280
Industrial users	Occasionally; studies of welding stresses relevant for nuclear power installations
Iron pin data	None
Picture	Fig. II–1
Can you provide diffraction elasticity constants (DECs) to be compiled into a database?	No experimental data, since no load frame available

TABLE II–7. VERSATILE INSTRUMENT FOR STRESS ANALYSIS — HB5, THE NETHERLANDS

Source	45 MW High Flux Reactor, HFR
Name of instrument	Versatile Instrument for Stress Analysis — HB5
Web link	http://ie.jrc.ec.europa.eu/ http://www.nrg.eu/product/irradiat/hfr/index.html
User facility?	No
Experiment proposal deadlines	—
Time from application to beam time for normal users	—
Measurement principle (monochromatic, TOF, RTOF, etc.)	Monochromatic
Wavelength (range)	0.256 nm
Take-off angle (range)	76°
Monochromator type and reflection(s)	Cu (111)
Resolution (intrinsic peak width, $\Delta d/d$, etc.)	Unknown
Neutron flux on specimen	$\sim 10^6$ cm^{-2}·s^{-1}
Specimen weight capacity	200 kg
Movement ranges of positioning stages	x ±125 mm y ±125 mm z >250 mm
Additional sample movement possibilities (Eulerian cradle, hexapod, robot arm, etc.)	ω-rocking during measurement possible with limitations; instrument rests on Tanzboden floor, change to different beam port possible, however, currently no second monochromator installed
Available sample environment (furnace, load frame, irradiated samples, etc.)	Limited purpose furnaces up to 1400°C
Description of detector	ORDELA type 1150 N single wire 1D position sensitive detector, 1 mm theoretical resolution, currently operated at about 0.04° of angle per pixel, surface area 100 × 50 mm, ^{3}He gas detector

TABLE II–7. VERSATILE INSTRUMENT FOR STRESS ANALYSIS — HB5, THE NETHERLANDS (cont.)

Source	45 MW High Flux Reactor, HFR
Beam opening: sizes, horizontal/vertical	1–5 mm horizontal 1–30 mm vertical
Beam defining optics (slits, radial collimators)	Slits
Software packages	Custom made software based on LabVIEW for instrument operation, PEAKFIT for data analysis
Data formats	ASCII
Typical applications	Mainly residual stress measurements on welds in steel
Operation (days/year)	Normally >280
Industrial users	Rarely; last customer study was a cast automotive engine part
Iron pin data	None
Picture	Fig II–2
Can you provide diffraction elasticity constants (DECs) to be compiled into a database?	No experimental data, since no load frame available

TABLE II–8. FSD — FOURIER STRESS DIFFRACTOMETER, RUSSIAN FEDERATION

Source	2 MW IBR-2 pulsed reactor, 1500 MW peak power in pulse
Name of instrument	FSD — Fourier Stress Diffractometer
Web link	http://flnp.jinr.ru/150/
User facility?	Yes
If yes, who are the users?	Beam time is available for scientists from any country via user programme (proposals)

TABLE II–8. FSD — FOURIER STRESS DIFFRACTOMETER, RUSSIAN FEDERATION (cont.)

Source	2 MW IBR-2 pulsed reactor, 1500 MW peak power in pulse
Experiment proposal deadlines	15 May and 15 October
Time from application to beam time for normal users	3 months
Measurement principle (monochromatic, TOF, RTOF, etc.)	RTOF
Wavelength (range)	0.09–0.8 nm
Resolution (intrinsic peak width, $\Delta d/d$, etc.)	0.0023
For backscattering and ±90° detectors	0.0040
Neutron flux on specimen	1.8×10^6 cm$^{-2}\cdot$s^{-1}
Specimen weight capacity	50 kg
Movement ranges of positioning stages	x 0–100 mm y 0–100 mm z 0–60 mm
Additional sample movement possibilities (Eulerian cradle, hexapod, robot arm, etc.)	Eulerian cradle
Available sample environment (furnace, load frame, irradiated samples, etc.)	Furnace (up to 1000°C), Stress rig LM-20 with maximal applied load 20 kN
Description of detector	ZnS(Ag) scintillator detectors in time focusing geometry
Beam opening: sizes, horizontal/vertical	10 mm horizontal 75 mm vertical
Beam defining optics (slits, radial collimators)	Slits and radial collimator
Software packages	MRIA (Rietveld method) and UPEAK (single peak processing)
Data formats	Binary, intrinsic format
Typical applications	Material mechanical properties, welds, microstress and particle size effects, fatigue damage due to cyclic load
Operation (days/year)	100

TABLE II–8. FSD — FOURIER STRESS DIFFRACTOMETER, RUSSIAN FEDERATION (cont.)

Source	2 MW IBR-2 pulsed reactor, 1500 MW peak power in pulse
Industrial users	Occasionally
Iron pin data	Not presently
Picture	Figs II–3 and II–4
Can you provide diffraction elasticity constants (DECs) to be compiled into a database?	Yes

TABLE II–9. EPSILON — STRESS/STRAIN DIFFRACTOMETER, RUSSIAN FEDERATION

Source	2 MW IBR-2 pulsed reactor, 1500 MW peak power in pulse
Name of instrument	EPSILON — stress/strain diffractometer
Web link	http://flnp.jinr.ru/154/
User facility?	Partially
If yes, who are the users?	Restricted access after consultation with responsible person
Experiment proposal deadlines	15 May and 15 October
Time from application to beam time for normal users	3 months (approx.)
Measurement principle (monochromatic, TOF, RTOF, etc.)	TOF
Wavelength (range)	0.08–0.76 nm
Resolution (intrinsic peak width, $\Delta d/d$, etc.)	$\Delta d/d = 4 \times 10^{-3}$ at $d = 2 \times 10{-}1$ nm (20' collimation)
Neutron flux on specimen	1×10^{6} cm^{-2}·s^{-1}
Specimen weight capacity	

TABLE II–9. EPSILON — STRESS/STRAIN DIFFRACTOMETER, RUSSIAN FEDERATION (cont.)

Source	2 MW IBR-2 pulsed reactor, 1500 MW peak power in pulse
Movement ranges of positioning stages	x 100 mm y 100 mm z 40 mm manually
Additional sample movement possibilities (Eulerian cradle, hexapod, robot arm, etc.)	Ω rotation: 0–360°
Available sample environment (furnace, load frame, irradiated samples etc.)	Uniaxial pressure device: F = 100 kN (P = 150 MPa) sample: Ø = 30 mm, l = 60 mm
Description of detector	81 ^{3}He single tubes (10 mm diameter)
Beam opening: sizes, horizontal/vertical	horizontal: 0–50 mm vertical: 0–85 mm
Beam defining optics (slits, radial collimators)	Collimators: Nine radial collimators, each with 48 Gd coated foils Collimator length: 500 mm 2θ-range: $82° \leq 2\theta \leq 98°$
Software packages	Instrument control: SONIX-VME-based measuring system running OS-9 and X WINDOW
Data formats	Binary, intrinsic format
Typical applications	Residual and applied stress/strain investigation in various geological samples
Operation (days/year)	Approx. 100 (9 reactor cycles with 11 work days for each cycle)
Iron pin data	Yes
Can you provide diffraction elasticity constants (DECs) to be compiled into a database?	Yes

TABLE II–10. RESIDUAL STRESS, SOUTH AFRICA

Source	20 MW SAFARI-1 Research Reactor (currently being refurbished)
Name of instrument	Residual Stress
Web link	www.necsa.co.za
User facility?	Yes
If yes, who are the users?	Geographical
Experiment proposal deadlines	Open call approach
Time from application to beam time for normal users	3 months
Measurement principle (monochromatic, TOF, RTOF, etc.)	Monochromatic
Wavelength (range)	1.5–1.8 Å
Take-off angle (range)	75–100°
Monochromator type and reflection(s)	Double focused Si multiwafer, 331
Resolution (intrinsic peak width, $\Delta d/d$, etc.)	5×10^{-3}
Neutron flux on specimen	5×10^{6} cm^{-2}·s^{-1}
Specimen weight capacity	250 kg
Movement ranges of positioning stages	x 250 mm y 250 mm z 250 mm manually
Additional sample movement possibilities (Eulerian cradle, hexapod, robot arm, etc.)	Eulerian cradle
Available sample environment (furnace, load frame, irradiated samples etc.)	None
Description of detector	Denex 300 × 300 mm^2 area detector
Beam opening: sizes, horizontal/vertical	Max: 10 mm (h) × 10 mm (v) Min: 1 mm (h) × 1 mm (v)
Beam defining optics (slits, radial collimators)	Fixed Cd slits No radial collimators
Software packages	None
Data formats	Nexus

TABLE II–10. RESIDUAL STRESS, SOUTH AFRICA (cont.)

Source	20 MW SAFARI-1 Research Reactor (currently being refurbished)
Typical applications	Laser deformed samples, weldments, autofrettaged materials, hard metals
Operation (days/year)	None presently. Reactor operation in excess of 300
Industrial users	Yes, as occasional users Local industries such as utilities company, rail transport, motor car manufacturers, hard metals manufacturers
Iron pin data	Not presently, but can be provided when facility is back in operation
Can you provide diffraction elasticity constants (DECs) to be compiled into a database?	XRD (X ray diffraction) values

TABLE II–11. PD-3, INDIA

Source	100 MW Dhruva research reactor
Name of instrument	PD-3
Web link	—
User facility?	—
Experiment proposal deadlines	—
Time from application to beam time for normal users	—
Measurement principle (monochromatic, TOF, RTOF, etc.)	Monochromatic
Wavelength (range)	1.76, 2.71×10^{-1} nm
Take-off angle (range)	90°
Monochromator type and reflection(s) :	BPC SI (220) (111)
Resolution (intrinsic peak width, $\Delta d/d$, etc.)	0.3%
Neutron flux on specimen	1×10^{7} cm^{-2}·s^{-1}
Specimen weight capacity	100 kg

TABLE II–11. PD-3, INDIA (cont.)

Source	100 MW Dhruva research reactor
Movement ranges of positioning stages	x 100 mm y 100 mm z 200 mm
Additional sample movement possibilities (Eulerian cradle, hexapod, robot arm, etc.)	—
Available sample environment (furnace, load frame, irradiated samples etc.)	—
Description of detector	Linear Position Sensitive Detector
Beam opening: sizes, horizontal/vertical	Variable 1–10 mm
Beam defining optics (slits, radial collimators)	Slits
Software packages	Custom data acquisition packages
Data formats	ASCII
Typical applications	—
Operation (days/year)	—
Industrial users	—
Iron pin data	—

TABLE II–12. BT8 (DARTS), UNITED STATES OF AMERICA

Source	20 MW NBSR research reactor
Name of instrument	BT8 (DARTS)
Web link	http://www.ncnr.nist.gov/instruments/darts/
User facility?	Yes
If yes, who are the users?	USA Mid-Atlantic Region
Experiment proposal deadlines	Continuously during the year
Time from application to beam time for normal users	0–3 months
Measurement principle (monochromatic, TOF, RTOF, etc.)	Monochromatic

TABLE II–12. BT8 (DARTS), UNITED STATES OF AMERICA (cont.)

Source	20 MW NBSR research reactor
Wavelength (range)	0.9–3.0 Å
Take-off angle (range)	30–120°
Monochromator type and reflection(s)	Si400,Si311,Si511,Cu200,Cu220
Resolution (intrinsic peak width, Δd/d, etc.)	$\Delta d/d =$
Neutron flux on specimen	8×10^5 cm^{-2}·s^{-1}
Specimen weight capacity	Up to 100 kg
Movement ranges of positioning stages	x 150 mm y 150 mm z 200 mm
Additional sample movement possibilities (Eulerian cradle, hexapod, robot arm, etc.)	Yes
Available sample environment (furnace, load frame, irradiated samples etc.)	2 tension–compression rigs (100 kN,12 kN), can be combined
Description of detector	1D-PSD 100 mm length, 2 mm spatial resolution
Beam opening: sizes, horizontal/vertical	10 × 30 mm
Beam defining optics (slits, radial collimators)	Slits
Software packages	Peak fitting, stress from strain, texture, elastic constants with and without texture
Data formats	ASCII
Typical applications	Stress scanning around the welds
Operation (days/year)	Depends on reactor, typically 180
Industrial users	Yes
Iron pin data	In process

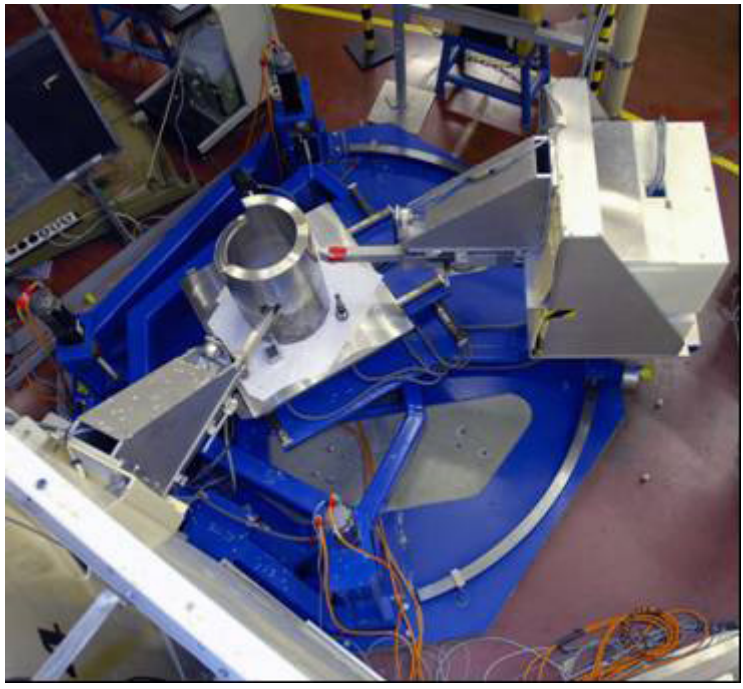

FIG. II-1. Large Component Neutron Diffraction Facility.

FIG. II-2. Fourier Stress Diffractometer.

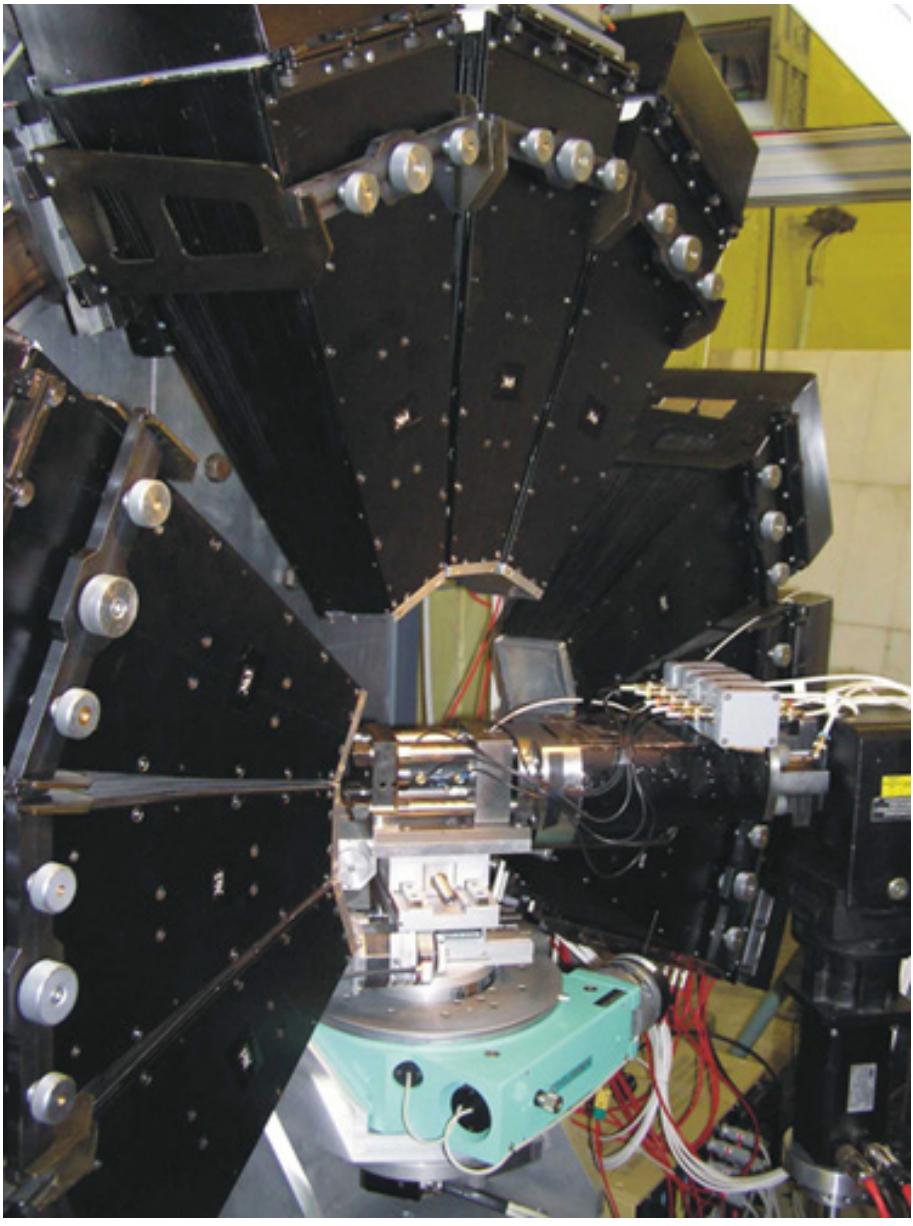

FIG. II–3. Strain/stress EPSILON diffractometer with uniaxial pressure device.

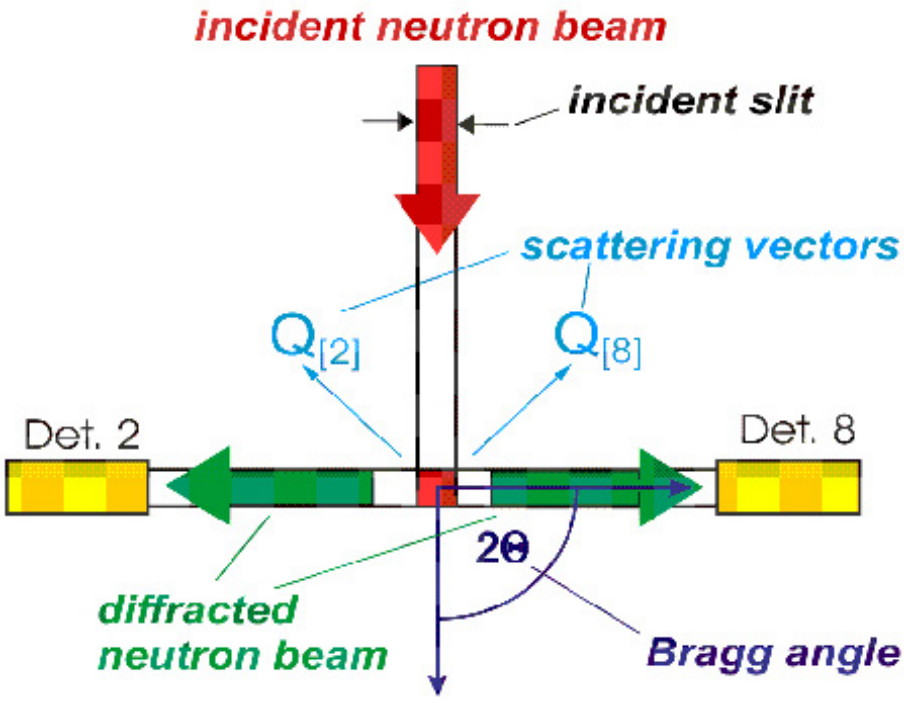

FIG. II–4. Geometrical setup of the EPSILON diffractometer.

CONTRIBUTORS TO DRAFTING AND REVIEW

Abriola, S.A.	International Atomic Energy Agency
Balagurov, A.	Joint Institute for Nuclear Research (JINR), Russian Federation
Bashir, J.	Pakistan Institute of Nuclear Science and Technology (PINSTECH), Pakistan
Das, A.	Bhabha Atomic Research Centre (BARC), India
Edwards, L.	Australia Nuclear Science and Technology Organization (ANSTO), Australia
Gnäupel-Herold, T.	National Institute of Standards and Technology (NIST), United States of America
Goh, B.	International Atomic Energy Agency
Ionita, I.	Nuclear Research Institute Piteşti, Romania
Mikula, P.	Nuclear Physics Institute (NPI), Czech Republic
Ohms, C.	European Commission DG Joint Research Centre, Institute for Energy, Netherlands
Peld, N.	International Atomic Energy Agency
Ridikas, D.	International Atomic Energy Agency
Schneider, R.P.	Helmholtz Zentrum Berlin (HZB), Germany
Sutiarso, S.	National Nuclear Energy Agency (BATAN), Indonesia
Torok, G.	Research Institute for Solid State Physics and Optics, Hungary
Venter, A.	South African Nuclear Energy Corporation (NECSA), South Africa
Wimpory, R.	Helmholtz Zentrum Berlin (HZB), Germany

Technical Meeting
Vienna, Austria: 20–24 April 2009

Consultants Meeting
Vienna, Austria: 16–18 May 2012

IAEA
International Atomic Energy Agency

No. 23

ORDERING LOCALLY

In the following countries, IAEA priced publications may be purchased from the sources listed below or from major local booksellers.

Orders for unpriced publications should be made directly to the IAEA. The contact details are given at the end of this list.

AUSTRALIA
DA Information Services
648 Whitehorse Road, Mitcham, VIC 3132, AUSTRALIA
Telephone: +61 3 9210 7777 • Fax: +61 3 9210 7788
Email: books@dadirect.com.au • Web site: http://www.dadirect.com.au

BELGIUM
Jean de Lannoy
Avenue du Roi 202, 1190 Brussels, BELGIUM
Telephone: +32 2 5384 308 • Fax: +32 2 5380 841
Email: jean.de.lannoy@euronet.be • Web site: http://www.jean-de-lannoy.be

CANADA
Renouf Publishing Co. Ltd.
5369 Canotek Road, Ottawa, ON K1J 9J3, CANADA
Telephone: +1 613 745 2665 • Fax: +1 643 745 7660
Email: order@renoufbooks.com • Web site: http://www.renoufbooks.com

Bernan Associates
4501 Forbes Blvd., Suite 200, Lanham, MD 20706-4391, USA
Telephone: +1 800 865 3457 • Fax: +1 800 865 3450
Email: orders@bernan.com • Web site: http://www.bernan.com

CZECH REPUBLIC
Suweco CZ, spol. S.r.o.
Klecakova 347, 180 21 Prague 9, CZECH REPUBLIC
Telephone: +420 242 459 202 • Fax: +420 242 459 203
Email: nakup@suweco.cz • Web site: http://www.suweco.cz

FINLAND
Akateeminen Kirjakauppa
PO Box 128 (Keskuskatu 1), 00101 Helsinki, FINLAND
Telephone: +358 9 121 41 • Fax: +358 9 121 4450
Email: akatilaus@akateeminen.com • Web site: http://www.akateeminen.com

FRANCE
Form-Edit
5 rue Janssen, PO Box 25, 75921 Paris CEDEX, FRANCE
Telephone: +33 1 42 01 49 49 • Fax: +33 1 42 01 90 90
Email: fabien.boucard@formedit.fr • Web site: http://www.formedit.fr

Lavoisier SAS
14 rue de Provigny, 94236 Cachan CEDEX, FRANCE
Telephone: +33 1 47 40 67 00 • Fax: +33 1 47 40 67 02
Email: livres@lavoisier.fr • Web site: http://www.lavoisier.fr

L'Appel du livre
99 rue de Charonne, 75011 Paris, FRANCE
Telephone: +33 1 43 07 50 80 • Fax: +33 1 43 07 50 80
Email: livres@appeldulivre.fr • Web site: http://www.appeldulivre.fr

GERMANY
Goethe Buchhandlung Teubig GmbH
Schweitzer Fachinformationen
Willstätterstrasse 15, 40549 Düsseldorf, GERMANY
Telephone: +49 (0) 211 49 8740 • Fax: +49 (0) 211 49 87428
Email: s.dehaan@schweitzer-online.de • Web site: http://www.goethebuch.de

HUNGARY
Librotade Ltd., Book Import
PF 126, 1656 Budapest, HUNGARY
Telephone: +36 1 257 7777 • Fax: +36 1 257 7472
Email: books@librotade.hu • Web site: http://www.librotade.hu

INDIA

Allied Publishers
1st Floor, Dubash House, 15, J.N. Heredi Marg, Ballard Estate, Mumbai 400001, INDIA
Telephone: +91 22 2261 7926/27 • Fax: +91 22 2261 7928
Email: alliedpl@vsnl.com • Web site: http://www.alliedpublishers.com

Bookwell
3/79 Nirankari, Delhi 110009, INDIA
Telephone: +91 11 2760 1283/4536
Email: bkwell@nde.vsnl.net.in • Web site: http://www.bookwellindia.com

ITALY

Libreria Scientifica "AEIOU"
Via Vincenzo Maria Coronelli 6, 20146 Milan, ITALY
Telephone: +39 02 48 95 45 52 • Fax: +39 02 48 95 45 48
Email: info@libreriaaeiou.eu • Web site: http://www.libreriaaeiou.eu

JAPAN

Maruzen Co., Ltd.
1-9-18 Kaigan, Minato-ku, Tokyo 105-0022, JAPAN
Telephone: +81 3 6367 6047 • Fax: +81 3 6367 6160
Email: journal@maruzen.co.jp • Web site: http://maruzen.co.jp

NETHERLANDS

Martinus Nijhoff International
Koraalrood 50, Postbus 1853, 2700 CZ Zoetermeer, NETHERLANDS
Telephone: +31 793 684 400 • Fax: +31 793 615 698
Email: info@nijhoff.nl • Web site: http://www.nijhoff.nl

Swets Information Services Ltd.
PO Box 26, 2300 AA Leiden
Dellaertweg 9b, 2316 WZ Leiden, NETHERLANDS
Telephone: +31 88 4679 387 • Fax: +31 88 4679 388
Email: tbeysens@nl.swets.com • Web site: http://www.swets.com

SLOVENIA

Cankarjeva Zalozba dd
Kopitarjeva 2, 1515 Ljubljana, SLOVENIA
Telephone: +386 1 432 31 44 • Fax: +386 1 230 14 35
Email: import.books@cankarjeva-z.si • Web site: http://www.mladinska.com/cankarjeva_zalozba

SPAIN

Diaz de Santos, S.A.
Librerias Bookshop • Departamento de pedidos
Calle Albasanz 2, esquina Hermanos Garcia Noblejas 21, 28037 Madrid, SPAIN
Telephone: +34 917 43 48 90 • Fax: +34 917 43 4023
Email: compras@diazdesantos.es • Web site: http://www.diazdesantos.es

UNITED KINGDOM

The Stationery Office Ltd. (TSO)
PO Box 29, Norwich, Norfolk, NR3 1PD, UNITED KINGDOM
Telephone: +44 870 600 5552
Email (orders): books.orders@tso.co.uk • (enquiries): book.enquiries@tso.co.uk • Web site: http://www.tso.co.uk

UNITED STATES OF AMERICA

Bernan Associates
4501 Forbes Blvd., Suite 200, Lanham, MD 20706-4391, USA
Telephone: +1 800 865 3457 • Fax: +1 800 865 3450
Email: orders@bernan.com • Web site: http://www.bernan.com

Renouf Publishing Co. Ltd.
812 Proctor Avenue, Ogdensburg, NY 13669, USA
Telephone: +1 888 551 7470 • Fax: +1 888 551 7471
Email: orders@renoufbooks.com • Web site: http://www.renoufbooks.com

United Nations
300 East 42nd Street, IN-919J, New York, NY 1001, USA
Telephone: +1 212 963 8302 • Fax: 1 212 963 3489
Email: publications@un.org • Web site: http://www.unp.un.org

Orders for both priced and unpriced publications may be addressed directly to:

IAEA Publishing Section, Marketing and Sales Unit, International Atomic Energy Agency
Vienna International Centre, PO Box 100, 1400 Vienna, Austria
Telephone: +43 1 2600 22529 or 22488 • Fax: +43 1 2600 29302
Email: sales.publications@iaea.org • Web site: http://www.iaea.org/books

SMALL ANGLE NEUTRON SCATTERING — REPORT OF A COORDINATED RESEARCH PROJECT 2000–2003
IAEA TECDOC Series No. 1486
(2006)
ISBN:92–0–102806–7 Price: €15.00

RESEARCH REACTORS: SAFE MANAGEMENT AND EFFECTIVE UTILIZATION — PROCEEDINGS OF AN INTERNATIONAL CONFERENCE, RABAT, MOROCCO, 14–18 NOVEMBER 2011
IAEA Proceedings Series (CD-ROM)
STI/PUB/1575 (2012)
ISBN: 978–92–0–184610–5 Price: €18.00

APPLICATIONS OF RESEARCH REACTORS
IAEA Nuclear Energy Series NP-T-5.3
STI/PUB/1627 (97 pp.; 2014)
ISBN: 978–92–0–145010–4 Price: €32.00

NEUTRON IMAGING: A NON-DESTRUCTIVE TOOL FOR MATERIALS TESTING
IAEA TECDOC Series No. 1604
(2008)
ISBN: 978–92–0–110308–6 Price: €15.00

UTILIZATION RELATED DESIGN FEATURES OF RESEARCH REACTORS: A COMPENDIUM
Technical Reports Series No. 455
STI/DOC/010/455 (606 pp.; 2009) Price: €80.00

CHARACTERIZATION AND TESTING OF MATERIALS FOR NUCLEAR REACTORS — PROCEEDINGS OF A TECHNICAL MEETING HELD IN VIENNA, 29 MAY–2 JUNE 2006
IAEA TECDOC Series No. CD-1545
(2006)
ISBN:978–92–0–156807–6 Price: €15.00

This publication is the result of an IAEA coordinated research project and presents a survey of the basic principles, requirements, preparation, design, execution and standardization of residual stress measurements using neutron beams. It includes details of experimental techniques, associated equipment and instrumentation, their commissioning, calibration and control, and data acquisition. A separate chapter is dedicated to data analysis and interpretation. Finally, the report provides, with a number of selected examples, applications of residual stress measurements as well as future trends for development and use of this powerful technique. The publication is a comprehensive and useful resource to the neutron beam user community including academia and industrial partners. It may serve as an introduction to the field for young researchers and graduate students and as guidelines to those operating or planning to implement or modernise their facilities for residual stress measurements. Ultimately, the document presents neutron beams as a valuable and effective tool for performing residual stress measurements both for basic research and various other applications.

INTERNATIONAL ATOMIC ENERGY AGENCY
VIENNA
ISBN 978–92–0–113313–7
ISSN 0074–1914